

The role of SLC7A11 in chemotherapy response of T-cell acute lymphoblastic leukemia

Amber Boutens

Student number: 01710497

Supervisor(s): Dr. Julie Morscio, Prof. Dr. Pieter Van Vlierberghe

A dissertation submitted to Ghent University in partial fulfilment of the requirements for the degree of
Master of science in the Biomedical Sciences

Academic year: 2021 - 2022

Preface

Five years ago, on 25 September 2017 to be exactly, I walked for the first time into the university to start one of the greatest adventures of my life: a Bachelor of Science in Biomedical Sciences. During that period, there were a lot of first times in relation to this study, such as my first lesson, my first practicum, my first report and my first exam. Even though it is already a considerable time ago, I still remember those moments as if it was yesterday. They say time flies when you are having fun, and I guess that is exactly how these years rushed by. Before I knew it, I had my Bachelor diploma in the pocket together with a well-defined life goal: doing cancer research that is related to the immune system.

I was very happy to start the Master of Science in Biomedical Sciences, because this would allow me to commit myself to my interests: cancer and the immune system. Unfortunately, both topics constituted a separate Major, forcing me to choose between either of the two. Moreover, students were appointed to a Major based on a top ten preference list, bringing uncertainty whether you could actually specialize yourself in your topic of interest. Luckily, I got my first choice Master's dissertation topic, allowing me to go further in cancer research. Since my thesis was on T-cell acute lymphoblastic leukemia, I could also stay close to my other interest: the immune system. I have always looked forward to doing a Master's dissertation, because that is the point where all those years of education come together in practice. However, I have also always been worried about a Master's dissertation, because it always seemed to be an enormous amount of work. Now, 2 years later, I am happy to say that doing research and writing a Dissertation is indeed challenging, but also a lot of fun. This dissertation has taken blood, sweat and tears, but I can say it was totally worth all the stress, because now it is finished, I can only be proud of the progress I have made during my Master. In addition, it made me realize even more that I absolutely want to pursue an academic career in cancer research. Therefore, I am very happy that I will be able to do a PhD, in which cancer and immunology are combined, as a first step into the academic world.

A Master's Dissertation is of course a project that is not performed by the student alone. Without a stimulating and supporting environment, it would never be possible to realize such a project. Therefore, I would first like to thank my promotor Dr. Julie Morscio, for helping and guiding me through my thesis. She has shown me the tricks of the trade, has read and improved my entire Master's dissertation, and was always prepared to answer my waterfalls of questions. Secondly, I would also like to thank my co-promotor Professor Dr. Van Vlierberghe, for putting the lab available for master students like me and proofreading a part of my Master's dissertation. Further, I would like to show my gratitude to the entire PVV group for always willing to help when I needed it. I think the atmosphere in this group is really unique, with all colleagues respecting each other and helping each other when needed. I was very happy to be a part of this group for a short time, and this group, together with the entire 1st floor of MRBII has ensured that I had a great time during this entire period. Lastly, I would also like to thank my parents, for judging my figures when I asked them, listening to my written text even though they had no idea what it was about, but also in general, for the moral support over the last 5 years.

On to the next adventure!

Content

1. Summary	1
2. Societal impact	1
3. Introduction	2
3.1 Introduction to T-cell acute lymphoblastic leukemia	2
3.1.1 T-ALL subclassification	3
3.1.2 Genomic landscape	5
3.1.3 Diagnosis, prognosis and treatment	6
3.1.4 Mechanisms of resistance and relapse	7
3.2 Seeking chemotherapy-induced resistance mechanisms	8
3.2.1 Solute carrier family 7 member 11 (SLC7A11)	9
3.2.2 Oxidative stress	10
3.2.3 Ferroptosis	10
3.2.4 Regulation of SLC7A11	11
3.2.5 SLC7A11 involvement in cancer	12
3.2.6 SLC7A11 inhibition	13
3.3 Metabolomics	14
3.3.1 Sample preparation	15
3.3.2 Metabolome measurement	15
4. Research aim	16
5. Materials and Methods	16
5.1 Cell culture	16
5.2 Quantitative RT-PCR (qRT-PCR) experiments	16
5.3 Cell stains	17
5.4 Metabolomics	17
5.4.1 Sample preparation	17
5.4.2 Metabolome measurement	18
5.4.3 Data analysis	18
5.5 Cell viability assay	19
5.6 Statistical analysis	19
6. Results	20
6.1 <i>SLC7A11</i> is upregulated in primary T-ALL samples	20
6.2 T-ALL cell lines are not dependent on SLC7A11 and variably express this antiporter subunit	21
6.3 <i>SLC7A11</i> is upregulated in T-ALL cell lines after L-asparaginase treatment	22
6.4 <i>SLC7A11</i> upregulation after L-asparaginase treatment modulates the expression of downstream components	23

6.5 Metabolomic analysis of T-ALL cells after L-asparaginase treatment	26
6.5.1 Targeted analysis of amino acid metabolism after L-asparaginase treatment	26
6.5.2 Untargeted analysis of T-ALL cell metabolism after L-asparaginase treatment	27
6.6 Inhibiting L-asparaginase upregulated SLC7A11 does not impair cell viability.....	31
6.7 <i>SLC7A11</i> is upregulated by the SLC7A11 inhibitor erastin	32
6.8 Combination treatment does not modulate the expression of SLC7A11 downstream components in accordance with its effect on <i>SLC7A11</i> expression	33
7. Discussion.....	35
8. References.....	40
9. Poster	
10. Addendum.....	

1. Summary

T-cell acute lymphoblastic leukemia (T-ALL) is an aggressive hematologic malignancy in which still up to 20% of children and 40% of adults do not respond to long-term high-dose multiagent chemotherapy, or relapse after initial response. Because the underlying mechanisms causing these relapsed/refractory (R/R) T-ALLs are generally unknown, salvage therapies are lacking, leaving these patients with a poor prognosis. Given the prominent need to elucidate the basis of R/R T-ALL for developing new therapeutic strategies, we explored the role of SLC7A11, the functional subunit of the cystine/glutamate antiporter system x_c^- , in the chemotherapy response of T-ALL and its potential as a chemotherapy-induced therapeutic target. Using RT-qPCR and flow cytometric analysis, we showed that L-asparaginase treatment of T-ALL cells upregulates *SLC7A11* expression and associated this with a decrease in cellular oxidative stress. Further metabolomic analysis revealed that, next to changes linked to SLC7A11 upregulation, a plethora of other cellular responses are provoked by L-asparaginase treatment, questioning the extent to which SLC7A11 is involved in the therapy response of T-ALL. Finally, a cell viability assay demonstrated that combining L-asparaginase treatment with the SLC7A11 inhibitor erastin does not decrease cell viability, although flow cytometry indicated an increase in cellular oxidative stress. RT-qPCR analysis suggested that this could be due to erastin induced *SLC7A11* upregulation. Collectively, our results imply SLC7A11 involvement in the therapy response of T-ALL, but further experiments are needed to determine the extent of this involvement, its exact role and its potential as chemotherapy-induced therapeutic target.

2. Societal impact

T-cell acute lymphoblastic leukemia (T-ALL) is an aggressive blood cancer, requiring patients still to be treated with a long-term high-dose multiagent chemotherapy. Unfortunately, a significant number of patients do not respond to therapy or relapse after initial response. In general, the reason why these patients cannot be cured with standard treatment is not known, and because there are no second line therapies, these patients are left with a poor prognosis. In line with the need for second line therapeutic strategies, this Master's dissertation showed that the amino acid transporter SLC7A11 might play a role in decreasing T-ALL therapy response. If further elaboration would confirm that this indeed the case, this transporter could be exploited in the future as a new therapeutic target. Given the lack of second line therapies, this would have a major impact on public health, improving the survival chances of at least a part of the described patient group. Moreover, if this would be demonstrated as a highly therapy potentiating strategy, it might even be possible to ameliorate the long-term high-dose multiagent therapy, reducing lifelong side effects, and therefore improving the quality of life of patients. The latter would also have a significant economic impact through reducing hospital time, and thus costs, due to shorter therapy time and less side effect related hospitalizations. Although further research will be needed to determine the exact role and potential of SLC7A11 as a chemotherapy-induced therapeutic target, it is a promising first step in the search for new second line therapies.

3. Introduction

3.1 Introduction to T-cell acute lymphoblastic leukemia

Throughout life, enormous numbers of all mature blood cells are constantly regenerated from a small heterogeneous population of self-renewing hematopoietic stem cells (HSCs) in a process that is called hematopoiesis (Figure 1)^{1,2}. During this process, HSCs in the bone marrow go through a hierarchy of differentiation stages, leading to progressive lineage commitment. In a first step, HSCs differentiate into multipotent progenitors (MPPs), which can produce all blood cells but have lost self-renewal ability^{2,3}. MPPs subsequently give rise to common myeloid progenitors (CMPs) and common lymphoid progenitors (CLPs). CMPs further differentiate into either megakaryocyte-erythroid progenitors (MEPs) or granulocyte-macrophage progenitors (GMPs), which eventually produce all mature myeloid cells. CLPs finally form all mature lymphoid cells, being the T-, B- and NK-cells. It is important to mention that the tree-like compartmentalized hematopoiesis as described in Figure 1, which suffices to conceptualize hematopoiesis, is an oversimplification. Recent research has shown that the acquisition of lineage-specific fates is a continuous process, suggesting that there are no clear boundaries between stem cells and progenitors^{2,4}. Elaborating on this would, however, go beyond the scope of this Master's dissertation.

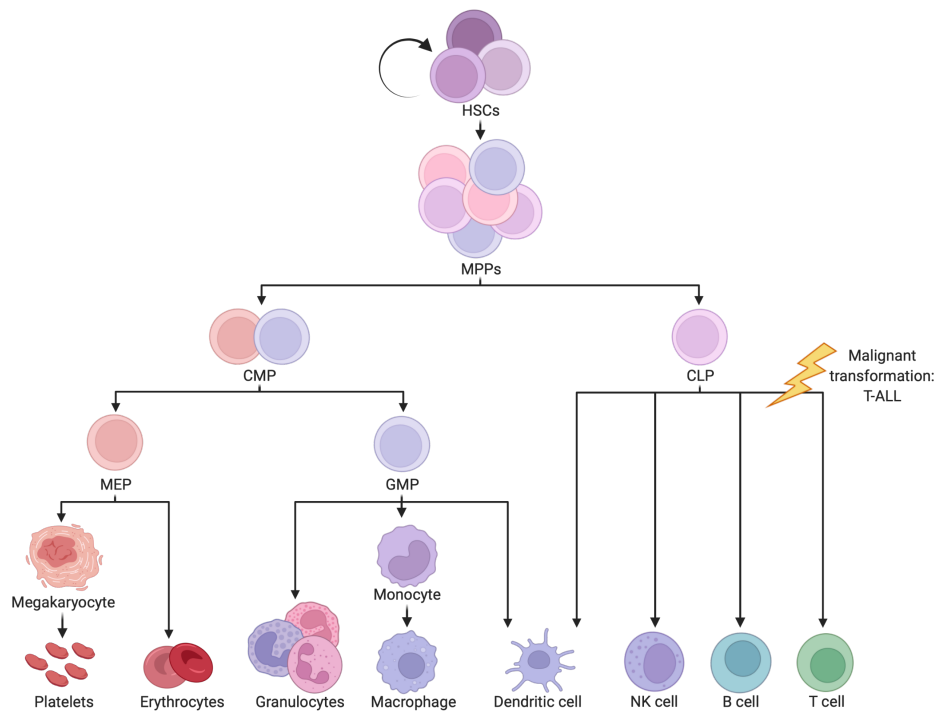


Figure 1 – Normal hematopoiesis and malignant transformation of T-cell progenitors into T-ALL. HSC, Hematopoietic stem cell; MPP, Multipotent progenitor; CMP, Common myeloid progenitor; CLP, Common lymphoid progenitor; MEP, Megakaryocyte-erythroid progenitor; GMP, granulocyte-macrophage progenitor. Created with BioRender.com.

Since the hematopoietic system must provide new blood cells during an individual's entire life, its protection is critical to maintain lifelong functional integrity³. The hematopoietic architecture is therefore inherently tumor suppressive, with HSCs kept to a small population, retaining in a quiescent, autophagy dependent and glycolytic state^{3,4}. Self-renewal, differentiation and lineage commitment are tightly controlled by both intrinsic and extrinsic factors, which induce or suppress gene programs based on the needs of an individual^{1,3}. Disruption of this balanced axis due to (epi)genetic alterations in these regulating factors or the HSCs themselves will directly impact normal hematopoiesis, leading to abnormal proliferation, increased self-renewal capacity and impaired differentiation of hematopoietic stem and progenitor cells (HSPCs). This phenomenon is defined as leukemia, a form of a hematologic malignancy. Leukemia can be

divided into several subclasses, depending on the rate of clinical progression and the transformed lineage of origin, being myeloid or lymphoid⁵⁻⁷. Acute leukemias are characterized by their rapid progression, plentitude of blasts and early symptoms of hematopoietic insufficiency, requiring immediate treatment. Chronic leukemias contrarily show a more indolent progression with some but not exclusive blasts, and do not need, given the late onset of symptoms, instantaneous treatment.

When a malignant transformation and subsequent clonal expansion aggressively occurs in T-cell progenitors, we designate it as T-cell acute lymphoblastic leukemia (T-ALL)⁸. ALL incidence follows a bimodal distribution, with peaks in childhood and around the age of 60 years^{9,10}. T-ALL accounts herein for approximately 15% of pediatric and 25% of adult cases and is twice as prevalent in males than females¹¹. Patients typically experience symptoms that reflect the accumulation of T-cell lymphoblasts within the bone marrow, peripheral blood and extramedullary sites such as the central nervous system, lymph nodes, liver and spleen⁸. They present with leukocytosis and bone marrow failure, leading to nonspecific symptoms such as infections, fever, fatigue, easy bruising/bleeding and bone/joint pain^{8,9,12}. In addition, patients frequently show mediastinal thymic masses and meningeal infiltration, giving symptoms such as dyspnea, headache, nausea and visual impairment¹². Involvement of other extramedullary sites can cause lymphadenopathy, splenomegaly or hepatomegaly⁸. The etiology of T-ALL is largely unknown since its relatively low incidence makes it difficult to obtain robust etiological data¹². However, in the majority of cases, T-ALL develops as a *de novo* malignancy in previously healthy individuals⁸. Furthermore, environmental exposures such as ionizing radiation, chemotherapy, chemicals and human T-lymphotropic virus type 1 have been associated with an increased risk of developing ALL^{9,13}. Also several genetic factors such as germline mutations in *PAX5* or *ETV6*, single nucleotide polymorphisms (SNPs) in *CDKN2A* and hereditary conditions including Down syndrome, Klinefelter syndrome, Bloom syndrome, Fanconi anemia, Nijmegen breakdown syndrome, neurofibromatosis type 1 and ataxia telangiectasia can predispose to a minority of ALL cases^{9,12,13}. Lastly, also ethnicity can predispose to ALL, with the highest incidence occurring in the Hispanic population¹⁴.

3.1.1 T-ALL subclassification

T-ALLs are usually classified into different subcategories based on unique gene expression signatures and immunophenotypes reflecting the stage of normal intrathymic T-cell maturation at which transformation occurred¹⁵. Indeed, in contrast to other hematologic lineages, T-cells do not complete their development in the bone marrow¹⁶. T-cells differentiation takes place in the thymus, a mediastinal organ that provides a highly specialized microenvironment to coordinate the development of functionally mature, self-tolerant T-cells¹⁷.

Structurally, the thymus can be divided into an outer cortex and an inner medulla, two functionally distinct regions with specific contributions to the differentiation of T-cells¹⁷ (Figure 2A). Because T-cell differentiation in humans is not yet extensively known, differentiation as observed in the mouse will be described. Bone marrow derived thymus-seeding progenitor cells (TSPs) arrive via vasculature at the corticomedullary junction, and transit into cortical early T-cell progenitors (ETPs) after the activation of NOTCH1 signaling^{17,18}. T-cell development progresses from this moment on through specific stages that can be distinguished through cell surface markers. Based on the expression of CD4 and CD8 molecules, thymocytes belong to either double negative (DN), double positive (DP) or single positive (SP) subsets. DN cells are further divided into four stages, depending on CD44 and CD25 expression. ETPs are part of the uncommitted DN1 population (CD25⁻CD44⁺), still retaining some NK and DC potential¹⁹. Due to the genetic program that is induced by NOTCH1 signaling, ETPs expand and differentiate into DN2 cells (CD25⁺CD44⁺)²⁰. During this phase, cells undergo T cell lineage commitment through gene arrangements at the *TCR γ* , *TCR δ* and *TCR β* loci, which is completed when cells enter the DN3 stage (CD25⁺CD44⁻) and choose the $\alpha\beta$ or $\gamma\delta$ cell fate²¹. DN3 cells complete TCR β rearrangement, leading to, when associated with an invariable pre-T α chain, expression of a pre-TCR. Pre-TCR signaling allows transition

through the β selection checkpoint, enabling DN3 thymocytes to further differentiate into DN4 (CD25⁻CD44⁻) and DP thymocytes. DP cells will rearrange their TCR α chain, inducing the expression of a complete TCR $\alpha\beta$ complex¹⁹. In case this TCR $\alpha\beta$ binds self-peptide-MHC complexes presented by cortical TECs with adequate affinity, DP thymocytes are positively selected and mature into CD4 or CD8 SP cells, which migrate into the medulla. Finally, only cells that express a TCR which does not bind self-peptide-MHC complexes with high affinity will survive negative selection, mature and leave the thymus via vasculature at the corticomedullary junction.

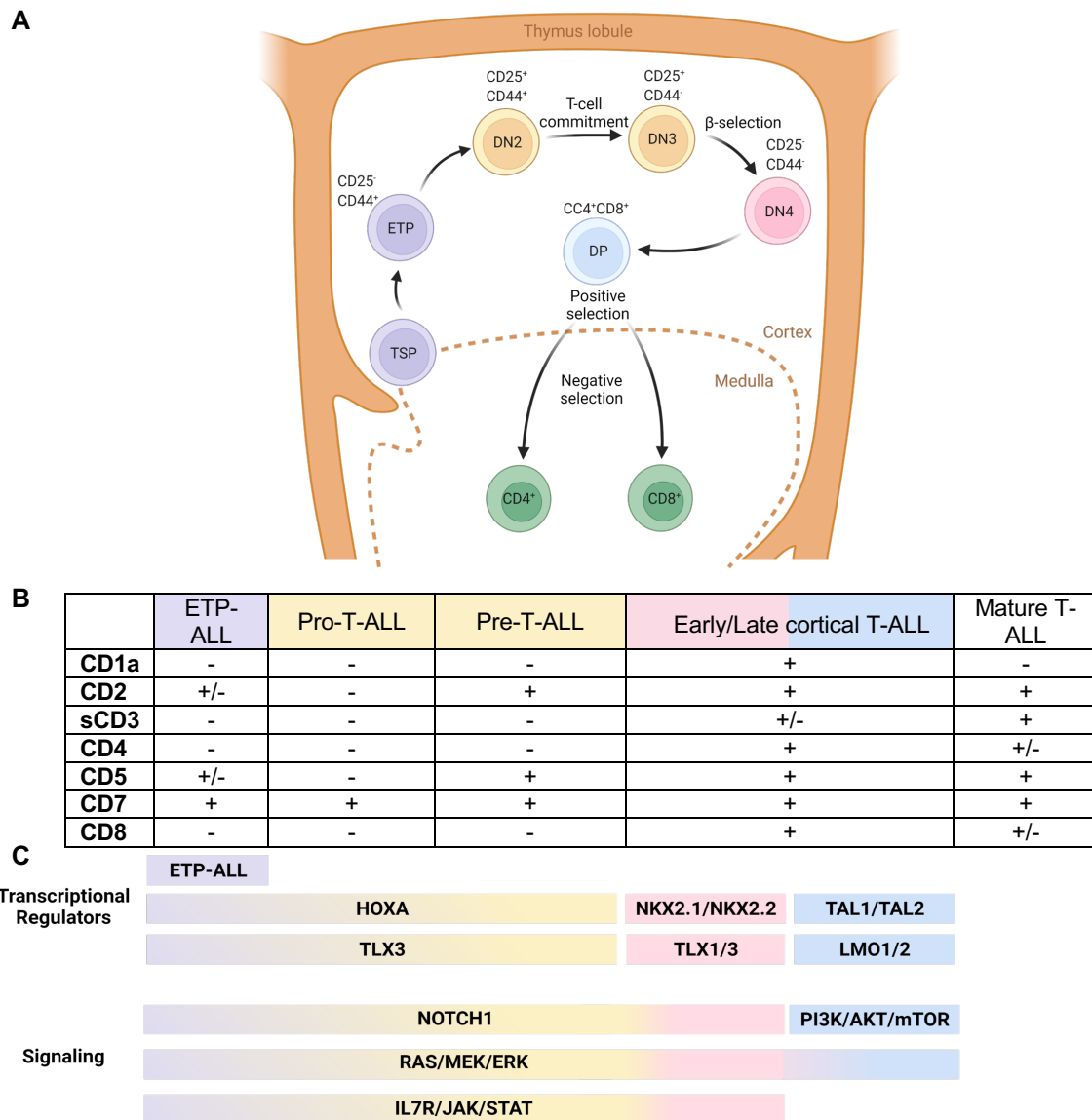


Figure 2 – (A) T-cell development, (B) immunophenotypic subclassification and (C) genetic subclassification of T-ALL (based on De Smedt et al.²²). TSP, Thymus seeding progenitor; ETP, Early T-cell progenitor; DN, Double negative; DP, Double positive. Created with BioRender.com.

One of the most commonly used immunophenotypic subclassifications of T-ALL is the stratification system proposed by the European Group for the Immunological Characterization of Leukemias (EGIL), which classifies T-ALL into four subtypes, being pro-, pre-, cortical and mature T-ALL²³ (Figure 2B). In recent years, this subclassification has been extended with a fifth subgroup, early T-cell precursor (ETP)-ALL, which is characterized by a differentiation arrest at the earliest stage of T-cell differentiation¹⁵. Since T-cell maturation is characterized by a change in the expression of CD markers, T-ALL subtyping is based on the constellation of CD markers found in T-ALL lymphoblasts¹². All lymphoblasts in T-ALL are terminal

deoxynucleotidyl transferase (TdT) positive and typically express cytoplasmic CD3, which is the only lineage specific marker for T-cell disease¹¹. Variable expression of CD1a, CD2, surface CD3 (sCD3), CD4, CD5, CD7 and CD8 allows to make the distinction between the different subcategories. In addition to this, ETP-ALL leukemias express, due to their close relationship with hematopoietic stem cells and myeloid progenitors, at least one of the following stem cell or myeloid markers: CD11b, CD13, CD33, CD34, CD65, CD117 or HLA-DR^{9,11}.

3.1.2 Genomic landscape

T-ALL is a genetically heterogeneous disease that results from a multi-step process in which a broad spectrum of genetic lesions collectively cooperate to alter key mechanisms that control cell growth, proliferation, differentiation and survival during thymocyte development^{11,24}. These genetic lesions are generally distributed into one of two main categories: anomalies that result in aberrant expression of transcription factor oncogenes (1), and molecular (epi)genetic abnormalities that affect signaling and/or the cell cycle (2)¹¹. The latter group is often present in combination with aberrant expression of transcription factors.

The aberrant expression of transcription factor oncogenes is a hallmark of T-ALL²⁰. It results from either chromosomal translocations to regulatory regions of TCR genes, chromosomal rearrangements with other regulatory sequences, duplications/amplifications, or mutations/small insertions generating novel regulatory sequences²⁵. Core affected transcriptional regulators include the basic helix loop helix (bHLH) family members TAL1, TAL2, LYL1 and BHLHB1, LIM-only domain family genes LMO1 and LMO2, homeobox family members TLX1, TLX3, HOXA, NKX2.1, NKX2.2 and NKX2.5, and genes including MYB, MYC and MEF2C^{20,26}. Hierarchical clustering of gene expression profiling data has revealed that, next to immunophenotypic subtypes, also well-defined molecular genetic subgroups can be identified in T-ALL (Figure 2C). These subgroups exhibit unique gene expression signatures of aberrantly expressed transcription factors, which also reflect T-ALL cell differentiation arrest at specific stages of T-cell development. In light of this, ETP-ALLs are associated with the aberrant expression of HOXA, LYL1, LMO2, TLX3 or MEF2C^{15,22,25,26}. Additionally, ETP-ALLs might show abnormalities in transcription factors important in hematopoiesis and acute myeloid leukemias, including RUNX1, ETV6, GATA3. Pro- and pre-T-ALLs harbor aberrations in HOXA²². Cortical T-ALLs are divided in early and late subclasses in genetic subtyping, the early subgroup having aberrant expression of TLX1, TLX3, NKX2.1 or NKX2.2, and the late subgroup having abnormalities in TAL1, TAL2, LMO1 or LMO2^{15,22,24}.

The second group of genetic lesions consists of a multitude of genetic and epigenetic defects that are shared among the different genetic subclasses^{11,22}. A common consequence of these defects is the activation of oncogenic signaling cascades, such as NOTCH1, IL7R/JAK/STAT, PI3K/AKT/mTOR and RAS/MEK/ERK pathways²². Constitutive activation of NOTCH1 signaling is the most common oncogenic event involved in the pathogenesis of T-ALL, especially in TLX1/3, NKX2.1/2 and HOXA positive T-ALLs. It results from either activating *NOTCH1* mutations or inactivating mutations or deletions targeting *FBXW7*, the latter impairing proteasomal degradation of activated NOTCH1. The IL7R/JAK/STAT pathway is often disturbed through activating mutations in *IL7R*, *JAK1*, *JAK3* and/or *STAT5B* or deletions in *PTPN2*, with the highest representation within TLX1/3⁺, HOXA⁺ and ETP-ALL patients. Further, also PI3K/AKT/mTOR signaling is frequently activated. Inactivation of PTEN, the main negative regulator of the pathway, or aberrant activation of PI3KCA, PI3KR1 and AKT1 form the most important causes hereof, and have almost been exclusively identified in TAL1/2⁺ and LMO1/2⁺ T-ALLs^{22,27}. Lastly, RAS/MEK/ERK signaling is regularly hyperactivated in T-ALL patients through activating mutations in *NRAS*, *KRAS* or *BRAF* or loss of function alterations in *NF1* or *PTPN11*. These genetic defects are highly enriched in ETP-ALL and HOXA⁺ T-ALL subtypes, and to a lesser extent in TLX1/3⁺ and NKX2.1/2⁺ leukemias, while almost absent in TAL1/2⁺ and LMO1/2⁺ subgroups. Another consequence of the (epi)genetic defects in T-ALL, is loss of cell cycle control. Deletions of *CDKN2A* or *CDKN2B*, encoding for the tumor suppressors p16^{INK4A} and P14^{ARF} or P15^{INK4B} respectively, occur in up to 70% of non ETP-ALL

patients, leading to abnormal proliferation control²⁶. Next to that, also deletions in RB1 and CDKN1B and high levels of cyclin D due to translocations with TCR loci are recurrent phenomena in T-ALL patients. Finally, (epi)genetic lesions in T-ALL also have several other consequences, including epigenetic deregulation, ribosomal dysfunction, and altered expression of oncogenic miRNAs or long non coding RNAs²⁴.

3.1.3 Diagnosis, prognosis and treatment

Diagnosis of T-ALL is generally established when patients present with at least 20% of lymphoblasts in the peripheral blood or bone marrow⁸. A detailed view of the disease is obtained by the combination of morphologic, immunophenotypic and cytogenetic evaluation, allowing for risk stratification and informing the clinician on treatment choices. Historically, clinical factors such as age (> 35 years) and white blood cell count (> 100*10⁹) were used to risk stratify patients based on their prognosis. However, with current chemotherapy regimens, treatment response as determined by minimal residual disease (MRD) has become the key prognostic determinant of outcome and is hence used for treatment allocation¹². The genetic and immunophenotypic subclasses as discussed before are also shown to be related to treatment response and prognosis, yet, they do not independently predict outcome in T-ALL²⁸.

Despite the broad knowledge on the heterogeneous genetic landscape of T-ALL, current treatment protocols still consist of high-dose multiagent chemotherapy, potentially followed by HSC transplantation (HSCT) in patients with high-risk or refractory disease¹³. There is considerable variation according to age and risk stratification, yet, all treatment protocols follow the same basic structure of treatment phases, comprising induction, consolidation and maintenance along with central nervous system (CNS) prophylaxis if needed. During a 4-6 weeks lasting induction, the bulk of leukemic cells is supposed to be eradicated by a combination of anthracyclines (daunorubicin/doxorubicin), vincristine, L-asparaginase and steroids (prednisone/dexamethasone)^{13,22}. After this, treatment is further intensified in the consolidation phase by the addition of high dose methotrexate and 6-mercaptopurine in an attempt to fully eradicate all residual leukemic cells²². Finally, during a maintenance phase of 2 years, disease relapse is countered by methotrexate and 6-mercaptopurine consolidation supplemented with pulses of vincristine and steroids¹³. In patients with CNS involvement, this treatment regimen is expanded by intrathecal chemotherapy in order to clear leukemic cells that are not accessible with systemic chemotherapy because of the blood brain barrier.

Even though this harsh and long treatment regimen, which goes along with considerable short- and long-term side effects, still up to 20% of children and 40% of adults do not respond to this therapy or relapse after a transient initial response^{22,25,29}. The prognosis of these patients is poor, since a second remission, a prerequisite to proceed to curative HSCT, is only achieved in 30-40% of patients due to the lack of standard of care salvage therapies in relapsed or refractory (R/R) setting¹⁰. In fact, the purine nucleoside analog Nelarabine is currently the only drug that is licensed specifically for R/R T-ALL²⁹. As its registration study showed a 1-year overall survival of approximately 28% in responders, there is still an urgent need for the development of novel agents.

Last years' advances in genetic characterization have paved the way for the development of targeted therapies, with the combined goal to reduce the lifelong side effects that come along with the high-dose chemotherapy regimens and to increase complete remission rates²⁹. Even though it is still in its infancy, some promising results have already emerged from the use of agents targeting aberrantly activated NOTCH1, IL7R/JAK/STAT, PI3K/AKT/mTOR and RAS/MEK/ERK pathways^{22,30}. On top of this, also immunotherapeutic approaches are on their way, including anti-CD38 monoclonal antibodies and CAR T-cell therapy^{30,31}. Nevertheless, most of these efforts concentrate on the drivers of newly diagnosed T-ALL, maintaining R/R the major hurdle to overcome in T-ALL²⁹.

3.1.4 Mechanisms of resistance and relapse

In a recent study, an extensive in-depth genetic characterization of diagnostic, remission and relapse samples of pediatric ALL patients treated according to the Shanghai Children's Medical Center ALL-2005 frontline treatment protocol suggested that there are three different clonal evolution models that may lead to relapse in T-ALL (Figure 3)³². In the first model, the *de novo* resistance scenario, most of the leukemic cells are resistant up-front, preventing the achievement of remission in newly diagnosed patients (Figure 3A). In the second model, the chemo-selection scenario, a minor drug-resistant subclone survives treatment, causing very early relapse (< 9 months) (Figure 3B). Lastly, in the chemo-induced mutation scenario, a not fully resistant subpopulation of cells present at diagnosis acquires therapy-induced resistance mutations, leading to the early and late relapses (> 9 months) that are observed in T-ALL (Figure 3C).

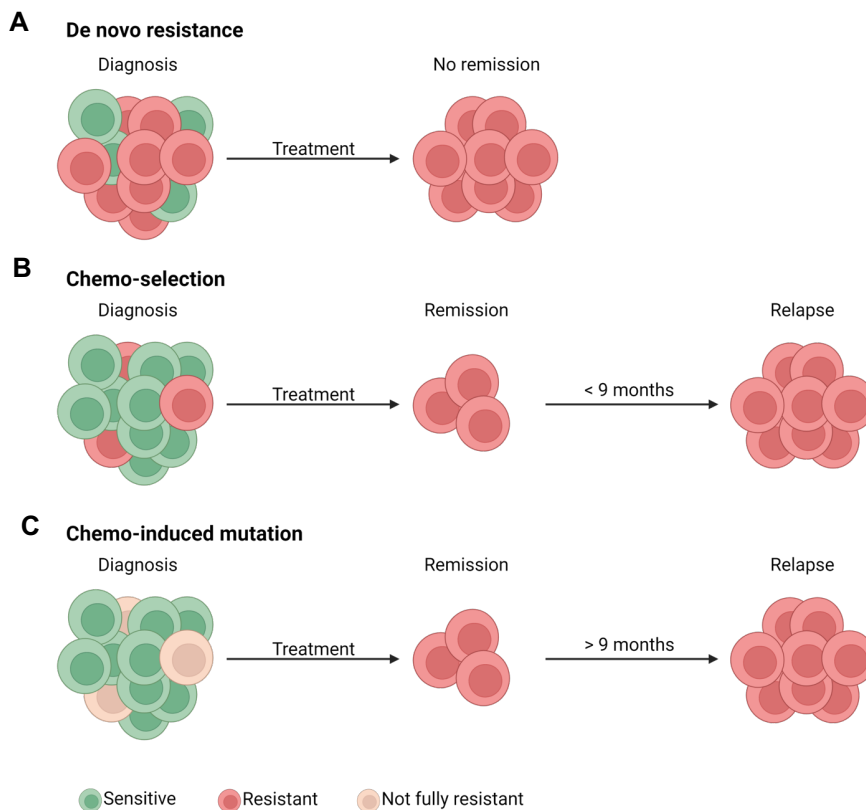


Figure 3 – Three different clonal evolution models of T-ALL relapses. Created with BioRender.com.

Apart from these clonal evolution models, as mentioned before, another distribution of relapses was described by Kunz *et al.* (Figure 4)³³. Here, relapses were divided into two types based on differences in mutational pattern between diagnostic, remission and relapse samples. Type 1 relapses originated from the major subclone present at diagnosis, which had acquired additional mutations until relapse. Type 2 relapses on the contrary resulted from a common pre-leukemic clone, which became malignant due to extensive mutational remodeling. Even though type 1 relapses tended to occur earlier (< 24 months), both subtypes were characterized by selection of subclones and acquisition of novel mutations.

As the variation in the described models of R/R T-ALL already implies, the underlying mechanisms of R/R T-ALL are generally unknown. Currently, only a few recurrent mutations have been associated with R/R T-ALL, amongst which activating mutations in cytosolic 5'-nucleotidase II (*NT5C2*) conferring leukemia cells resistant against 6-mercaptopurine are most commonly known²⁹. Also aberrant activation of MDM2 is an established resistance mechanism, leading to aberrant ubiquitination of the tumor suppressor protein p53. Furthermore, RAS/MEK/ERK activating mutations (*KRAS*, *NRAS*, *BRAF*, *FLT3*, *NF1*,

PTPN11) have been reported to be associated with steroid and/or methotrexate resistance, however, the exact mechanisms remain to be elucidated³⁴. Similarly, overactivation of PI3K/AKT/mTOR and IL7R/JAK/STAT signaling has been linked to steroid resistance, still requiring a more extensive understanding^{26,34}. Based on findings in B-ALL, it is hypothesized that also epigenetic changes such as PRC2 downregulation and WHSC1 or SMARCA4 upregulation may also correlate with chemoresistance. Finally, also non-genetic mechanisms may alter therapy response. An example of this is the upregulation of the oncogenic kinase proviral integration site for Moloney-murine leukemia 1 (PIM1), which has been associated with reduced dexamethasone response³⁵.

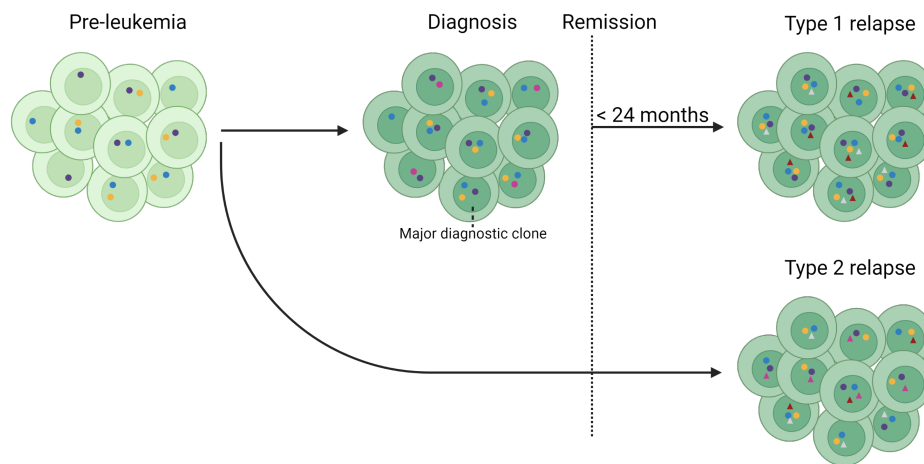


Figure 4 – Suggested T-ALL relapse models based on mutational analysis of diagnostic, remission and relapse samples. Created with BioRender.com.

3.2 Seeking chemotherapy-induced resistance mechanisms

Because elucidating the basis of acquired chemotherapy-resistance will help to identify therapeutic strategies to prevent or eradicate relapsed disease, our group performed a preliminary experiment to identify chemotherapy-induced resistance mechanisms. For this, T-ALL PDX models received a short-term chemotherapy treatment with a cocktail of vincristine, dexamethasone and L-asparaginase on day 1, followed by single shots of dexamethasone on days 2-4. A bulk RNA-Seq analysis on hCD45⁺ T-ALL cells collected from the bone marrow and spleen showed that during this treatment period, a transient change in gene expression could be observed in several genes, amongst which the upregulation of the solute carrier family 7 member 11 (*SLC7A11*) gene was most consistent (Figure 5A). Subsequently, a qPCR analysis on different T-ALL cell lines treated with each of the single components of the cocktail demonstrated that this upregulation could be attributed to specifically one component, namely L-asparaginase (Figure 5B).

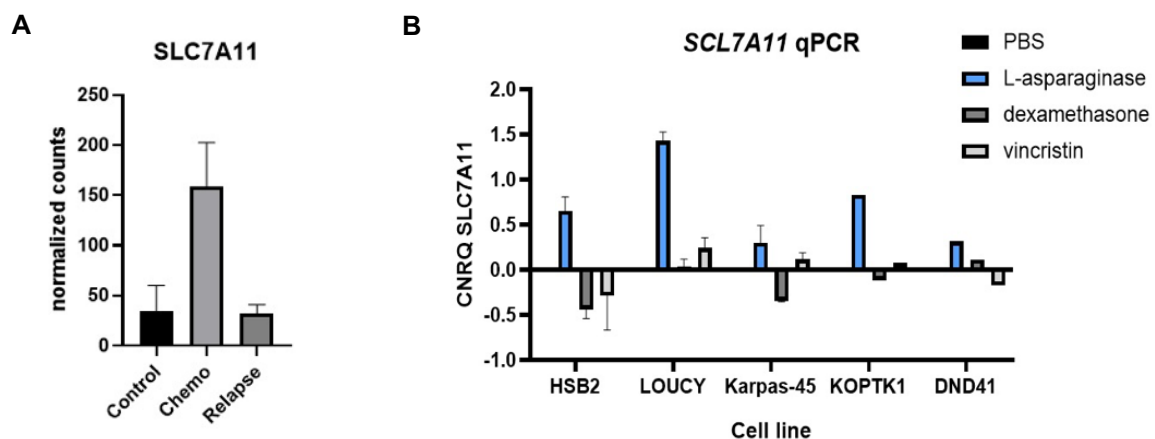


Figure 5 – Preliminary data on the therapy induced upregulation of *SLC7A11*. (A) RNA-Seq data of *SLC7A11* expression in T-cells collected from the bone marrow and spleen. (B) qPCR analysis on different T-ALL cell lines treated with each of the single components of the cocktail used in A.

3.2.1 Solute carrier family 7 member 11 (SLC7A11)

SLC7A11 (also known as xCT) is the light chain functional subunit of the cystine/glutamate antiporter system x_c^- , a Na^+ -independent, Cl^- -dependent transporter that belongs to the family of heterodimeric amino acid transporters (HATs)(Figure 6)³⁶. System x_c^- consists of two subunits, including the light chain subunit SLC7A11 and the heavy chain subunit solute carrier family 3 member 2 (SLC3A2, also known as CD98hc or 4F2hc), linked by a disulfide bond. It is expressed on the cell surface, where it mediates the uptake of extracellular cystine in exchange for intracellular glutamate in a ratio of 1:1³⁷. The human *SLC7A11* gene is located on chromosome 4, contains 14 exons and has orthologs in all vertebrates^{37,38}. Its resulting protein comprises 12 transmembrane domains, with both N- and C-termini located within in the cytoplasm, and has a restricted expression pattern with primary expression in the brain^{37,39}. In contrast to SLC3A2, a chaperone protein for several members of the HAT family that maintains both SLC7A11 protein stability and membrane localization, SLC7A11 is highly specific for system x_c^- , hence providing it its substrate specificity³⁷.

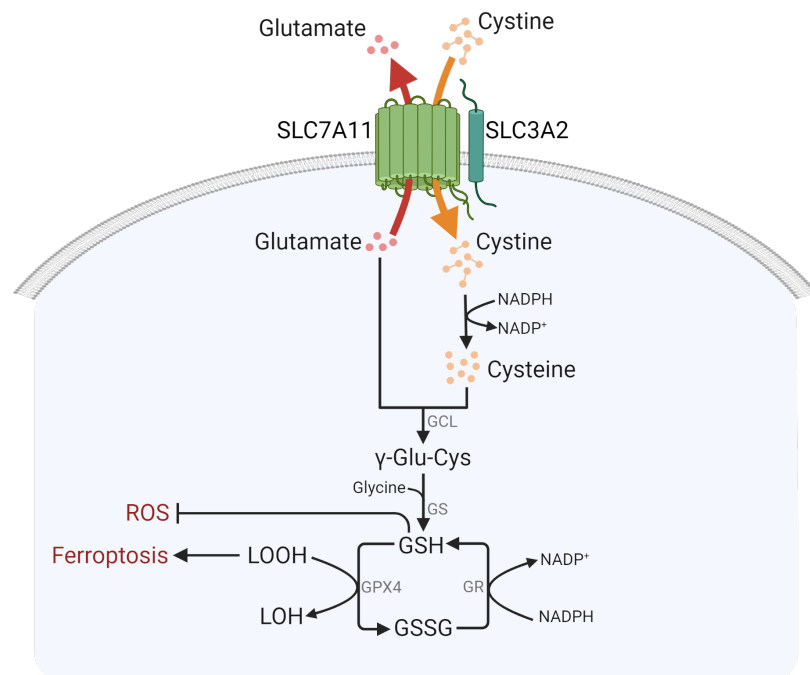


Figure 6 – Function of SLC7A11 in system x_c^- . SLC7A11 is the functional subunit of system x_c^- that imports one molecule of cystine in exchange for one molecule glutamate. Once imported, cystine is converted into two cysteine molecules. Subsequently, cysteine is utilized to synthesize glutathione (GSH) through a two-step process. This GSH can directly protect cells from oxidative stress caused by reactive oxygen species (ROS) through the scavenging of free radicals. In addition to this, GSH can also protect cells from ferroptosis through its function as co-factor for the lipid hydroperoxide detoxifying enzyme glutathione peroxidase 4 (GPX4). GCL, glutamate-cysteine ligase; GS, glutathione synthetase; GPX4, glutathione peroxidase 4; GR, glutathione reductase; GSSG, oxidized glutathione; LOOH, lipid hydroperoxide; LOH, lipid alcohol; ROS, reactive oxygen species. Created with BioRender.com.

Once cystine is imported into the cell via SLC7A11, it is immediately converted into two cysteine molecules through a NADPH-consuming reduction reaction (Figure 6)^{39,40}. Subsequently, cysteine is utilized as the rate-limiting precursor for glutathione (GSH) synthesis³⁹. GSH, the most abundant intracellular antioxidant, is a tripeptide consisting of cysteine, glutamate and glycine. It is produced via a two-step process. In the first rate-limiting step, cysteine and glutamate are catalyzed into γ -glutamyl-L-cysteine (γ -Glu-Cys) by glutamate cysteine ligase (GCL)³⁷. Then, in the second step, glycine is added to the C-terminus of γ -Glu-Cys by GSH synthetase (GS) to produce GSH^{37,38}. GSH functions as an intracellular antioxidant via both enzymatic and non-enzymatic mechanisms³⁶. In the latter, GSH directly protects cells from oxidative stress caused by reactive oxygen species (ROS) by scavenging free radicals⁴¹. However, in the enzymatic process, GSH functions as a co-factor for ROS-

detoxifying enzymes such as glutathione peroxidase 4 (GPX4), which detoxifies lipid hydroperoxides into lipid alcohols³⁹. This enzymatic process is known to inhibit ferroptosis, an iron-dependent cell death triggered by the accumulation of lipid peroxidation products⁴¹. In both enzymatic and non-enzymatic mechanisms, GSH is converted into its oxidized form (GSSG), which is recycled back to GSH via glutathione reductase (GR) at the expense of NADPH³⁹.

3.2.2 Oxidative stress

ROS are a group of highly reactive molecules containing free oxygen radicals that are formed by redox reactions^{37,42}. They are involved in various intracellular signaling pathways that contribute to molecular responses that are part of normal biological processes. However, excessive ROS levels due to an imbalance in the production of free radicals and their removal by the antioxidant defense system induces oxidative stress, which causes oxidative damage to proteins, lipids and DNA^{36,42}. This imbalance mostly arises due to an insufficiency of detoxifying mechanisms, including GSH reserves and antioxidant enzyme activity⁴².

Normal healthy cells usually do not experience disproportionate levels of oxidative stress⁴⁰. This is because their intracellular cysteine levels derived by *de novo* biosynthesis or protein degradation often suffice to produce adequate GSH levels. Cancer cells, however, often extensively reprogram their metabolic pathways to support their increased biosynthetic and bioenergetic demands³⁹. As a result, cancer cells often experience high levels of oxidative stress, causing the traditional biosynthesis and protein catabolism to fall short in meeting their high demand for antioxidant defense^{39,40}. In response to this, cancer cells upregulate their antioxidant mechanisms, including the amino acid transporter SLC7A11, to maintain their redox balance and to prevent ferroptosis.

3.2.3 Ferroptosis

In 2012, a new form of regulated cell death (RCD) associated with cysteine depletion in the cell was discovered after pharmacological blockade of the SLC7A11 antiporter subunit⁴³. Since this form of cell death required intracellular iron, it was self-evidently termed *ferroptosis*. Ferroptosis is highly distinct from other forms of regulated cell death⁴⁰. At morphological level for example, ferroptotic cells exhibit shrunken, dense mitochondria, while DNA fragmentation in the nucleus or plasma membrane blebbing/rupture, typical characteristics of apoptosis and necrosis, are absent³⁹. Also biochemical features of other forms of RCD are not present in ferroptotic cells, indicating its distinctiveness.

As mentioned before, ferroptosis occurs due to the accumulation of lipid peroxidation products. These products typically result from the oxidation of polyunsaturated fatty acids (PUFAs) in the cellular lipid bilayer via a non-enzymatic or enzymatic multistep process⁴⁴ (Figure 7). In the first step of the non-enzymatic process, a bis-allylic hydrogen atom, which is located on the carbon between two carbon-carbon double bonds, is abstracted by a radical. Next, the formed lipid radical (L[•]) reacts with oxygen, leading to a lipid peroxy radical (LOO[•]), which will remove a hydrogen from an adjacent PUFA phospholipid, forming lipid hydroperoxide (LOOH). In the enzymatic process, this LOOH product is thought to be directly formed from PUFA lipids via iron-dependent lipoxygenase (LOX) or cytochrome P450 oxidoreductase (POR) enzymes, however, the exact mechanism remains to be elucidated. In case this hydroperoxide is not immediately converted to its corresponding alcohol (LOH) by GPX4, it can react with cellular labile iron to generate an alkoxide radical (LO[•]). This radical then finally forms a non-toxic lipid alcohol (LOH) by retrieving a hydrogen from an adjacent PUFA phospholipid, initiating a new round of lipid oxidation^{44,45}. This chain reaction will eventually lead to a myriad of secondary products, including PUFA fragments and oxidized and modified proteins. How these events finally cause irreversible cell death is still unclear⁴⁵. However, it is hypothesized that either the hydrophilization of the lipid bilayer by the lipid alcohols or the inactivation of essential intracellular proteins by the radicals pushes the cell into ferroptotic cell death^{44,45}.

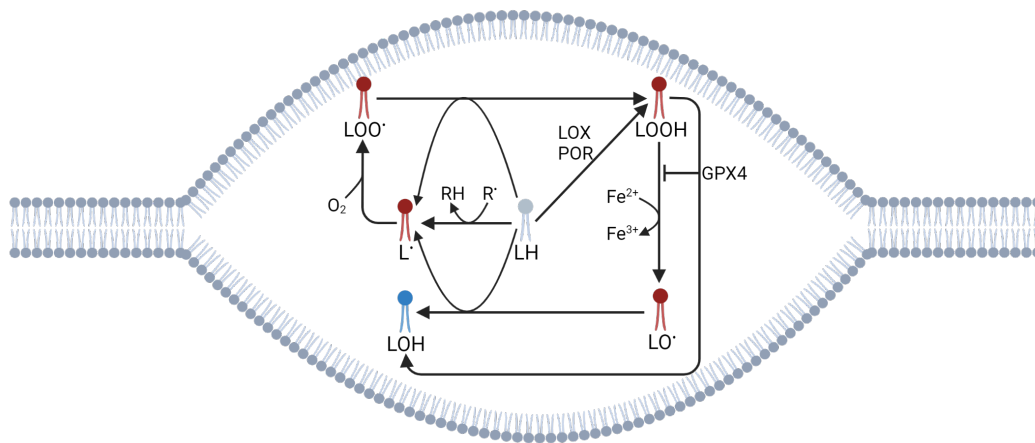


Figure 7 – Ferroptosis. LH, Lipid hydrogen; R[•], radical; L[•], lipid radical; LOO[•], lipid peroxy radical; LOOH, lipid hydroperoxide; LO[•], alkoxide radical; LOH, lipid alcohol; LOX, lipoxygenase; POR, cytochrome P450 oxidoreductase; GPX4, glutathione peroxidase 4. Created with BioRender.com.

Normal healthy cells usually contain sufficient GSH to fuel GPX4 mediated detoxification of lipid hydroperoxides, thereby suppressing ferroptosis^{39,40}. Cancer cells, however, often consume significantly higher levels of GSH than normally available, thereby putting them at risk of ferroptosis⁴². Consequently, SLC7A11 upregulation is critical for cancer cells, increasing intracellular cysteine and GSH levels, protecting the cells from lipid peroxidation and ferroptotic cell death.

3.2.4 Regulation of SLC7A11

As one might expect from its function, SLC7A11 expression and activity is primarily modulated by various stress-inducing conditions such as oxidative stress, amino acid starvation and genotoxic stress with the aim to restore redox homeostasis and antagonize cell death^{37,38,42}. This modulation occurs through a variety of mechanisms, including transcriptional, post-transcriptional and post-translational regulation⁴¹ (Figure 8).

At the transcriptional level, activating transcription factor 4 (ATF4) and nuclear factor erythroid 2-related factor 2 (NRF2) constitute the two major regulating transcription factors of *SLC7A11* expression⁴⁰. Under amino acid starvation stress, ATF4 is induced via enhancement of mRNA translation. Indeed, stress causes the phosphorylation of eukaryotic initiation factor 2 α (eIF2 α) by general control nondepressible 2 (GCN2), preventing the translation of the ATF4 upstream open reading frames (uORFs) and thus liberating ATF4 mRNA translation and protein production³⁹. ATF4 will then move to the nucleus to bind amino acid response elements (AAREs) in gene promoter regions of stress involved genes, amongst which *SLC7A11*, stimulating their transcription. In case of oxidative stress, Kelch-like ECH-associated protein 1 (KEAP1) mediated proteasomal degradation of NRF2 is impaired, resulting in NRF2 stabilization and translocation into the nucleus^{38,42}. There, it will bind antioxidant response elements (AREs) in gene promoter regions, inducing transcription of a variety of antioxidant defense genes, including *SLC7A11*. ATF4 and NRF2 are generally thought to cooperatively regulate *SLC7A11* expression by interacting with each other on the promoter, however, hard evidence is often lacking⁴⁰. In contrast to *SLC7A11* upregulation, *SLC7A11* transcription can also be repressed. The best known transcription factors for this are p53 and ATF3³⁸. Next to transcription factors, also epigenetic regulators modulate *SLC7A11* expression at the transcriptional level by chemical modifications on DNA or DNA-associated histones⁴⁰. For example, polycomb repressive complex 1 (PRC1) mediated mono-ubiquitination and paradoxically BRCA1 associated protein 1 (BAP1) mediated deubiquitination of histone 2A both repress *SLC7A11* transcription. Similarly, also mono-ubiquitination of histone 2B (H2Bub) by ubiquitin-specific-processing protease 7 (USP7), whose nuclear translocation is promoted by p53, restrains *SLC7A11* expression. Conversely, demethylation of H3K9 by lysine demethylase 3B (KDM3B), causes *SLC7A11* upregulation. Lastly, chromatin modeling at the

SLC7A11 transcriptional start site by ARID1A, a component of the SWI/SNF complex, also promotes *SLC7A11* expression by facilitating NRF2 mediated transcriptional activation.

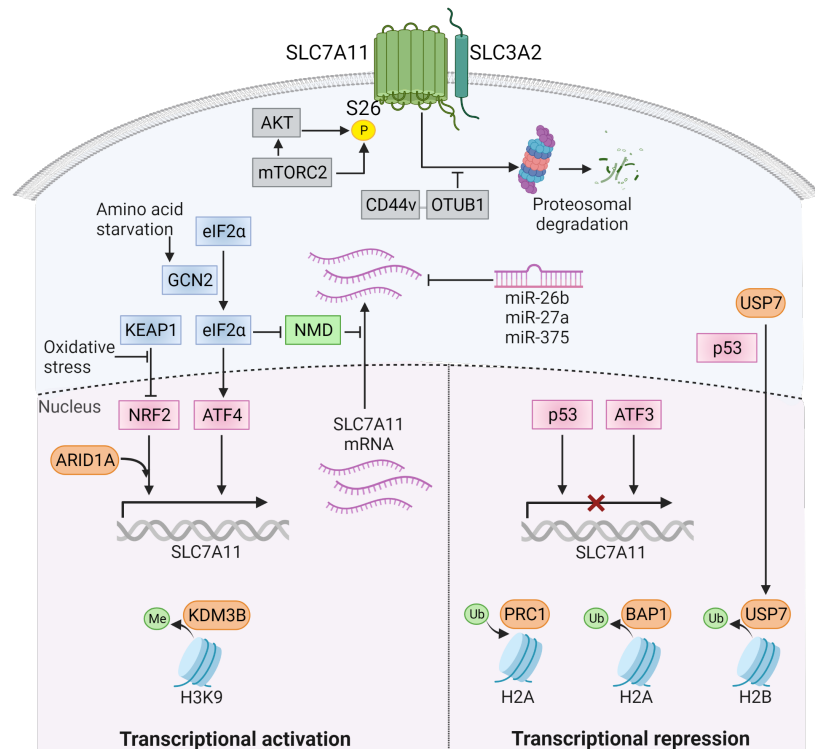


Figure 8 – Regulation of *SLC7A11*. ATF4, activating transcription factor 4; NRF2, nuclear factor erythroid 2-related factor 2; eIF2 α , eukaryotic initiation factor 2 α ; GCN2, general control nondepressible 2; KEAP1, Kelch-like ECH-associated protein 1; ATF 3, activating transcription factor 3; PRC1, polycomb repressive complex 1; BAP1, BRCA1 associated protein 1; USP7, ubiquitin-specific-processing protease 7; KDM3B, lysine demethylase 3B; NMD, nonsense-mediated RNA decay; CD44v, CD44 variant; OTUB1, OUT Domain-containing ubiquitin aldehyde-binding protein 1. Created with BioRender.com.

At the post-transcriptional level, nonsense-mediated RNA decay (NMD) and microRNAs (miRNAs) constitute the most common regulators of *SLC7A11* expression^{37,39}. Under cellular stress, NMD, a surveillance pathway that constantly degrades both mutated and non-mutated RNA, is inhibited via phosphorylated eIF2 α , resulting in *SLC7A11* mRNA stabilization and protein level upregulation. Further, *SLC7A11* mRNA is also regulated by miRNAs including miR-27a, miR-26b and miR-375, which silence *SLC7A11* mRNA by binding to its 3' untranslated region.

Lastly, at the post-translational level, *SLC7A11* expression is mediated via regulation of its protein stability, localization and transporter activity³⁸. As earlier discussed, SLC3A2 is essential to maintain *SLC7A11* protein stability and membrane localization. In addition, also CD44 variant (CD44v) has been identified as a *SLC7A11* binding partner, stabilizing the *SLC7A11* protein via OTU Domain-containing ubiquitin aldehyde-binding protein 1 (OTUB1), which preserves the protein from ubiquitination and proteasomal degradation⁴⁰. Last of all, *SLC7A11* transporter activity itself can also be regulated by mTORC2 which, either directly or via AKT, phosphorylates serine 26 at the N-terminal cytoplasmic tail of *SLC7A11* in response to growth factor stimulation, resulting in an impaired transporter activity^{38,40}.

3.2.5 *SLC7A11* involvement in cancer

To date, *SLC7A11* overexpression has been reported in a wide variety of human cancers, showing an association with proliferation, growth, invasion and metastasis through the enhancement of antioxidant defense and the suppression of ferroptosis^{37,38,41,46}. In non-small

cell lung cancer (NSCLC) for example, inhibiting SLC7A11 transport activity ameliorated tumor cell proliferation and invasion both *in vitro* and *in vivo*⁴⁷. Furthermore, high SLC7A11 levels were correlated with increased melanoma cell proliferation, but also with tumor invasion in both glioblastoma and colorectal cancer⁴⁸⁻⁵⁰. Overexpression of SLC7A11 was also associated with tumor metastasis in CRC as well as oral cavity squamous cell carcinoma^{49,51}. On top of this, high SLC7A11 expression has been linked with a poor prognosis, causing one study to propose the incorporation of SLC7A11 expression in AML risk assessment at diagnosis^{47,49-52}.

In addition, numerous studies have described the role of SLC7A11 in GSH-mediated treatment resistance^{37,38,41}. SLC7A11 overexpression has for instance been shown to confer resistance to cisplatin in gastric cancer, temozolomide in glioblastoma and gemcitabine in pancreatic cancer⁵³⁻⁵⁵. Furthermore, radiation therapy was shown to induce SLC7A11 upregulation, thereby promoting radioresistance^{56,57}. Finally, SLC7A11 has also been shown to be involved in cancer stem cell (CSC) propagation, which emanates from its interaction with CD44v, a well-established CSC marker³⁷. Its expression has proved to be critical in breast CSC maintenance, and its overexpression was shown to confer glioblastoma cells stem cell-like properties^{58,59}. As a consequence, several studies have indicated that inhibition of SLC7A11 in drug resistant CSCs either sensitizes them to standard treatment, or directly depletes them, the latter also attenuating therapy resistance⁶⁰⁻⁶².

Considering the prominent role of SLC7A11 in cancer progression and resistance, its restricted expression patterns in healthy individuals and its dispensability in normal development⁶³, SLC7A11 could potentially function as a highly targetable chemotherapy-induced resistance mechanism in T-ALL.

3.2.6 SLC7A11 inhibition

Since the discovery of SLC7A11's function in ferroptosis, a plethora of compound and drugs have been identified to inhibit this antiporter subunit^{36,39}. Amongst these, the most prominently known and used ones are sulfasalazine, erastin and sorafenib³⁷. Sulfasalazine, a FDA-approved drug commonly used to treat chronic inflammatory diseases such as rheumatoid arthritis, emerged long before the discovery of ferroptosis as a suppressor of lymphoma growth via inhibition of SLC7A11⁶⁴. Erastin, the most selective and potent of the three, originated from a high-throughput screening for synthetic lethal compounds in RAS mutant cancer cells, and led to the discovery of ferroptosis^{43,65}. Lastly, also the FDA-approved multi-kinase inhibitor sorafenib appeared to exert its anti-cancer effect via SLC7A11 inhibition, however, it remains to be elucidated whether this is due to a direct or indirect effect on SLC7A11⁴⁵.

All three inhibitors are able to induce ferroptosis by blocking SLC7A11 mediated cystine uptake and GSH synthesis⁴². However, from a therapeutic point of view, each has its pros and cons. Sulfasalazine for example, does not give better outcomes in phase I/II clinical trials due to its unfavorable pharmacological properties^{66,67}. Similarly, erastin exhibits poor pharmacological characteristics, preventing it from progressing to preclinical studies⁴⁰. Luckily, two recently developed analogues, imidazole ketone erastin (IKE) and piperazine erastin (PE), have brought a solution for this, showing improved water solubility, potency and metabolic stability^{37,68}. On top of this, both sulfasalazine and sorafenib have mechanisms of action besides inhibiting SLC7A11, being prostaglandin and multi-kinase inhibition respectively, going along with significant adverse clinical events⁴².

Since all currently available SLC7A11 inhibitors have off-target effects, new strategies targeting the SLC7A11-GSH axis more specifically are highly needed³⁹. Amongst the ongoing developments, several immunotherapeutic strategies have shown some promising results³⁷. For instance, anti-SLC7A11 DNA vaccines using full length SLC7A11 expressing plasmids have shown to attenuate stem-like behavior and metastatic progression in breast cancer⁵⁸. Similar results were obtained with virus-like particles displaying human and mouse homologous sixth extracellular loop of SLC7A11⁶⁹. Finally, also a bovine herpes virus 4 vector based

vaccine was shown to protect against breast cancer metastases via antibodies against breast CSCs⁷⁰.

3.3 Metabolomics

Metabolomics is the comprehensive analysis of endogenous metabolites, the metabolome, of a biological system⁷¹. The metabolome consists of low molecular weight organic and inorganic molecules that belong to a wide variety of compound classes (e.g. amino acids, lipids, fatty acids, steroids, sugars, estrogens, etc.) with highly diverse physical and chemical properties⁷¹⁻⁷³. Because the metabolome represents the endpoint of the omics cascade, the metabolome is most directly related to the functional phenotype of a cell (Figure 9)^{72,74}. Nevertheless, metabolomics has lagged behind upstream omics research for a long time due to the high complexity and wide concentration ranges of metabolites in a cell⁷². Luckily, last decade's advances in analytical techniques and data analysis tools have boosted metabolome research, establishing metabolomics as a new highly evolving research field⁷⁵.

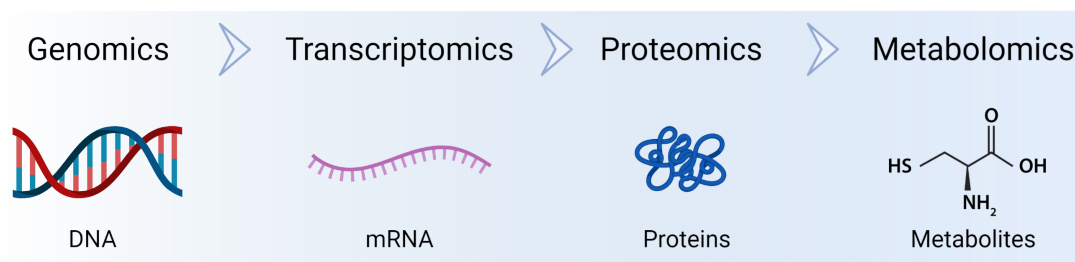


Figure 9 – Omics cascade. Created with BioRender.com.

The metabolome is highly dynamic and context-dependent, causing the levels of each metabolite to depend on the physiological or pathological state of a cell, tissue or organism⁷⁶. Since cancer cells are known to extensively reprogram their metabolic pathways in support of their increased biosynthetic and bioenergetic demands, studying their metabolome could provide critical information on targetable features that would otherwise not have been found through higher omics techniques^{39,77}. In addition, metabolomics also allows the analysis of anti-cancer therapy induced metabolomic changes that could possibly contribute to therapy resistance⁷⁸. An example of this is the study of Schraw *et al.*, in which metabolic profiling of diagnostic childhood ALL samples allowed the identification of pathways associated with MRD⁷⁹. Therefore, exploiting this technique in cancer research is highly relevant.

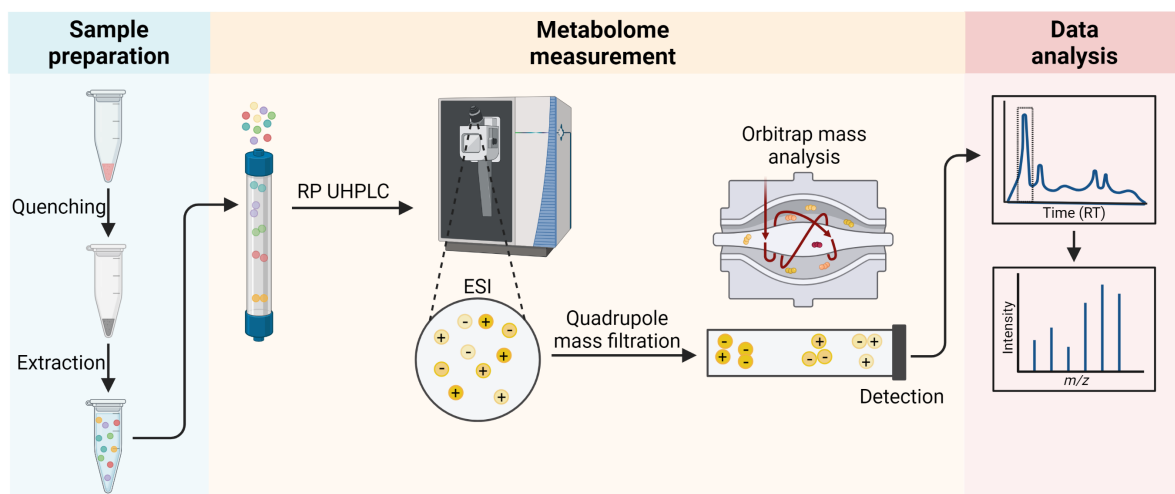


Figure 10 – Schematic overview of the different steps of a metabolomic experiment. RP UHPLC, reversed phase ultra-high pressure liquid chromatography; ESI, electrospray ionization; RT, retention time. Created with BioRender.com.

At this moment, two complementary approaches, targeted and untargeted, are typically employed for metabolomic analyses⁸⁰. Targeted analysis is usually a hypothesis-driven strategy, focusing on the identification and quantification of selected metabolites with known chemical properties. Untargeted analysis on the contrary explores as many metabolites as analytically possible in a given sample, mostly generating new hypotheses for further experiments. Irrespective of the approach, a metabolomics experiment generally consists of three steps: sample preparation, metabolome measurement and data analysis (Figure 10).

3.3.1 Sample preparation

Although sample preparation usually depends on the experimental design, it always consists of two key steps: quenching and extraction⁷² (Figure 10). As the metabolome is a highly dynamic set of compounds that swiftly reflects changes induced by any (unnoticed) variation in the environment of the cell, rapid quenching of all biochemical processes is the first critical step⁷⁶. For cultured cells, this is typically done by snap freezing in liquid nitrogen and storage in -80°C until extraction⁸¹. In the second step, intracellular metabolites must be extracted from the cell to allow their analysis. Since this is the most time-consuming step, analyte losses will inevitably occur, indicating the importance of an optimized extraction protocol for maximum metabolite recovery⁷⁶. To control for losses, analyte standards are spiked into the samples to determine metabolite recovery and to track the extent of metabolite degradation⁷¹. Intracellular metabolites are usually extracted with organic solvents, with polar solvents such as methanol, methanol-water mixtures or ethanol extracting polar metabolites, and non-polar solvents such as chloroform, ethyl acetate, or hexane extracting lipophilic components⁷⁶. In addition, organic solvents also permanently denature enzymes, therefore decreasing metabolite degradation⁸².

3.3.2 Metabolome measurement

Once the metabolites are extracted, the challenge is to measure as many of them as accurately as possible⁸². Mass spectrometry (MS), a technique characterized by high sensitivity, high selectivity and high-throughput, is therefore the analytical tool of choice^{72,76}. MS operates by converting the metabolites to a charged (ionized) state, after which the ions and their fragments are analyzed based on their mass and charge^{75,83}. Highly abundant metabolites can generally be analyzed in an extremely high-throughput fashion by directly injecting the extract into the ionization source of the mass spectrometer^{72,83}. Yet, this approach is inherently associated with two important disadvantages: ion suppression and inability of isobar (compounds with identical mass but different structure) discrimination. Ion suppression is the phenomena that occurs when multiple components are simultaneously present in the ion source, resulting in competition for ionization and thus reduction in detectable signal^{81,83}. Consequently, MS is often coupled to a separation technique, which will reduce the complexity of mass spectra by separating the metabolites in a time dimension (Figure 10).

Currently, one of the most commonly exploited separation technique in metabolomics is reversed phase (RP) ultra-high pressure liquid chromatography (UHPLC)⁷³. In this system, metabolites are separated based on their polarity, which causes differences in partitioning between the solvent and the stationary phase⁸². In RP-UHPLC, the stationary phase consists of non-polar micron-sized beads, requiring the mobile phase (solvent) to have a lower polarity⁷⁵. As a result, elution occurs via a gradient from water to organic solvent causing polar compounds to elute first^{75,82}. It is a standard tool for the separation of medium polar and non-polar analytes in untargeted analysis due to its wide coverage of chemical classes^{72,75}. UHPLC discerns itself from HPLC by the use of columns packed with sub-2 µm particles that operate at high pressure, giving narrow chromatographic peaks that result in both better resolution and lower detection limits^{72,73}.

After separation by UHPLC, the metabolites are led to the mass spectrometer, which is typically composed of three major parts: ion source, mass analyzer and detector⁷¹. Electrospray ionization (ESI) is an ion source that can interface UHPLC to MS⁸³. It applies high

voltage to the liquid sample as it flows out the tip of a needle, converting it into a fine spray of charged droplets^{82,83}. These droplets are then rapidly evaporated by the application of heat and dry nitrogen, transferring the residual electrical charge to the analytes. ESI is considered a 'soft' ionization technique, only little fragmentation occurs during this process, and is therefore preferred for untargeted metabolomics^{75,83}. Ionization is often performed in polarity switching mode, creating both positive and negative ions to maximize metabolome coverage as some metabolites only form either positive or negative ions⁷¹. After ionization, the charged analytes are led to the mass analyzer via a quadrupole. The quadrupole functions as a low resolution mass filter, and will filter out all ions except those of particular mass-to-charge (m/z)-ratio of interest⁸². Most modern devices employ the most recently developed orbitrap technique as mass analyzer, which monitors ion oscillation up and down a spindle-shaped electrode^{75,82}. After ions enter the orbitrap, they rotate around the spindle with their electrostatic attraction balanced by the centripetal force⁸². In addition, due to the shape of the spindle, the ions also oscillate along its long axis with the frequency of these Z-axis oscillations dependent on the ion m/z -ratio. The frequency of these oscillations will be registered by the detector and can be used to determine the m/z -ratio of the analyte.

4. Research aim

Despite the harsh and long treatment regimens in T-ALL, still up to 20% of children and 40% of adults do not respond to this therapy or relapse after an initial response, leaving them with a poor 5-year survival due to the lack of second line therapies. Since the underlying mechanisms of R/R T-ALL are mostly unknown, there is a prominent need to elucidate the basis of acquired chemotherapy-resistance in view of identifying new therapeutic strategies to prevent or eradicate R/R T-ALL. In light of this, a preliminary experiment has shown that the expression of the light chain antiporter of system x_c^- , *SLC7A11*, is upregulated after L-asparaginase treatment. Since this antiporter has shown to be involved in proliferation, growth, invasion, metastasis and, most importantly, resistance in a wide variety of cancers, it is likely that this antiporter might also affect therapy response in T-ALL. Therefore, this Master's dissertation will explore the role of *SLC7A11* in the chemotherapy response of T-ALL and its potential as a chemotherapy-induced therapeutic target.

5. Materials and Methods

5.1 Cell culture

Loucy (10%), KOPT-K1 (10%), DND-41 (10%), HSB2 (10%), KARPAS-45 from Jan Cools lab (20%) and HPB-ALL (20%) cells were cultured in RPMI-1640 medium supplemented with fetal calf serum (FCS, % indicated per cell line), 1% penicillin/streptomycin and 1% L-glutamine. PER-117 cells were grown in RPMI-1640 medium supplemented with 10% FCS, 1% non-essential amino acids, 1% sodium pyruvate and 0.2% β -mercaptoethanol. All cells were maintained in a humidified environment at 37°C and 5% CO₂ in an incubator and split twice a week to their recommended seeding densities. Medium and supplements, except FCS (Bovogen Biologicals), were obtained from Life Technologies. T-ALL cells, except KARPAS-45, were acquired from ATCC.

5.2 Quantitative RT-PCR (qRT-PCR) experiments

The qRT-PCR for baseline *SLC7A11* expression in a T-ALL panel was performed on an in-lab stock of cDNA produced from T-ALL cell lines that were kept in culture without any manipulations. In exploration of *SLC7A11* expression after treatment with L-asparaginase, dexamethasone or vincristine, Loucy, DND-41, KARPAS-45 and HSB2 cells were seeded at a density of 500,000 cells/ml and treated with IC₅₀ concentrations of each of the components or PBS (control) (Life technologies) for 48h, after which they were pelleted for RNA extraction. Pegylated L-asparaginase (Oncaspar, 750 IU/ml), dexamethasone (Aacidexam, 5 mg/ml) and vincristine (Vincrisin, 1 mg/ml) were acquired from the University Hospital of Ghent. To confirm the role of L-asparaginase in *SLC7A11* upregulation, leftovers of cells treated for the

metabolomics experiments (§5.4.1) were employed. In search of the potential of *SLC7A11* as a chemotherapy induced therapeutic target, Loucy, PER-117, DND-41, HSB2, KARPAS-45 and HPB-ALL cells were seeded at a density of 500,000 cells/ml and treated with L-asparaginase at IC_{50} concentrations. After 24h of treatment, cell cultures were split in two and treated with either erastin (IC_{50})(Sigma-Aldrich, 329600-5MG) or DMSO (control) (Life technologies) for another 24h followed by cell pelleting for RNA extraction.

In all experiments, RNA was extracted using the RNeasy[®] Plus Mini Kit (Qiagen) followed by RNA concentration determination with NanoDrop[®]-1000 technology (Isogen Lifescience). 500 ng RNA was then converted into cDNA via the iScript[™] Advanced cDNA Synthesis Kit, which was subsequently diluted to 2.5 ng/ μ l. In preparation of the qRT-PCR, wells of a 384-well qRT-PCR plate were filled with 3 μ l of a premade mix per gene of interest, incorporating 2.5 μ l SsoAdvanced Universal SYBR Green Supermix (Bio-Rad), 0.25 μ l forward primer and 0.25 μ l reverse primer (Supplementary table 1), together with 2 μ l of cDNA. Data analysis was performed with qbase⁺ software (Biogazelle), using *UBC*, *TBP*, *HMBS* and *YWHAZ*, or *B2M*, *HPRT*, *RPL13A* and *UBC* (qRT-PCR after L-asparaginase, dexamethasone and vincristine therapy) as reference genes for normalization.

5.3 Cell stains

To explore the effect of L-asparaginase and/or erastin on downstream components of *SLC7A11*, cells were seeded at a density of 500,000 cells/ml and treated with IC_{50} concentrations of L-asparaginase or PBS (control). After 24h, both cultures were split in two and treated with either erastin (IC_{50}) or DMSO (control) for the remaining 24h. Next, 100,000 cells for the CM-H2DCFDA general oxidative stress indicator (ThermoFisher Scientific, C6827) and BioTracker Cystine-FITC Live Cell Dye (Sigma-Aldrich, SCT047) or 500,000 cells for the Intracellular glutathione (GSH) Detection Assay Kit (Abcam, ab112132) were transferred to FACS tubes and washed twice with either PBS (CM-H2DCFDA and GSH) or RPMI-1640 (Cystine-FITC). Cell pellets were subsequently resuspended in 100 μ l (CM-H2DCFDA and Cystine-FITC) of 5 μ M dye working solution or 500 μ l (GSH) of a 1/200 working solution and incubated for 20 (CM-H2DCFDA), 30 (GSH) or 45 (Cystine-FITC) minutes at 37°C. Post incubation, non-bound remainders of the dye were washed away with the earlier mentioned washing fluids. Before measurement, a propidium iodide (PI) live-dead staining was added, after which cells were analyzed using a BD LSR II flow cytometer (BD Biosciences) and FlowJo 10 software.

5.4 Metabolomics

5.4.1 Sample preparation

To explore whether L-asparaginase treatment induces *SLC7A11* related metabolic changes, Loucy, PER-117, KOPT-K1 and KARPAS-45 cells were seeded at a density of 500,000 cells/ml (5 million cells per condition) and treated with IC_{50} concentrations of L-asparaginase or PBS (control) for 48h. Subsequently, 2 million cells were pelleted per condition, washed twice with PBS, snap frozen in liquid nitrogen and stored in -80°C until 5 - 7 replicates were acquired. Metabolites were extracted by adding 1 ml of ice cold methanol/ultrapure (UP) water (1:1) to the cell pellets followed by thorough vortexing and sonification (2 min) at room temperature, the latter after the addition of 27 μ l internal standard mixture (25 ng/ μ l of L-alanine-d3 and dopamine-d4). Cell debris was removed by centrifugation for 5 minutes at 16,200 x *g* and 4°C. Next, 100 μ l of supernatant was collected, passed over to a new Eppendorf tube and dried using a Gyrovap centrifugal evaporator (35 °C, vacuum conditions) (Howe, Banbury, UK). Dried pellets were dissolved in 375 μ l of a solvent mixture at UHPLC starting conditions (0.1% formic acid in UP water and 0.1% formic acid in acetonitrile in 98/2 ratio respectively) after which 100 μ l was transferred to a glass HPLC vial with insert. In addition, 100 μ l of each sample was added to a single vial, forming the quality control (QC) sample that will be used for normalization. All solvents and internal standards were acquired from Sigma-Aldrich, while UP water was obtained by usage of a purified-water system (Millipore, Brussels, Belgium).

5.4.2 Metabolome measurement

Chromatographic separation (Vanquish Duo UHPLC, Thermo Fisher Scientific) was performed on an Acquity HSS T3 C18 column (1.8 μm , 150 mm x 2.1 mm, Waters) that was kept at 45°C. A binary solvent system consisting of UP water (A) and acetonitrile (B), both acidified with 0.1% formic acid, was used according to the following gradient profile of solvent A: 0–1.5 min at 98%, 1.5–7.0 min from 98% to 75%, 7.0–8.0 min from 75% to 40%, 8.0–12.0 min from 40% to 5%, 12.0–14.0 min at 5%, 14.0–14.1 min from 5 to 98%, followed by 4.0 min of re-equilibration at 98%. The injection volume was 10 μl and flow rate was set at 400 $\mu\text{l}/\text{min}$.

Metabolite detection was performed on an Orbitrap Exploris instrument, which was preceded by heated electrospray ionization (HESI-II source) in polarity switching mode. Ionization source and instrumental parameters were as follows: sheath, auxiliary and sweep gas flow rates 50, 25 and 3 arbitrary units respectively, heater and capillary temperature 350°C and 250°C, S-lens RF level 50 V and spray voltage 2.7 kV. The scan range was set to 50–800 m/z with a maximum injection time of 70 ms, a resolution of 120,000 full width at half maximum (FWHM) and an automatic gain control target of 1×10^6 ions.

Prior to MS detection, the Orbitrap Exploris instrument was calibrated by infusing ready-to-use calibration mixtures (Thermo Fisher Scientific, San José, CA, USA). In addition, standard mixtures of 349 target analytes, including all amino acids, with concentrations of 5 ng/ μl (Supplementary Figure 1) were injected before and after the analysis of samples both to check the operational conditions of the device and to allow targeted metabolomics data analysis (§5.4.3). The QC sample was run six times at the beginning of the analytical run to stabilize the system as well as after each set of 10 samples to correct for instrumental fluctuations within the analytical batch. Samples were analyzed in a random order to avoid temporal biases.

5.4.3 Data analysis

Targeted analysis

Since standard mixtures were run before and after the analysis of samples, retention times (RT), which represent the time at which the metabolite eluted from the column, were known for each amino acid. Chromatograms were therefore evaluated for the presence of peaks at those amino acid specific RTs using Xcalibur 3.0 software (Thermo Fisher Scientific, San José, CA, USA), and the area under the curve (AUC), representing the abundance of a metabolite, was adjusted manually in case a peak was not included correctly (Supplementary Figure 2). AUCs were subsequently quantified, exported to an excel file and normalized per 10 samples using the average AUC value of the QC sample run after those samples. These normalized data were then further processed in GraphPad Prism 9.0 to explore whether amino acid abundance differed between L-asparaginase and control samples.

Untargeted analysis

Using Compound Discoverer software (Thermo Fisher Scientific), a list of all detected positively and negatively ionized metabolites together with their AUCs was generated and exported to excel. AUC values were subsequently normalized using the internal QC samples identically as described for the targeted analysis (Supplementary Figure 3). After this, pre-processed data were subjected to multivariate statistics using SIMCA™ software (Umetrics), which searches for trends in the detected metabolites by creating either unsupervised or supervised statistical models. First, principal component analysis was performed for data exploration by creating a PCA-X model. This model shows the unsupervised clustering of all samples based on their metabolic fingerprint, revealing natural patterning of samples and potential outliers. Second, OPLS-DA (orthogonal partial least squares - discriminant analysis) was performed on data that was pareto scaled and log₂ transformed for data normalization. These predictive models allowed for pairwise comparison of control and L-asparaginase treated samples of the individual cell lines. OPLS-DA models were considered successful in

case the following three criteria were fulfilled: C-ANOVA: $P < 0.05$ (1), R^2Y and $Q^2 > 0.5$ (2) and a good permutation test ($n=100$) (3). From these criteria, R^2Y reflects the total sum of variation in the Y-variable, being L-asparaginase or control treatment, Q^2 forms the goodness of prediction and the permutation test indicates the reliability of the model. Only if a OPLS-DA model was successful, it could be considered to be predictive for the Y-variable when started from the metabolic fingerprint.

In a next step, metabolites discriminating control and L-asparaginase treated samples in validated OPLS-DA models were identified based on three selection parameters: the VIP-score (1), representing the relative importance of a metabolite to discriminate the two groups, the Jack-knifed confidence interval (2), indicating the reliability of the VIP-score, and the S-plot score (3), summarizing the VIP score on the x-axis and the Jack-knifed confidence interval on the y-axis. These selection parameters were required to be > 1 , > 0 and $0.5 < y < -0.5$ for the VIP-score, Jack-knifed confidence interval and S-plot score respectively. In a final step, Xcalibur 3.0 software was used in an attempt to identify these discriminating metabolites. Based on the relative abundancies of isotope 12 carbon (m/z) and isotope 13 carbon ($m/z + 1.008$), the number of carbon atoms in the metabolite was predicted using the following formula: $\% \text{ }^{13}\text{C} / \% \text{ }^{12}\text{C} * 100/1.1$. This number was then used to identify a putative chemical formula from a list of possible chemical formulas suggested by the software (Supplementary Figure 4). Entering this formula in the Human Metabolome Database (<https://hmdb.ca/>) then finally allowed to identify the metabolite.

Separately from this untargeted analysis to identify differentially expressed metabolites between L-asparaginase and control samples, also pathway analyses were performed on the normalized data lists of all detected positively and negatively ionized metabolites. For this, a list of either positive or negative ionized metabolites were entered in the Functional Analysis module of MetaboAnalyst (<https://www.metaboanalyst.ca/>), in which data were normalized by sum, log transformed and pareto scaled. Finally, pathway level integration was performed by applying the mummichog algorithm with default settings, resulting in an overview of differently represented pathways between control and L-asparaginase treated samples.

5.5 Cell viability assay

In examination of the dose-dependent responses of various T-ALL cell lines to L-asparaginase and/or erastin treatment, 100 μl cell suspension containing 50,000 cells/ml was added to each well of a 96-well plate according to design. Next, dilution series ($1/2$) of L-asparaginase, starting at 100 nIU/ml (Loucy, PER-117, KOPT-K1, HSB2, HPB-ALL) or 400 nIU/ml (DND-41 and KARPAS-45), were administered. Control samples and samples that were single treated with erastin received an identical volume of PBS. After 24h of culturing, a $1/2$ dilution series of erastin was added, starting from 10 nM in all cell lines. Control and L-asparaginase mono-treated samples received an identical volume of DMSO. Following a total treatment time of 48h, CellTiter-Glo® Reagent (50 μl) (Promega) was administered and luminescence was analyzed according to manufacturer's protocol at a GloMax® Explorer Multimode Microplate Reader (Promega).

5.6 Statistical analysis

GraphPad Prism 9.0 software (GraphPad Software) was used for statistical analyses. A one tailed paired parametric student's t-test was performed to analyze differences in *SLC7A11* expression between L-asparaginase and control groups. Differences in abundance of metabolites observed in targeted metabolomics data were analyzed with paired t-tests using the two-stage step-up method of Benjamini, Krieger and Yekutieli. Finally RT-qPCR data comparing *SLC7A11* expression between control, L-asparaginase, erastin or L-asparaginase + erastin was evaluated using one way ANOVA with a Tukey post hoc test. P -values < 0.05 were considered statistically significant and significance was indicated as displayed in table 1.

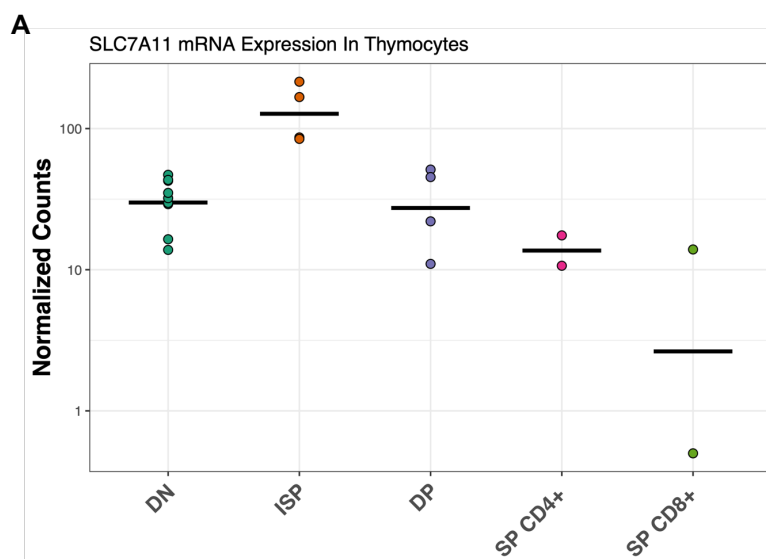
Symbol	P-value
ns	> 0.05
*	≤ 0.05
**	≤ 0.01
***	≤ 0.001
****	≤ 0.0001

Table 1 – Overview of symbols used to indicate significance based on the calculated P-values.

6. Results

6.1 *SLC7A11* is upregulated in primary T-ALL samples

The fact that preliminary data have shown an upregulation of *SLC7A11* expression in xenograft T-ALL models after L-asparaginase treatment implies, but does not guarantee, that a similar phenomenon occurs in T-ALL patients. To explore the relevance of *SLC7A11* in T-ALL patients, several datasets containing genome wide sequencing data were consulted to determine the *SLC7A11* expression in healthy thymocytes and T-ALL lymphoblasts^{84,85}. During normal thymocyte development, *SLC7A11* appeared to be variably expressed over the different differentiation stages, with the highest expression during the intermediate single positive stage (ISP), a stage that has been reported to be a transition phase between DN and DP T-cells¹⁷ (Figure 11A). This is consistent with the knowledge that T-cell development goes along with various cellular stresses⁸⁶ and might implicate that *SLC7A11* also plays an important role in counteracting lethal stresses during normal thymocyte differentiation. When comparing *SLC7A11* expression in normal thymocytes and T-ALLs, *SLC7A11* was clearly upregulated in T-ALL primary samples (Figure 11B). This showed that next to *SLC7A11* upregulation in response to L-asparaginase, as observed in preliminary experiments, *SLC7A11* baseline expression is already upregulated in T-ALL patients. Another interesting observation that could be made is that *SLC7A11* expression appears to be equally upregulated in the Mullighan cohort (n = 265) regardless of T-ALL subtype. The fact that this was not the case in the Soulier cohort can be attributed to the small sample size (n = 25), causing sample variance to play a prominent role in distorting the true population average. Based on these genome wide sequencing data, it is fair to state that *SLC7A11* is not only involved in xenograft T-ALL models, but also in human T-ALL patients, validating the relevance of exploring its role in the chemotherapy response of T-ALL.



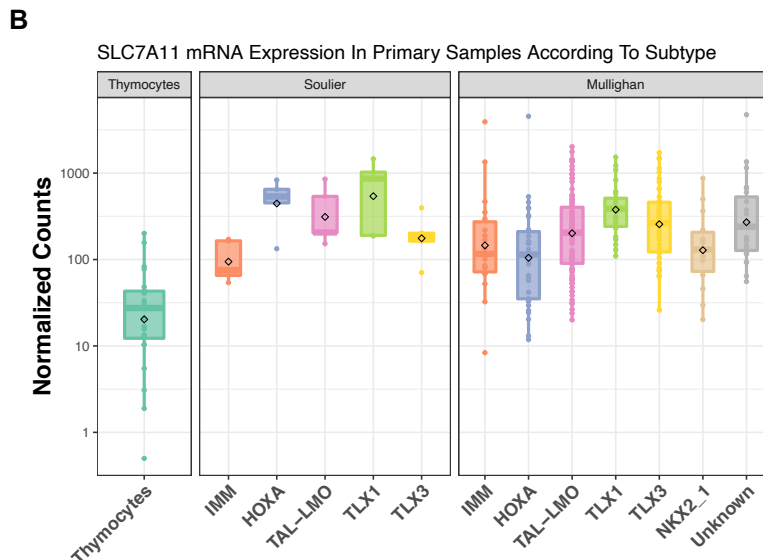


Figure 11 – SLC7A11 baseline expression is upregulated in primary T-ALL samples. (A) SLC7A11 mRNA expression in thymocytes at different developmental stages (data generated at the lab of Professor Tom Taghon, Ghent University). (B) Comparison of SLC7A11 mRNA expression between healthy thymocytes and different T-ALL genomic subgroups of the Soulier⁸⁵ and Mullighan⁸⁴ cohorts. DN, double negative; ISP, intermediate single positive; DP, double positive; SP, single positive; IMM, immature.

6.2 T-ALL cell lines are not dependent on SLC7A11 and variably express this antiporter subunit

Since T-ALL cells upregulate their *SLC7A11* expression in response of L-asparaginase treatment, treated cells presumably depend on this antiporter subunit for their survival. However, this does not imply that this is also the case for untreated T-ALL cells. Therefore, the Cancer Dependency Map (DepMap, Broad Institute) was consulted to evaluate the dependency of untreated T-ALL cell lines on SLC7A11. DepMap is an initiative that performs genome wide CRISPR-Cas9 loss of function screens to identify genes that are essential for survival in human cancer cell lines. It provides scientists with a CERES score, a value incorporating a correction for the antiproliferative effect of Cas9-mediated DNA cleavage, an effect which mainly occurs in regions with high copy numbers, therefore allowing unbiased gene dependency interpretation at all levels of copy numbers⁸⁷. The lower the score, the more a cell line depends on this gene for its survival, with a score of ≤ -0.5 indicating gene dependency and a score of 0 indicating gene independency. When plotting the CERES scores for SLC7A11 in T-ALL cell lines against the scores of other leukemia cell lines and solid tumors, it became clear that, albeit the low sample size, SLC7A11 is not an essential gene for survival in T-ALL cell lines (Figure 12A). In fact, all leukemia cell lines turned out to be independent of SLC7A11 for their survival. This indicates that, in line with the preliminary data, SLC7A11 most likely only starts to play a role in T-ALL cell survival in response to anti-cancer treatment.

Following the knowledge that SLC7A11 is not essential for T-ALL cell survival, *SLC7A11* baseline expression was also determined in untreated T-ALL cell lines to verify whether a similar expression pattern could be observed as in primary T-ALL samples (Figure 11B). In contrast to this earlier finding, the expression of *SLC7A11* was highly variable between the different cell lines, with the highest expression in the ETP-ALL cell lines Loucy and PER-117 and the lowest expression in the early cortical T-ALL cell lines HPB-ALL and KARPAS-45 (Figure 12B). In view of this, it was decided to take along Loucy, PER-117, HSB2, KOPT-K1, DND-41, HPB-ALL and KARPAS-45 cells in further experiments to cover the whole range of *SLC7A11* baseline expression levels. This allowed to explore whether a varying *SLC7A11* baseline expression would affect either the role of SLC7A11 in the chemotherapy response of T-ALL, or its potential as a chemotherapy-induced therapeutic target.

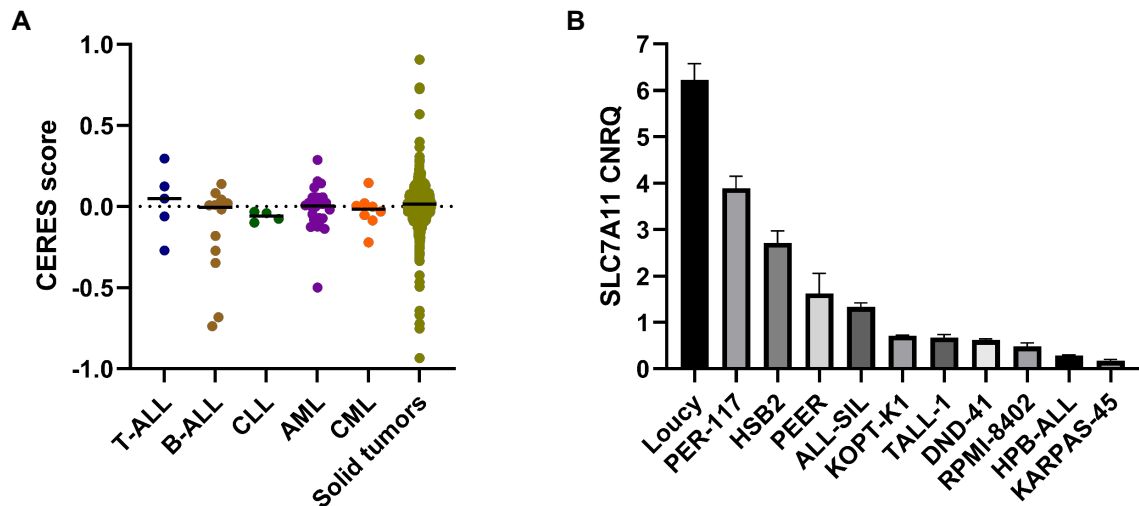
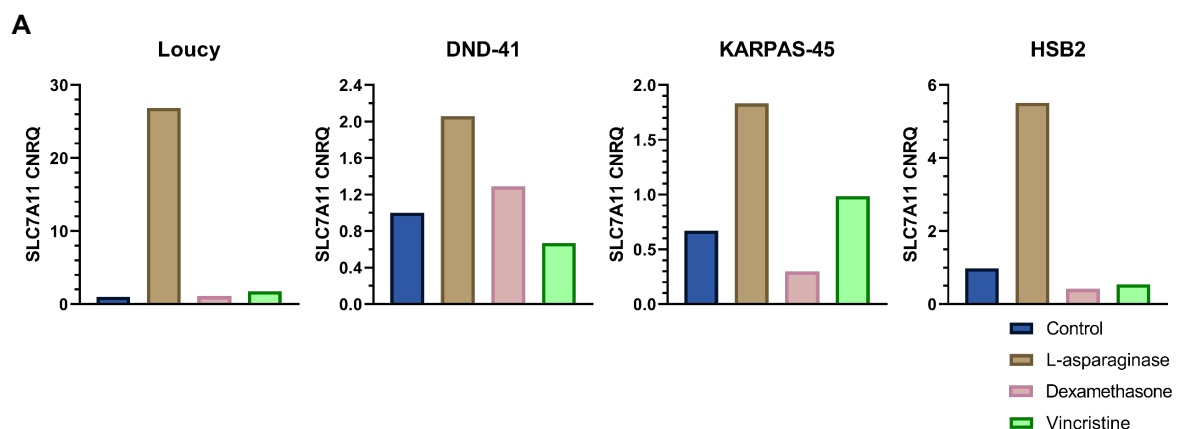


Figure 12 – *SLC7A11* is a non-essential gene for T-ALL cell survival and is variably expressed in different T-ALL cell lines. (A) CERES scores indicating *SLC7A11* gene dependency for the survival of T-ALL ($n = 5$), B-ALL ($n = 12$), CLL ($n = 4$), AML ($n = 26$), CML ($n = 8$) and solid tumor ($n = 944$) cell lines. (B) *SLC7A11* baseline mRNA expression in T-ALL cell lines covering different T-ALL subtypes. Error bars represent the SD of two technical replicates. B-ALL, B-cell acute lymphoblastic leukemia; CLL, chronic lymphocytic leukemia; AML, acute myeloid leukemia; CML, chronic myeloid leukemia.

6.3 *SLC7A11* is upregulated in T-ALL cell lines after L-asparaginase treatment

To validate the preliminary experiment that demonstrated *SLC7A11* upregulation after L-asparaginase treatment, *SLC7A11* expression was determined in various T-ALL cell lines after monotherapy with either L-asparaginase, dexamethasone and vincristine. These components are all part of the induction therapy, and are therefore the first stressors with which T-ALL cells are confronted, suggesting that therapy-induced resistance mechanisms will most likely occur in response to these components. A qRT-PCR confirmed that from the components in the treatment cocktail used for the preliminary experiment, L-asparaginase is responsible for *SLC7A11* upregulation (Figure 13A). Remarkably, *SLC7A11* expression was downregulated in KARPAS-45 and HSB2 cells lines after dexamethasone treatment, as well as in DND-41 and HSB2 cells after vincristine treatment. Even though these components have different mechanisms of action than L-asparaginase, this is rather unexpected since both aim at perturbing normal cell homeostasis, which is assumed to induce cellular stress. It might however be that these components induce other forms of stress than L-asparaginase, and therefore induce anti-stress responses different than the *SLC7A11*-GSH axis. However, further investigation of this would be beyond the scope of this thesis.



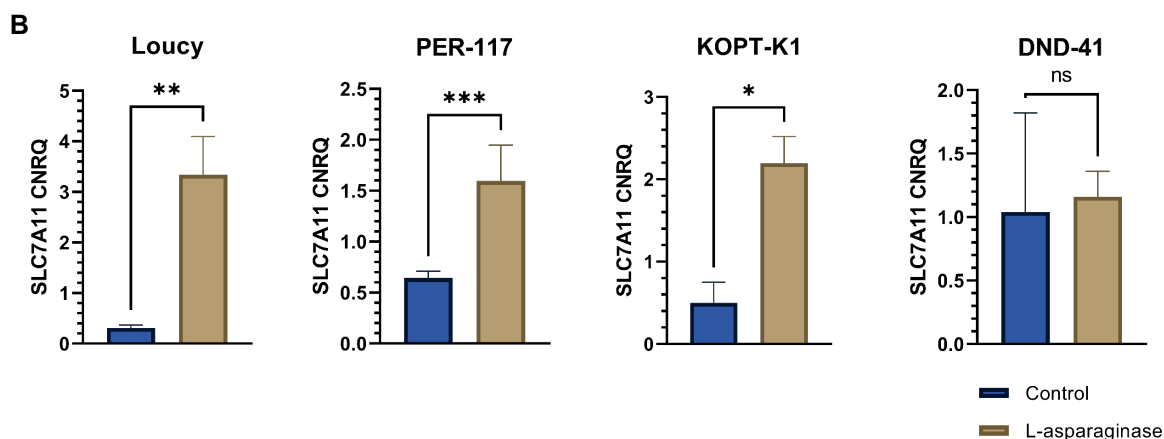


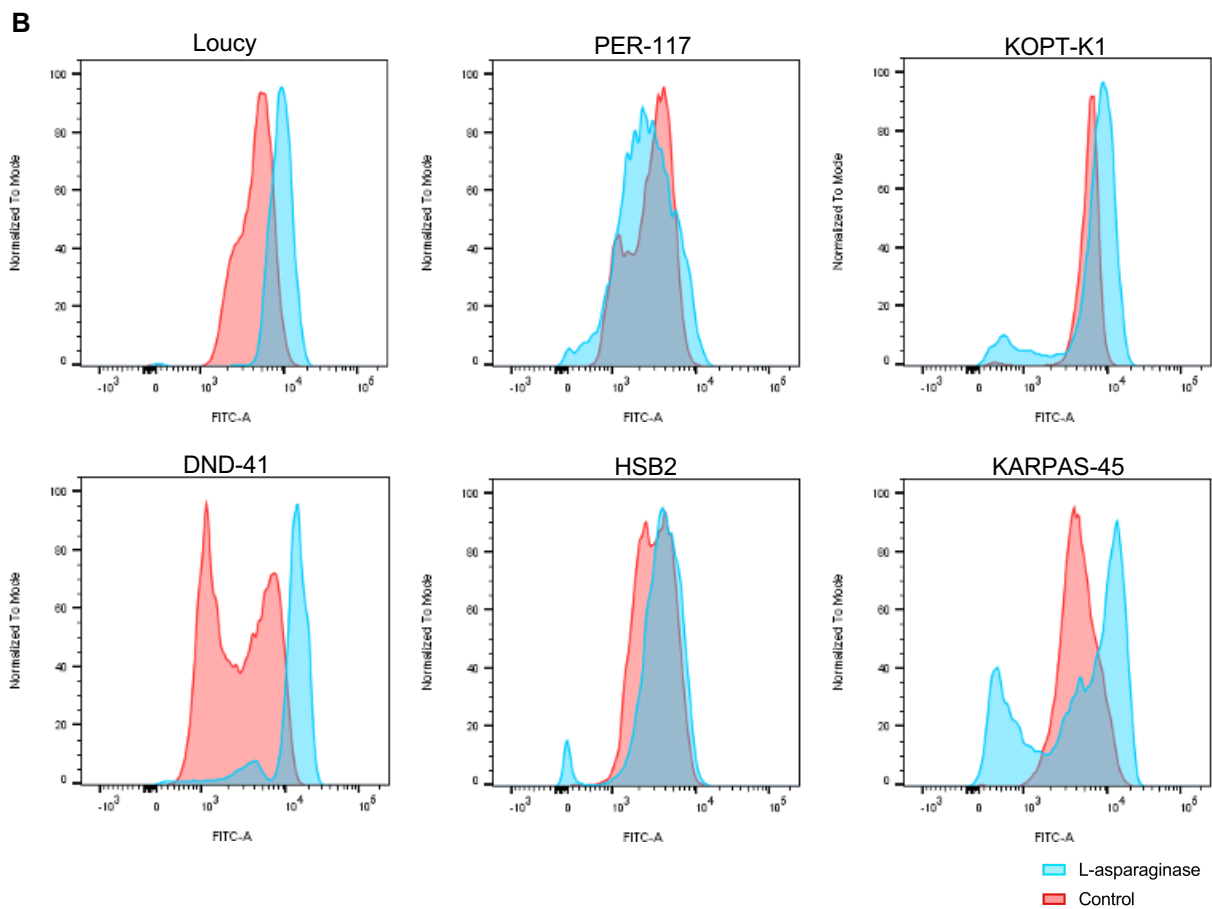
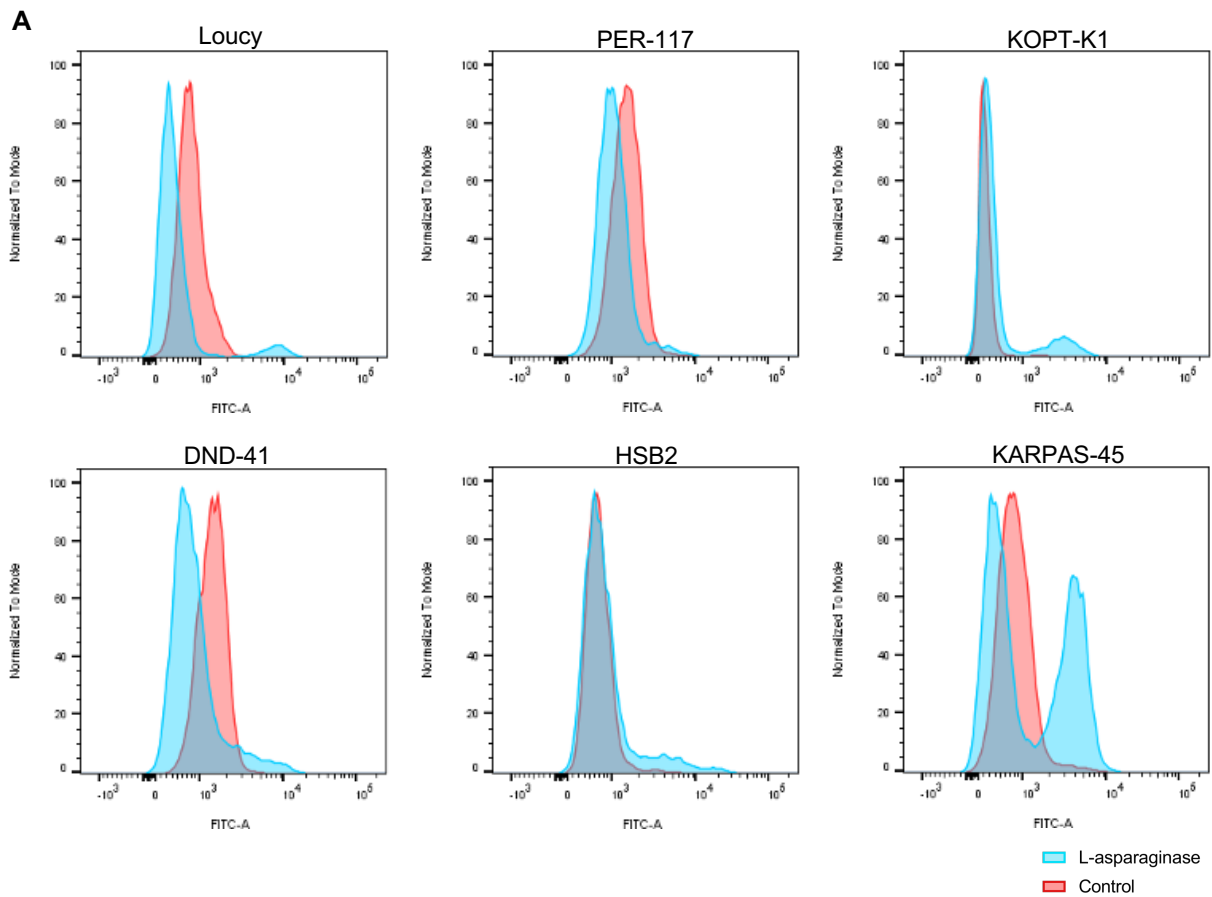
Figure 13 – SLC7A11 is upregulated in T-ALL cell lines after L-asparaginase treatment. (A) qRT-PCR analysis for SLC7A11 expression in Loucy, DND-41, KARPAS-45 and HSB2 T-ALL cell lines treated (48h) with either L-asparaginase, dexamethasone or vincristine. (B) qRT-PCR analysis for SLC7A11 expression in Loucy ($P = 0.0017$), PER-117 ($P = 0.0010$), KOPT-K1 ($P = 0.0154$) and DND-41 ($P = 0.3877$) T-ALL cell lines treated (48h) with L-asparaginase. Error bars represent the SD of three (KOPT-K1 and DND-41), four (Loucy) or six (PER-117) independent biological replicates.

After it was validated that L-asparaginase is indeed responsible for the observed upregulation of SLC7A11 in the T-ALL xenograft models of the preliminary experiment, a confirmatory qRT-PCR experiment was performed on T-ALL cell lines of different subtypes to explore whether this upregulation is significant. Figure 13B shows that in three out of four cell lines, SLC7A11 was significantly upregulated after L-asparaginase treatment. Notably, this upregulation was most significant in the two ETP-ALL cell lines Loucy and PER-117, which were previously shown to have the highest baseline expression (Figure 12B). This indicates that a high baseline expression does not hamper cells to upregulate this gene in response to cellular stresses. In addition, this also raises the question whether this suggests that these cell lines are most resistant after treatment since they have the highest SLC7A11 expression levels, or that, notwithstanding the high baseline expression, a certain degree of upregulation will always be required as these cells have adapted their metabolism to this high baseline antioxidant. Based on the IC₅₀ values of L-asparaginase in these cell lines, the question whether these cells would be more resistant can be refuted, since both Loucy and PER-117 cell lines have similar IC₅₀ values as all other T-ALL cell lines (except KOPT-K1 which has a higher IC₅₀).

6.4 SLC7A11 upregulation after L-asparaginase treatment modulates the expression of downstream components

Because it was shown that SLC7A11 is indeed upregulated after L-asparaginase treatment, it was hypothesized that this upregulation should be reflected in its downstream components, since these ought to be the ones responsible for the increased antioxidant effect according to the earlier described pathway (Figure 6). In exploration of this hypothesis, T-ALL cells that were treated with L-asparaginase were stained for flow cytometric analysis of cystine, GSH and general oxidative stress. Based on the earlier described pathway, both cystine and GSH were expected to be upregulated following increased SLC7A11 expression, while general oxidative stress was expected to be downregulated.

Surprisingly, intracellular cystine levels were shown to be downregulated in the majority of the cell lines (Figure 14A, Supplementary Figure 5A). Indeed, in Loucy, PER-117, DND-41 and KARPAS-45 cell lines, the majority of the cells displayed lower cystine levels after L-asparaginase treatment. KOPT-K1 and HSB2 cell lines generally did not show differences in intracellular cystine levels. An additional striking observation was that next to the major peak of downregulated/constant cystine expression, most cell lines also had an extra peak of increased cystine expression after L-asparaginase treatment. This extra peak is in accordance



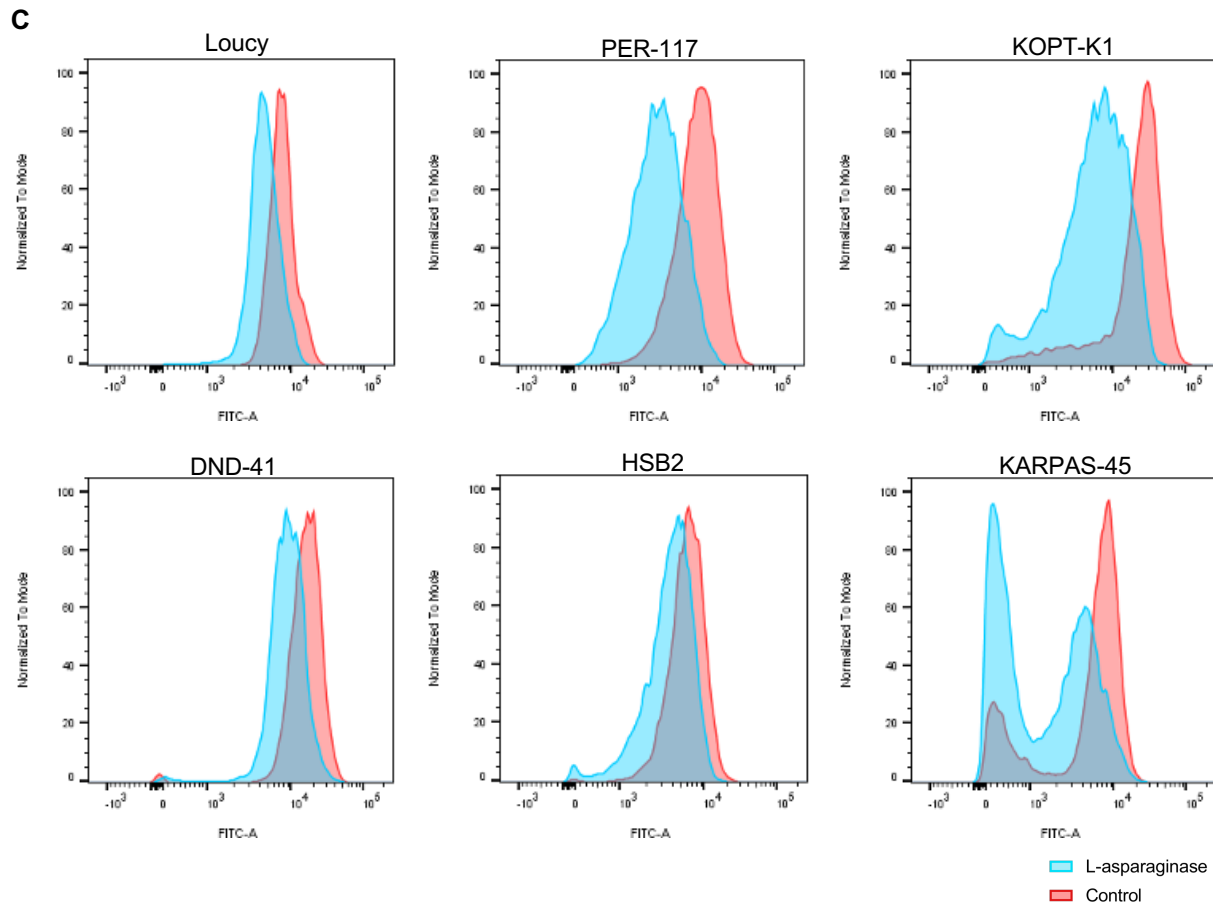


Figure 14 – L-asparaginase induced *SLC7A11* upregulation modulates downstream cystine, GSH and general oxidative stress levels. Flow cytometric analysis of (A) intracellular cystine levels, (B) cellular GSH and (C) general oxidative stress after L-asparaginase treatment.

with the hypothesis, however, since it is only observed in the minority of cells, it raises the question whether upregulation of *SLC7A11* only occurs in a subpopulation, or causes only in this minority of cells higher intracellular cystine levels, suggesting that only few T-ALL cells would have survival benefit. If the latter would be the case, also the downstream components GSH and general oxidative stress should have a double expression pattern: a major peak inversely of what was hypothesized, and a minor peak as hypothesized.

However, analysis of GSH levels in T-ALL cells treated with L-asparaginase refuted this. All cell lines, except PER-117, showed after treatment a major peak at a higher GSH level in accordance with what was hypothesized based upon the *SLC7A11* pathway (Figure 14B, Supplementary Figure 5B). In addition, KOPT-K1, HSB2 and KARPAS-45 cell lines had an extra peak of lower GSH expression as compared to control cells, raising similar questions as described for the cystine staining. What was remarkable is that control cells of both DND-41 and PER-117 also showed a double peak of GSH expression, questioning the significance of the double peaks in treated cells.

Finally, general oxidative stress was analyzed in T-ALL cells after L-asparaginase treatment. In contrast to cystine and GSH, general oxidative stress levels did follow the hypothesis in all cell lines, as all cell lines showed decreased general oxidative stress after treatment (Figure 14C, Supplementary Figure 5C). Interestingly, even DND-41 cells, which did not have a significant *SLC7A11* RNA upregulation after treatment (Figure 13B), clearly had lower levels of ROS, suggesting that the *SLC7A11*-GSH axis might not solely be responsible for this observed effect. Based on this staining, it can be speculated that *SLC7A11* upregulation is

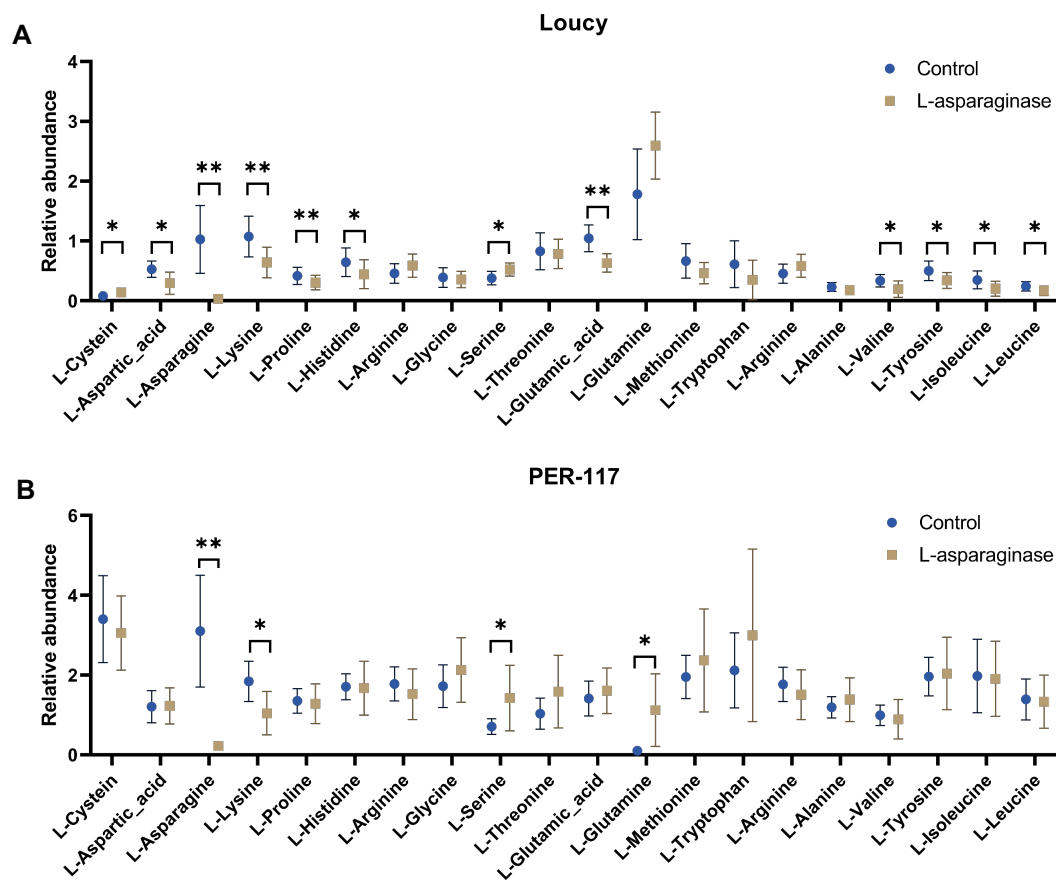
indeed involved in a therapy-induced survival response by contributing to a decrease in cellular oxidative stress.

6.5 Metabolomic analysis of T-ALL cells after L-asparaginase treatment

6.5.1 Targeted analysis of amino acid metabolism after L-asparaginase treatment

In consequence of the finding that L-asparaginase might provide T-ALL cells an advantage by decreasing oxidative stress via the SLC7A11-GSH axis, which involves upregulation of the amino acid L-cysteine, the effect of L-asparaginase on the entire amino acid metabolism was investigated using targeted metabolomic analysis. Even though flow cytometric analysis showed a general decrease in intracellular cystine levels, it was expected that L-cysteine levels would significantly increase after L-asparaginase treatment, as this would confirm that the observed decrease of oxidative stress was indeed via the SLC7A11-GSH axis. In addition, L-asparagine was expected to decrease, since L-asparaginase exerts its function by depleting this amino acid into L-aspartic acid and ammonia⁸⁸. Moreover, L-glutamine was also hypothesized to decrease after treatment, because L-asparaginase is known to deplete L-glutamine, to a lesser extent than L-asparagine, into L-glutamic acid and ammonia.

Surprisingly, analysis of normalized abundance levels revealed that L-asparaginase did not increase intracellular L-cysteine in most of the analyzed T-ALL cell lines (Figure 15). Indeed, L-cysteine was only significantly more abundant in Loucy cells. KOPT-K1 cells even showed a significant decrease in L-cysteine expression, questioning whether the observed decrease in intracellular oxidative stress might be fully attributed to the SLC7A11-GSH axis. Further analysis revealed that L-asparagine levels were, as expected, significantly downregulated in all T-ALL cell lines. L-glutamine levels on the contrary were mostly upregulated, going against the known glutaminase activity of L-asparaginase. Remarkably, most cell lines also showed a decrease in both L-aspartic acid and L-glutamic acid.



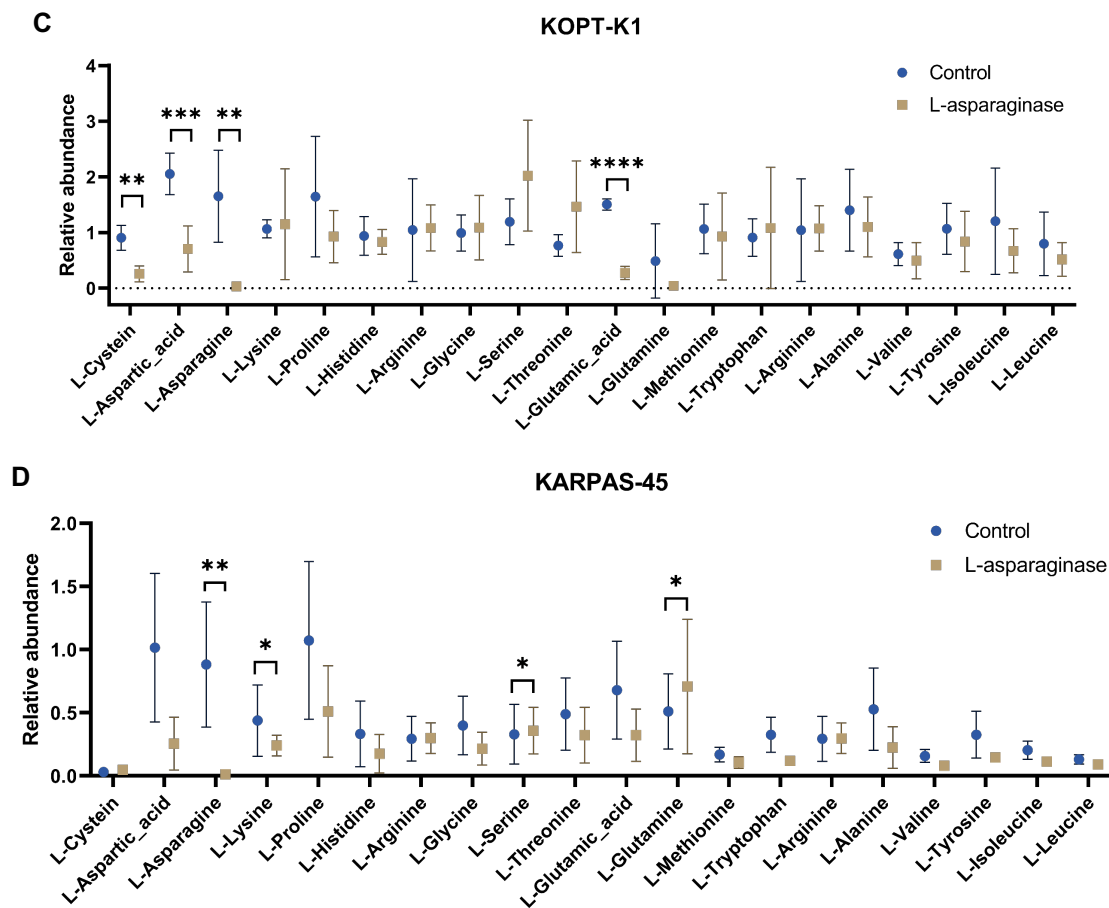


Figure 15 – Targeted analysis of amino acid metabolism after L-asparaginase treatment. Relative abundancies of all 20 amino acids in control and L-asparaginase treated (A) Loucy (L-cystein: $P = 0.010636$, L-aspartic acid: $P = 0.015912$, L-asparagine: $P = 0.003313$, L-lysine: $P = 0.006888$, L-proline: $P = 0.007376$, L-histidine: $P = 0.031876$, L-serine: $P = 0.043769$, L-glutamic-acid: $P = 0.003341$, L-valine: $P = 0.027969$, L-tyrosine: $P = 0.037890$, L-isoleucine: $P = 0.012869$, L-leucine: $P = 0.019763$) (B) PER-117 (L-asparagine: $P = 0.001820$, L-lysine: $P = 0.024315$, L-serine: $P = 0.047380$, L-glutamine: $P = 0.024174$), (C) KOPT-K1 (L-cystein: $P = 0.005365$, L-aspartic acid: $P = 0.000471$, L-asparagine: $P = 0.002168$, L-glutamic acid: $P < 0.000001$), and (D) KARPAS-45 (L-aspartic acid: $P = 0.019622$, L-proline: $P = 0.032198$, L-glutamic acid: $P = 0.027785$, L-alanine: $P = 0.044013$) T-ALL cells. Error bars represent the SD of five (KARPAS-45) or seven (Loucy, PER-117 and KOPT-K1) independent biological replicates.

6.5.2 Untargeted analysis of T-ALL cell metabolism after L-asparaginase treatment

Targeted metabolomic analysis is a hypothesis-driven strategy focusing on selected metabolites, and might therefore magnify differences that are only of minor importance in the metabolome as a whole. Therefore, all detected metabolites were also analyzed in an untargeted manner to identify in an unbiased manner the largest differences between the metabolomes of control and L-asparaginase treated T-ALL cells.

Using Compound Discoverer, a total of 1554 metabolites, of which 473 negatively ionized and 1081 positively ionized, were picked up from all samples. These metabolites were subsequently subjected to SIMCA™ software, in search for trends distinguishing control and L-asparaginase treated samples. To evaluate natural patterning of the samples and control for potential outliers, a PCA-X model including all samples and QCs was created (Figure 16). In this model, the two groups that were compared, being L-asparaginase and control, did not cluster together, indicating that is no general trend over all cell lines that allows to make a distinction between both groups. Clustering of the internal QCs (iQCs) indicated stability of the

entire metabolome measurement process. Importantly, this model also showed that one of the KARPAS-45 control samples formed an outlier.

After this, OPLS-DA was performed per cell line, to allow pairwise comparison of control and L-asparaginase treated samples. However, before these models could be used to compare both groups, they had to be validated. Based on the evaluation of all validation parameters, it could be concluded that only the models of KOPT-K1 and PER-117 were predictive for pairwise comparison of control and L-asparaginase treated samples (Table 2). As shown in Figure 17, both models showed a clear separation of the two sample groups. As a consequence, only these two models were used for identification of differentiating metabolites. Metabolites discriminating control and L-asparaginase treated samples in those models were identified based on several selection parameters, retaining 6 metabolites (3 positive and 3 negative ions) for the KOPT-K1 cell line and 64 metabolites (42 positive and 22 negative ions) for PER-117 (Supplementary Figure 6, 7). Using Xcalibur 3.0 software, putative chemical formulas were chosen for these metabolites and entered in the Human Metabolome Database to identify the corresponding metabolite. However, this database did not allow to identify any relevant metabolites from these chemical formulas.

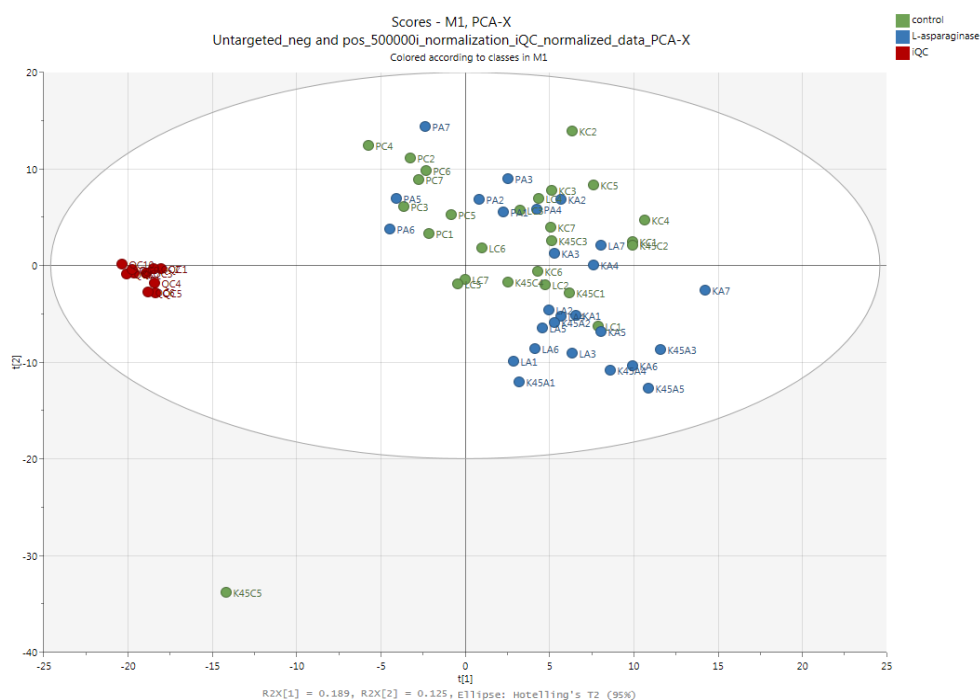


Figure 16 – Score plot of a PCA-X model that was created based on all 1554 metabolites, 473 negatively ionized and 1081 positively ionized, that were picked up from all samples. LA, Loucy L-asparaginase; LC, Loucy control; PA, PER-117 L-asparaginase; PC, PER-117 control; KA, KOPT-K1 L-asparaginase; KC, KOPT-K1 control; K45A, KARPAS-45 L-asparaginase; K45C, KARPAS-45 control.

	C-ANOVA	R ² Y	Q ²	Permutation
all samples (n=52)	0,237	0,421	0,0571	not ok
KARPAS-45	0,8	1	0,8	ok
Loucy	0,24	1	0,757	ok
KOPT-K1	0,0216	1	0,876	ok
PER-117	0,04	1	0,849	ok

Table 2 – Evaluation of validation parameters indicated that only KOPT-K1 and PER-117 OPLS-DA models were predictive for pairwise comparison of control and L-asparaginase treated samples. A model was considered predictive in case three criteria were fulfilled: C-ANOVA < 0.05 (1), R²Y and Q² > 0.5 (2) and a good permutation test (n = 100).

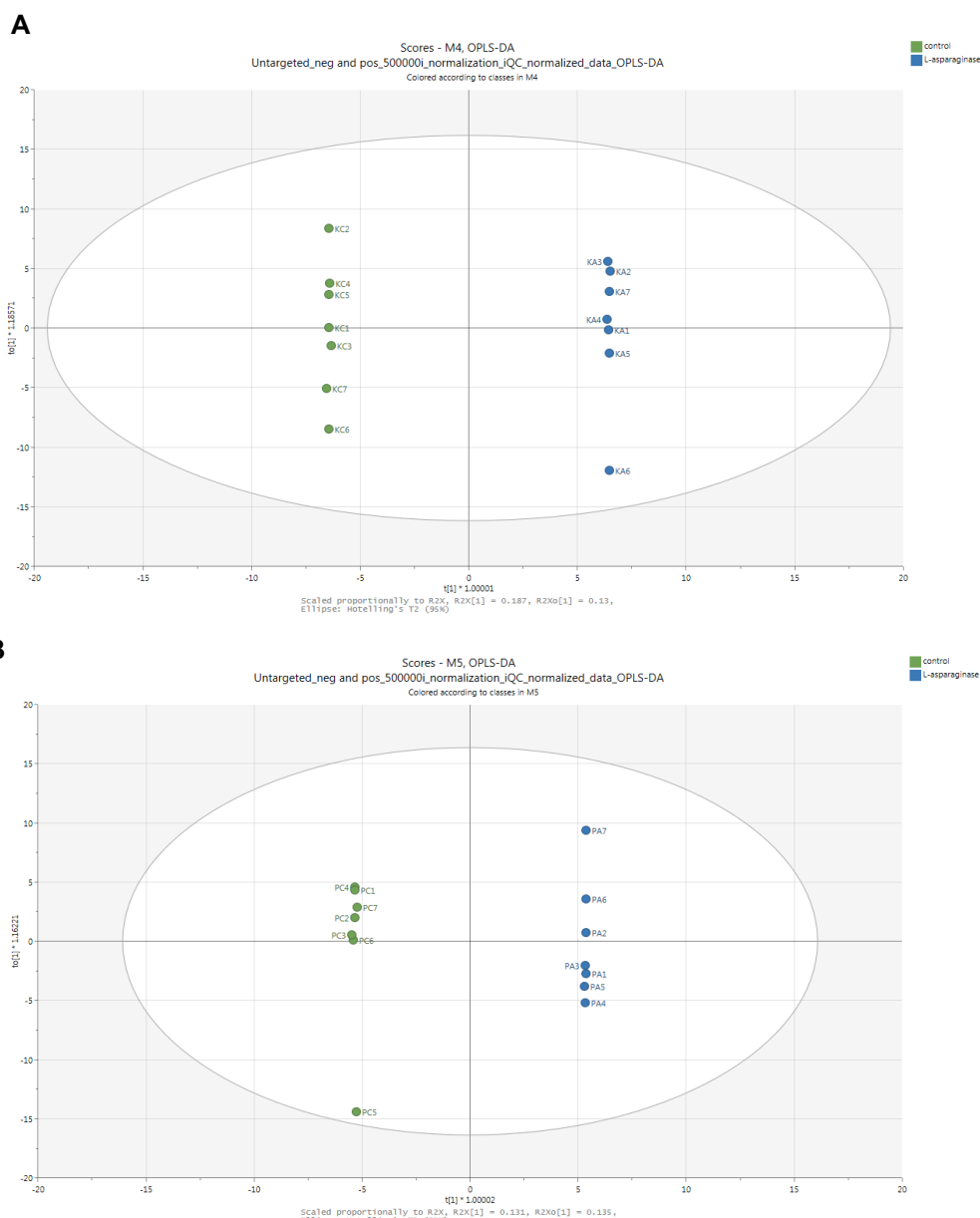


Figure 17 – Score plots of validated OPLS-DA models that were created for each cell line based on all 1554 metabolites, 473 negatively ionized and 1081 positively ionized, that were picked up from all samples. OPLS-DA model for (A) KOPT-K1 and (B) PER-117 cell lines, showing metabolite variation contributing to the difference between L-asparaginase and control samples on the x-axis and variation between the different replicates on the y-axis. PA, PER-117 L-asparaginase; PC, PER-117 control; KA, KOPT-K1 L-asparaginase; KC, KOPT-K1 control.

Separately from this untargeted analysis in which it was tried to identify differentially expressed metabolites between L-asparaginase and control samples, also pathway analyses were performed to explore differential pathways between L-asparaginase treated and control samples. For KARPAS-45 cells, no differentially expressed pathways could be identified, potentially because of the lower number of replicates and the outlier in the control samples. In the other cell lines, several pathways were shown to repeatedly differ between the two groups as displayed in both Figure 18 and Supplementary Figure 8-10. When analyzing the differentially expressed pathways, it was observed that all cell lines showed differences in either the alanine and aspartate metabolism, the aspartate and asparagine metabolism or both, referring to the mechanism of action of L-asparaginase. Methionine and cysteine metabolism was different in KOPT-K1 cells and glutathione metabolism was expressed differently in both PER-117 and KOPT-K1 samples, pinpointing the role of L-asparaginase in the SLC7A11-GSH axis. An additional interesting observation in relation to the SLC7A11-GSH axis was the fact that KOPT-

K1 cells showed differences in the pentose phosphate pathway. Remarkably, glycine, alanine and threonine metabolism was changed in all cell lines, suggesting that L-asparaginase also affects these amino acids. Lastly, also the sialic acid, pyrimidine and/or purine metabolism pathways were identified to differ between control and L-asparaginase samples in all cell lines.

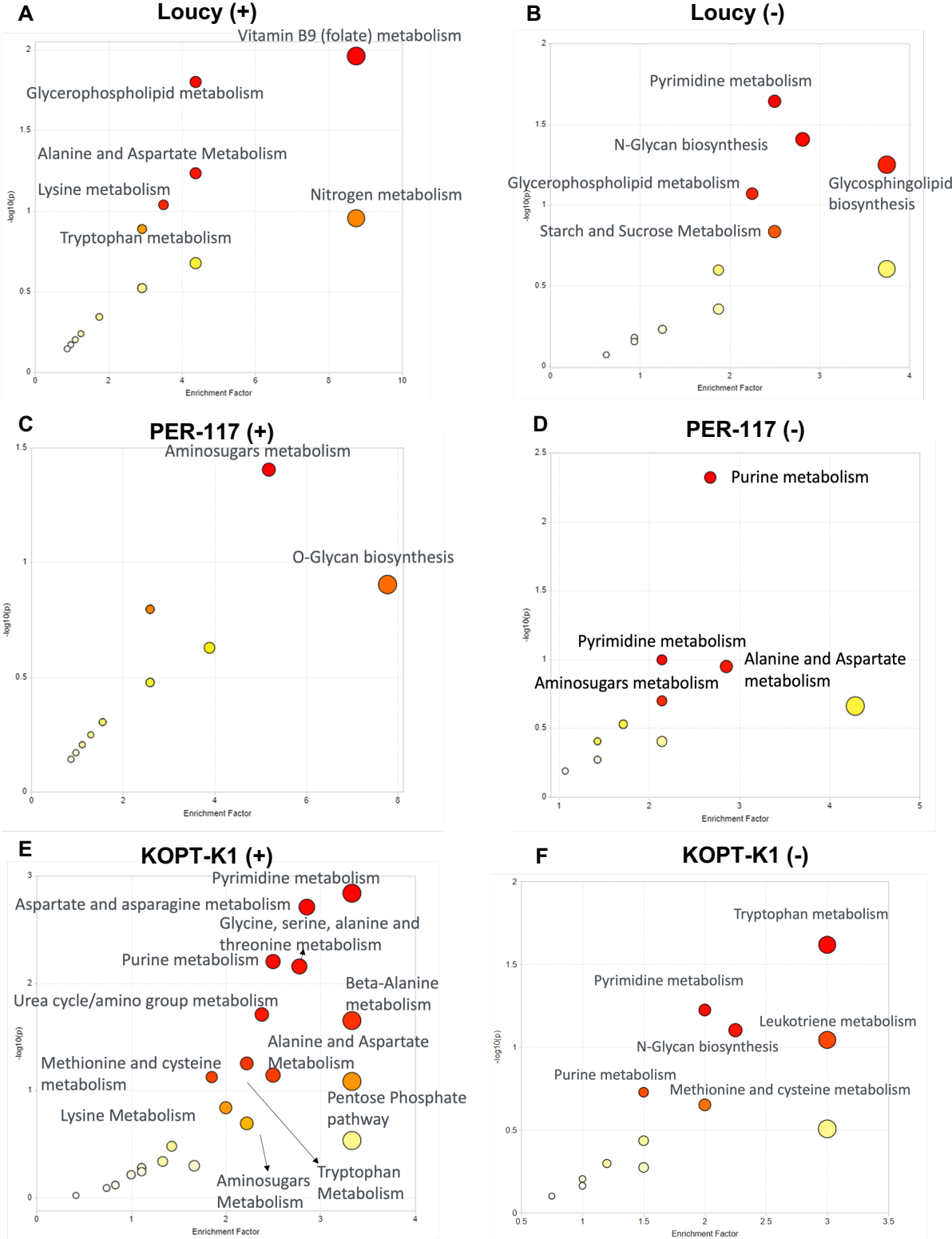


Figure 18 – Differentially expressed pathways between control and L-asparaginase treated T-ALL cell lines. Pathway analysis was performed for (A-B) Loucy, (C-D) PER-117 and (E-F) KOPT-K1 cell lines using all identified positively (+) and negatively ionized metabolites (-).

Together, this metabolomic data showed that L-asparaginase treatment indeed induces metabolomic changes in T-ALL cells that align with the observed effect of L-asparaginase on the SLC7A11-GSH axis. However, both targeted analysis and untargeted analysis have also revealed that L-asparaginase also influences amino acids and therefore cellular pathways independent of this upregulated axis, again suggesting that the observed reduction in cellular oxidative stress might not solely be due to upregulation of *SLC7A11*.

6.6 Inhibiting L-asparaginase upregulated SLC7A11 does not impair cell viability

The aforementioned data has associated L-asparaginase induced *SLC7A11* upregulation in T-ALL cell lines to a reduction of intracellular oxidative stress. This presumably provides the cells a survival advantage and chances are therefore high that *SLC7A11* indeed functions as a chemotherapy induced resistance mechanism. In consequence, it was explored whether *SLC7A11* could function as a chemotherapy-induced therapeutic target. For this, the effect of inhibiting *SLC7A11* by erastin after L-asparaginase induced upregulation was evaluated by CellTiter-Glo viability assays.

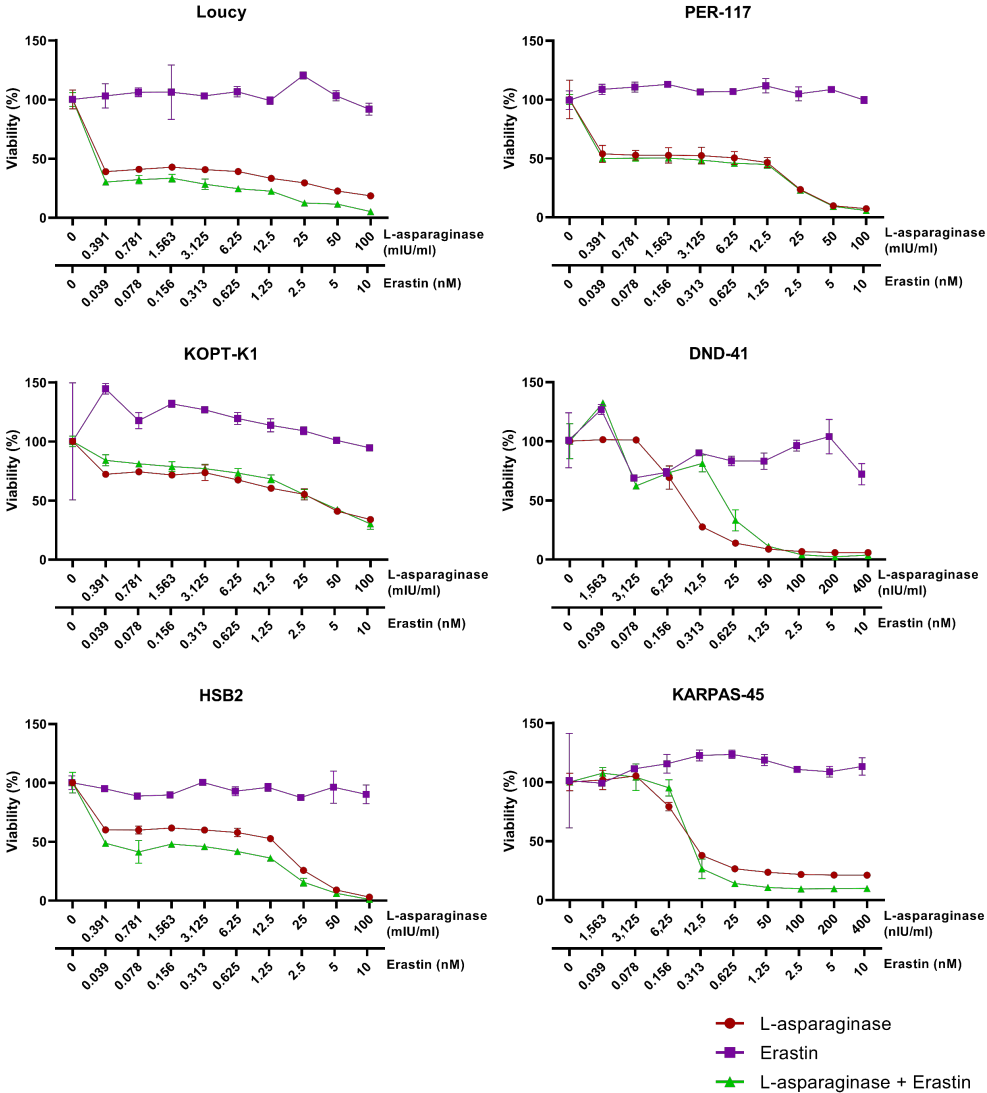


Figure 19 – Inhibiting L-asparaginase upregulated SLC7A11 with erastin does not decrease cell viability. Viability of Loucy, PER-117, KOPT-K1, DND-41, HSB2 and KARPAS-45 cells measured by CellTiter Glo viability assay after L-asparaginase/erastin mono-treatment or combination treatment. Error bars represent the SD of two technical replicates.

Combination therapy of L-asparaginase and erastin resulted in Loucy, HSB2, KARPAS-45 and HPB-ALL cell lines in a slightly decreased viability as compared to L-asparaginase mono-treatment (Figure 19, Supplementary Figure 11). In both KARPAS-45 and HPB-ALL cell lines, this decreased viability only occurred at high concentrations. Remarkably, cell viability increased or remained constant after combination treatment of PER-117, KOPT-K1 and DND-41 cells. Erastin mono-treatment did not have a notable effect on cell viability. However, considering that SLC7A11 only starts to play an important role for cell survival after treatment with L-asparaginase, the latter was not totally unexpected. In short, this cell viability experiment showed that, against expectations, inhibiting L-asparaginase upregulated SLC7A11 with erastin does not affect cell viability of T-ALL cells.

6.7 SLC7A11 is upregulated by the SLC7A11 inhibitor erastin

In search for an explanation for the absence of an increased effect of combination treatment on T-ALL cell viability, SLC7A11 expression levels were determined by RT-qPCR after treatment with L-asparaginase, erastin or a combination of both. Surprisingly, treating T-ALL cells with both L-asparaginase and erastin increased the expression of SLC7A11 in all T-ALL cell lines (Figure 20). This increase was even significant in HPB-ALL cell lines (data not shown), suggesting that erastin induces, similar to L-asparaginase, SLC7A11 upregulation. SLC7A11 expression levels determined after erastin monotherapy confirmed this, since they were, albeit not significant in most cell lines except HPB-ALL, prominently upregulated in contrast to control cells. Because both L-asparaginase and erastin were proven to upregulate SLC7A11 expression, it was remarkable that SLC7A11 expression was not in all cell lines the highest for combination treatment. However, the fact that L-asparaginase on itself generally did not induce a significant upregulation of SLC7A11 as seen in Figure 13B could play a part in this observation. The fact that erastin upregulated SLC7A11 expression presumably explains why combination therapy did not decrease cell viability.

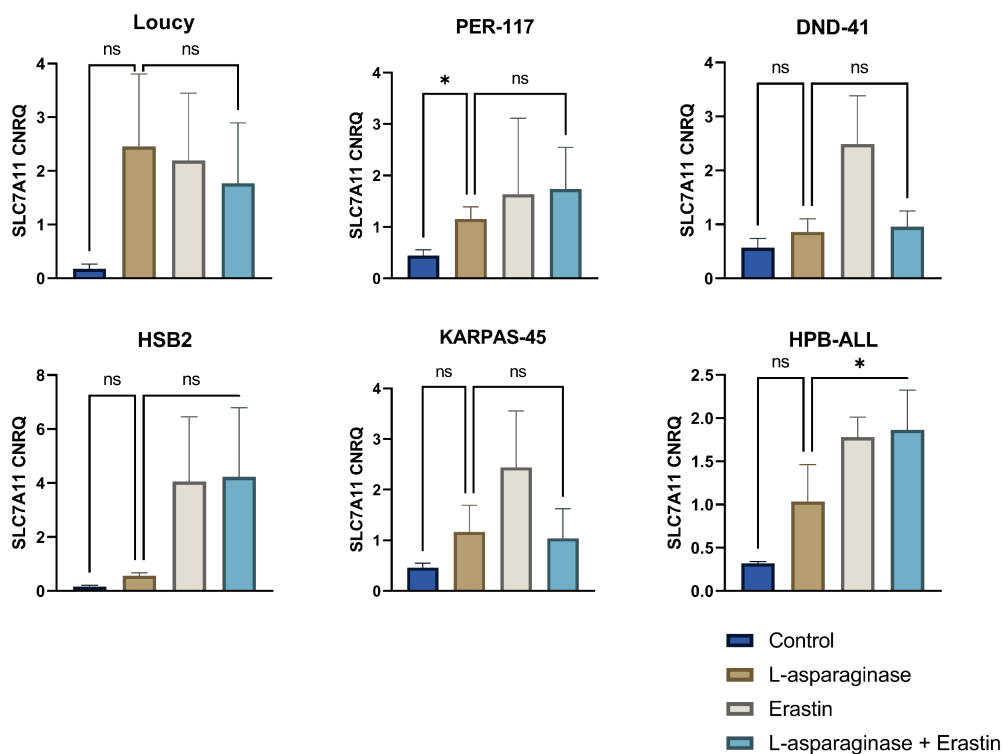


Figure 20 – SLC7A11 expression is upregulated by the SLC7A11 inhibitor erastin. qRT-PCR analysis for SLC7A11 expression in Loucy, PER-117 ($P = 0.0319$), DND-41, HSB2, KARPAS-45 and HPB-ALL ($P = 0.0243$) T-ALL cell lines treated (48h) with either L-asparaginase, erastin or a combination of both. Error bars represent the SD of three independent biological replicates.

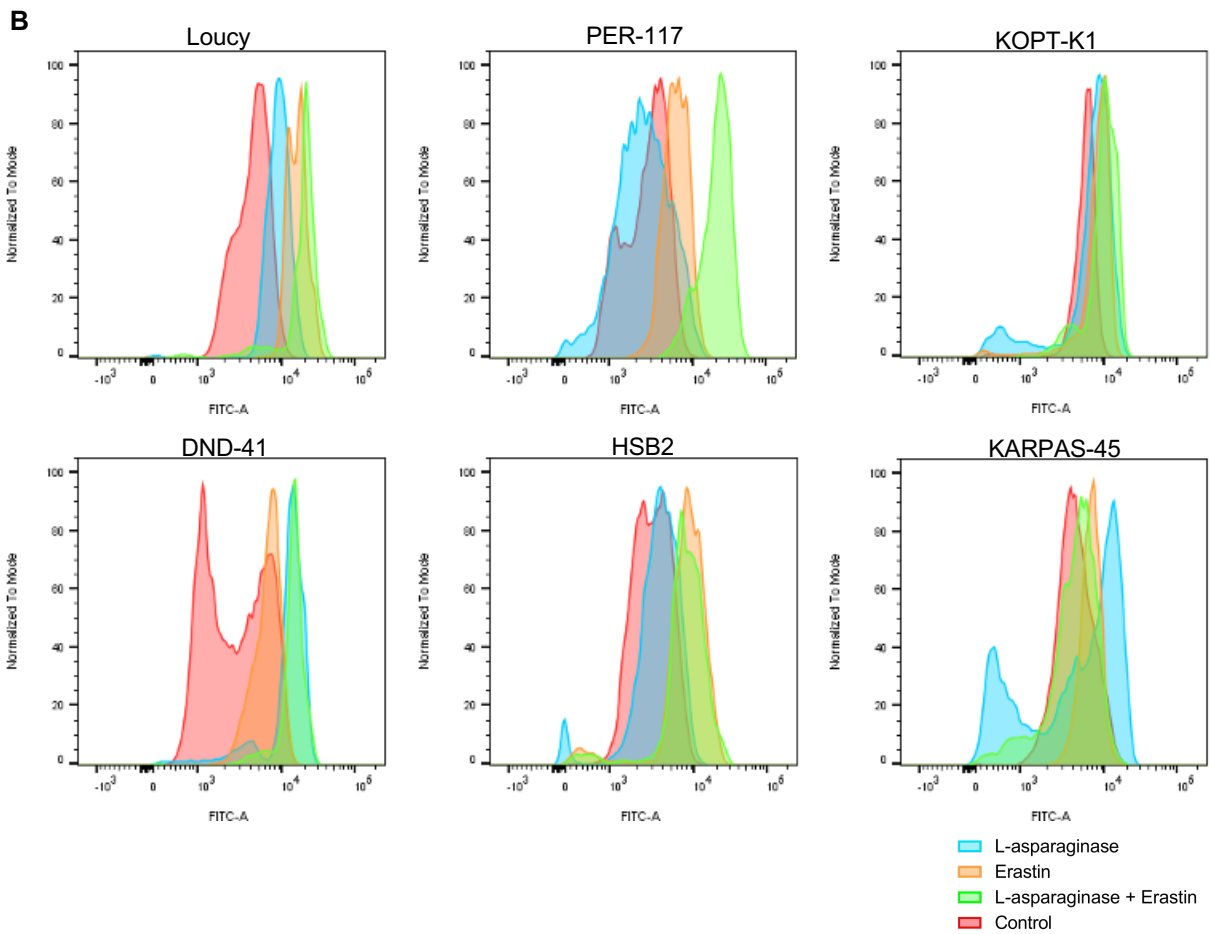
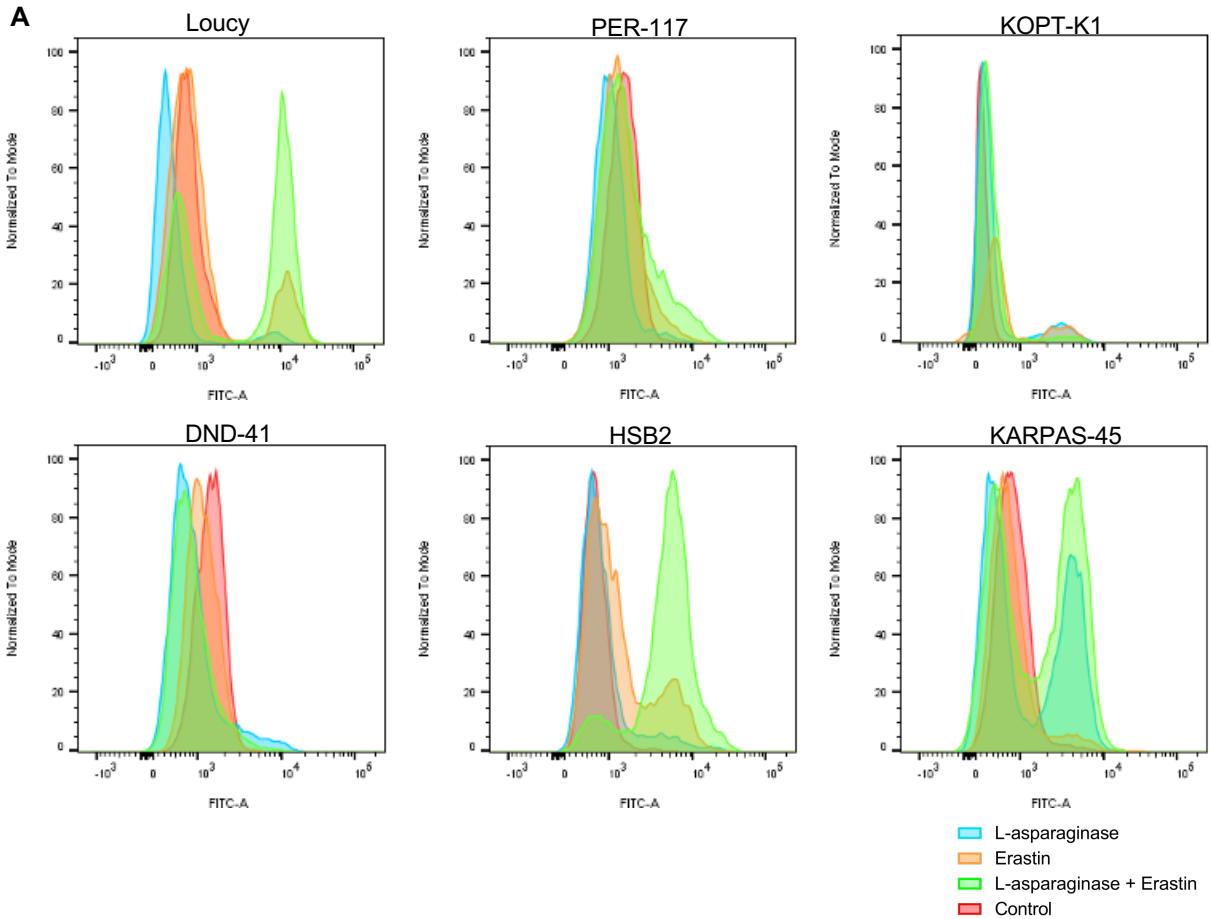
6.8 Combination treatment does not modulate the expression of SLC7A11 downstream components in accordance with its effect on SLC7A11 expression

To validate whether the insufficiency of combination therapy on decreasing T-ALL cell viability was indeed due to erastin induced upregulation of *SLC7A11*, T-ALL cells treated with L-asparaginase, erastin or a combination of both were stained for flow cytometric analysis of intracellular cystine, GSH and general oxidative stress. Following the earlier findings, it was expected that erastin mono-therapy would increase cystine and GSH levels, thus decreasing general oxidative stress. For combination treatment, expectations were that cystine, GSH and general oxidative stress levels would change depending on the cell line. This is because cell viability only decreased in certain cell lines. In those cell lines, it is supposed that cystine and GSH levels will be downregulated after treatment, inducing increased general oxidative stress.

Similarly to the earlier stains for cystine (Figure 14A), the majority of the cell lines did not follow the hypothesis stated for erastin mono-therapy since cystine levels mainly remained constant (Figure 21A, Supplementary Figure 12A). In addition to this major peak, most cell lines again displayed an extra minor peak of increased cystine expression. In both PER-117 and DND-41 cell lines, cystine levels remained constant, which was remarkable given the fact that *SLC7A11* was also shown to be upregulated in these cells after erastin mono-treatment (Figure 20, 21A). Surprisingly, combination therapy resulted in both HSB2 and Loucy, two cell lines that previously displayed lower cell viability after combination therapy (Figure 19), in higher cystine levels compared to L-asparaginase treated cells. The remaining cell lines did not show altered levels after combination treatment, raising the question whether the lack of effect on cell viability observed with combination treatment is attributable to the additional *SLC7A11* upregulation induced by erastin.

However, analysis of GSH levels in T-ALL cells after erastin mono-treatment treatment took this question away. Erastin mono-treatment led in all cell lines to higher GSH levels when compared to control cells, suggesting that *SLC7A11* upregulation by erastin indeed provides cells a survival advantage via the *SLC7A11*-GSH axis (Figure 21B, Supplementary Figure 12B). In addition, combination treatment also increased GSH levels in Loucy, PER-117, KOPT-K1 and HSB2 cells, however, this was not in every cell line evenly outspoken. GSH levels remained constant in DND-41, and HPB-ALL cells and were downregulated in KARPAS-45 cells. For both DND-41 and KARPAS-45, these findings were completely in line with the observations from the cell viability and RT-qPCR experiments. For Loucy and HSB2 cells on the contrary, these results were fully the reverse of what would be expected based on the cell viability assays. Since both cell lines showed a slight decrease in cell viability, this notable increase in GSH brings forth the question whether the observed decrease in cell viability in these cells lines is only partly attributable to the *SLC7A11*-GSH axis.

Flow cytometric analysis showed that erastin mono-treatment did not change general oxidative stress in the majority of cell lines as compared to control cells (Figure 21C, Supplementary Figure 12C). Combination therapy on the other hand induced general oxidative stress in the majority of cell lines when compared with L-asparaginase single treatment. Only in DND-41 cells, levels remained constant, again consistent with earlier findings. In general, this staining did not match with what was expected based on the cystine and GSH stains, implying that the insufficiency of combination therapy on decreasing T-ALL cell viability will not only be due to effects on the *SLC7A11*-GSH axis, but also due to additional underlying effects that were not investigated.



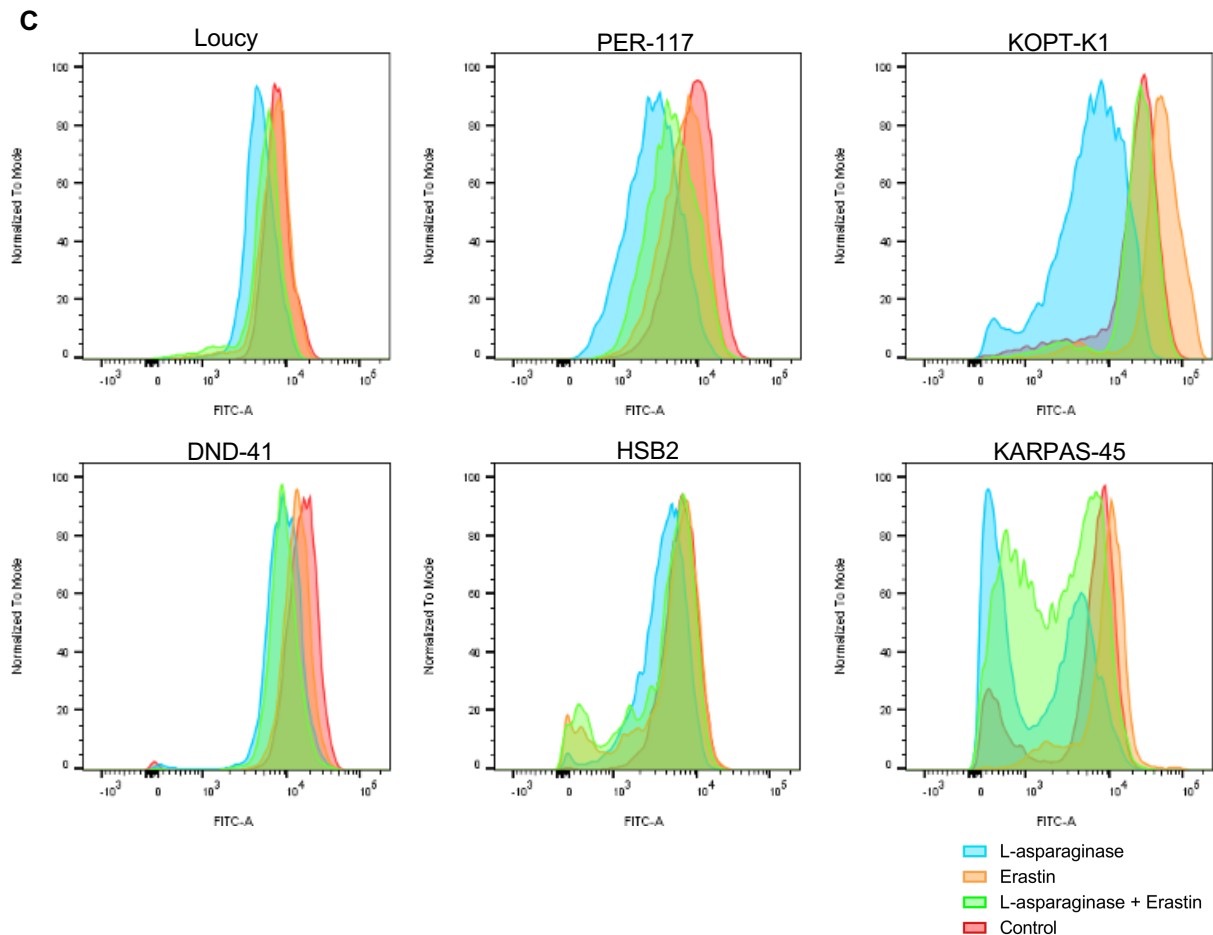


Figure 21 – Inhibiting L-asparaginase induced *SLC7A11* with erastin does not modulate downstream cystine, GSH and general oxidative stress levels in accordance with its effect on *SLC7A11* expression levels. Flow cytometric analysis of (A) intracellular cystine levels, (B) cellular GSH and (C) general oxidative stress after L-asparaginase, erastin or combination treatment.

7. Discussion

In spite of the fact that T-ALL patients are treated with a long-term high-dose multiagent chemotherapy regimen, currently still up to 20% of children and 40% of adults do not respond to this, or relapse after a transient initial response^{13,29}. Because the underlying mechanisms causing these R/R T-ALLs are generally unknown, standard of care salvage therapies are lacking, causing R/R T-ALL patients to have a poor prognosis¹⁰. In search for new therapeutic strategies to prevent or eradicate R/R T-ALL, our group had found the expression of the light chain functional subunit of system x_c⁻, *SLC7A11*, to be upregulated after L-asparaginase treatment. Because several studies have associated this antiporter with proliferation, growth, invasion, metastasis and resistance in a wide variety of cancers^{37,38,41,46}, this Master's dissertation explored its role in the chemotherapy response of T-ALL and its potential as a chemotherapy-induced therapeutic target.

Because prior studies in breast cancer^{89,90}, ovarian cancer⁹¹ and liver cancer⁹² have shown that cell lines do not always represent the primary tumors, we first validated the relevance of the earlier observed upregulation of *SLC7A11* in healthy thymocytes and primary T-ALL samples. In healthy thymocytes, *SLC7A11* turned out to be variably expressed over the various differentiation stages, with the highest expression during the ISP stage. This could be explained by the fact that T-cells switch their metabolic profile during this phase, going from aerobic glycolysis to oxidative phosphorylation, a process known for its high production of ROS^{93,94}. Because uncontrolled ROS production would result in cell death, *SLC7A11* presumably fine-tunes the balance between ROS production, which has been shown to be

essential for T-cell differentiation, and antioxidation during this stage^{93,95}. When we compared the expression in these healthy thymocytes with *SLC7A11* expression in primary T-ALL samples, *SLC7A11* was notably upregulated in the latter group. This is in accordance with an earlier study, which showed that *SLC7A11* baseline expression in NSCLC cells is higher than in normal airway epithelial cells⁴⁷, and suggests that *SLC7A11* is not only exploited in the therapy response of T-ALL cells.

Based on the observation that *SLC7A11* baseline expression is upregulated in T-ALL primary samples, one might expect that these cells depend on this antiporter for their survival. In consequence, we performed a cell dependency analysis in DepMap of untreated T-ALL cell lines, proving that, for the few T-ALL cell lines taken into analysis, *SLC7A11* is not essential for T-ALL cell survival. This was in contrast to the study on NSCLC, in which knocking out of *SLC7A11* significantly hampered cell viability⁴⁷. However, a genome-wide sequencing experiment on ALL cells confirmed the cell dependency analysis⁹⁶, indicating that in T-ALL, *SLC7A11* only starts to play a role in response to anti-cancer treatment.

Although *SLC7A11* was proven to be non-essential for survival of untreated T-ALL cells, we determined baseline expression in various untreated T-ALL cell lines to control whether a similar constant *SLC7A11* expression pattern could be observed over the different subtypes as in primary T-ALL samples. Remarkably, *SLC7A11* expression was highly variable between the different cell lines, contradicting the findings in T-ALL primary samples. The fact that ETP-ALL cell lines, representing a harsher T-ALL subtype that requires more intensive treatment regimens¹⁵, showed the highest expression levels might suggest that *SLC7A11* baseline expression could be predictive for R/R T-ALL. Indeed, high baseline *SLC7A11* expression levels have been associated with a poor prognosis in a variety of cancers, including NSCLC⁴⁷, ovarian cancer⁹⁷, glioma^{50,98}, liver cancer⁹⁹ and AML^{52,100}. However, care should be given by stating such a hypothesis, since for asparagine synthetase (*ASNS*), the rate limiting enzyme for *de novo* biosynthesis of L-asparagine¹⁰¹, a study on rectal cancer contradicted all previous findings by demonstrating that low *ASNS* expression constituted a negative prognostic factor for L-asparaginase therapy response¹⁰². In addition, it was also reported that not *ASNS* mRNA, but *ASNS* protein levels functioned as a predictor of resistance in ALL¹⁰³. Therefore, even though it is highly plausible that the observed high baseline *SLC7A11* mRNA expression levels in cell lines of a dedicated T-ALL subtype might be predictive for R/R T-ALL, further research, including clinical studies, will be needed to confirm this hypothesis.

A validation experiment of the preliminary experiments forming the basis of this Master's dissertation confirmed that from the components used in induction therapy, L-asparaginase is responsible for *SLC7A11* upregulation. However, remarkable was that both dexamethasone and vincristine decreased *SLC7A11* expression in several cell lines. Because both are assumed to induce cellular stress by perturbing normal cell homeostasis, this was rather unexpected. Nevertheless, this might indicate that even though L-asparaginase mono-therapy increases *SLC7A11* significantly, this effect might be suppressed by these other components, attenuating the role of *SLC7A11* in R/R T-ALL. Notably, *SLC7A11* upregulation was most significant in the ETP-ALL cell lines having the highest baseline expression, indicating that a high baseline expression does not hamper cells to upregulate this antiporter in response to cellular stresses. In consequence, this finding raised the question whether these cell lines were most resistant against L-asparaginase compared to cell lines of other T-ALL subtypes. However, both the fact that L-asparaginase usage in ETP-ALL patients has been associated with improved progression-free survival¹⁰⁴, and the fact that ETP-ALL cell lines had similar IC₅₀ values as other T-ALL subtype cell lines implied that this was not the case. As a consequence, we hypothesize that notwithstanding the high baseline expression, a certain degree of upregulation will always be required since these cells have adapted their metabolism to their high baseline antioxidation³⁹.

Because we hypothesized based on the SLC7A11-GSH axis that a possible cellular advantage of upregulating *SLC7A11* should come from its downstream components, we explored the effect of L-asparaginase treatment on cystine, GSH and general oxidative stress levels. Against expectations, cystine levels were only upregulated in small cell populations. Indeed, intracellular cystine levels were downregulated in the majority of L-asparaginase treated cell lines. Since all stains were optimized, the argument that the cystine staining failed was most likely not applicable. An earlier publication has reported a similar observation in SLC7A11 overexpressing renal carcinoma cell lines and suggested that this was due to the rapid intracellular reduction into cysteine¹⁰⁵. However, this would still not clarify the origin of the small cell populations displaying higher cystine levels.

In view of the fact that cystine is normally rapidly reduced, it might in those small cell populations be that cystine was converted less rapidly into cysteine due to a cellular defect causing shortage of NADPH. Yet, this is purely hypothetical. To further elucidate this, experimental blockage of NADPH production should be carried out to explore whether all cells then indeed exhibit high cystine levels. In addition, it is also important to keep in mind that L-asparaginase induces next to SLC7A11 upregulation plenty of additional metabolic changes in the cell. This also influences the expression of other amino acid transporters as illustrated by a STRING analysis of published microarray data on L-asparaginase treated ALL cells (Supplementary Figure 13), presumably contributing to the observed heterogeneity in cystine levels⁹⁶. Another hypothesis we first had based on this observed double peak pattern was that L-asparaginase induced *SLC7A11* upregulation either occurred only in a subpopulation of cells, or caused only in a minority of cells higher intracellular cystine levels. However, analysis of GSH levels showed that neither of two was the case, since GSH was increased in most cell lines. Similarly as for cystine, also an inexplicable second peak of lower GSH expression was observed in the majority of L-asparaginase treated cells.

Lastly, analysis of general oxidative stress levels, the final effector affected by SLC7A11 upregulation, showed that cells treated with L-asparaginase experience lower levels of cellular stress. Notably, the majority of cell lines did not show double peaks, contrasting the patterns observed in both cystine and GSH stains. Both upregulation of GSH and downregulation of oxidative stress were in accordance with the earlier study on renal carcinoma cell lines¹⁰⁵, strengthening the hypothesis that L-asparaginase induced SLC7A11 upregulation indeed provides T-ALL cells an advantage by decreasing oxidative stress.

L-asparaginase is known to exert its function by perturbing T-ALL cellular metabolism via the depletion of L-asparagine from the extracellular environment⁸⁸. However, both a study on ALL¹⁰⁶ as well as the above described upregulation have shown that T-ALL cells reprogram their metabolism as one of the mechanisms to survive this perturbation. In consequence, we performed a metabolomic analysis to explore whether L-asparaginase treatment induced metabolomic changes that could be linked to the upregulation of the SLC7A11-GSH axis. Using targeted analysis of amino acid metabolism, we found that intracellular cysteine levels were decreased in the majority of T-ALL cell lines, contrasting the earlier study on renal carcinoma in which, notwithstanding decreased cystine levels, L-asparaginase treatment significantly upregulated intracellular cysteine¹⁰⁵. Because the earlier described double peak pattern of GSH was not reflected in cellular ROS, this observation critically questions whether the observed decrease in intracellular oxidative stress could be fully attributed to the SLC7A11-GSH axis.

L-asparagine levels were, as expected, significantly downregulated in all T-ALL cell lines. However against expectations, glutamine levels were increased while both aspartic acid and glutamic acid were decreased in the majority of cell lines. This was not in line with an earlier metabolomic study on adherent cells, which showed the reverse of what was observed in this thesis¹⁰⁷. A possible explanation for this observation could be the fact that L-asparaginase exerts its function extracellularly. Indeed, intracellular L-asparagine levels are suggested to be decreased due to L-asparaginase induced exportation and rapid extracellular degradation of L-asparagine¹⁰⁷. It might be that a similar gradient for glutamine does not exist in T-ALL cells. An explanation for the observed upregulation could be that L-asparaginase induced

metabolomic changes hamper the functionality of glutaminase to convert L-glutamine into glutamate. Another explanation could be that due to the decrease of extracellular glutamine levels and increase of SLC7A11 mediated glutamate export, intracellular glutamate levels fall short to fuel both the tricarboxylic acid (TCA) cycle and GSH synthesis, causing an upregulation of glutamine transporters and thereby increasing intracellular glutamine levels (Supplementary Figure 14). The latter hypothesis is strengthened by the STRING analysis of microarray data of L-asparaginase treated cells (Supplementary Figure 13), showing that also glutamine transporters are upregulated after L-asparaginase treatment⁹⁶.

However, to confirm such a hypothesis, metabolomic analysis of the media in which cells are cultured should be performed to control whether extracellular glutamine levels indeed decrease after treatment. In addition, it is important to note that there was a significant heterogeneity in cellular metabolism depending on the cell line studied. Indeed, amino acid abundance was not altered consistently over the various cell lines, illustrating the complexity and variability of L-asparaginase induced metabolic changes in various cell lines.

To identify in an unbiased manner the largest differences between the metabolomes of control and L-asparaginase treated T-ALL cells, we also performed untargeted analysis of all detected metabolites. Unfortunately, this analysis did not bring forward any relevant metabolite from the identified putative chemical formulas of differently expressed metabolites. This might be due to fact that metabolomics is a relatively recent research field, as illustrated by the fact that next to 253.245 annotated metabolites, the Human Metabolome Database currently contains almost 7 times as much unannotated metabolite entries. Importantly, those metabolites are not only derived from the human metabolome, but also from food, drugs and the microbiome. As a consequence, typically less than 2% of the *m/z*-ratio based putative chemical formulas can be linked to a corresponding metabolite in an untargeted analysis¹⁰⁸. Since even among targeted metabolomic studies mostly less than 1% of the known human metabolome can be identified¹⁰⁸, it can be concluded that both the metabolite coverage and the MS spectral coverage in the Human Metabolome Database are inadequate and incomplete thus far, presumably explaining the failure of metabolite identification.

Although no metabolites could be identified from untargeted analysis, pathway analyses did bring forward that, in line with the observations in targeted analysis, metabolites involved in the alanine and aspartate and/or the aspartate and asparagine metabolism were modulated after L-asparaginase treatment. In a minority of cell lines, also methionine and cysteine as well as glutathione metabolism were altered due to L-asparaginase treatment, referring to an altered SLC7A11-GSH axis. An important notion to be made is that pathway analysis does not provide information on the direction of the change. It only indicates a pathway differs between the two conditions, here control and L-asparaginase.

An additional interesting observation in relation to the SLC7A11-GSH axis was the fact that the pentose phosphate pathway (PPP) was differently expressed in KOPT-K1 cells after L-asparaginase treatment. Indeed, since SLC7A11 upregulation results in higher import of cystine^{39,40}, its reduction into cysteine depletes intracellular NADPH levels¹⁰⁹, demanding a larger supply to fulfill the cellular needs. This supply mainly comes from glucose via the PPP^{39,40} (Supplementary Figure 14), as confirmed by an earlier study which demonstrated that SLC7A11 upregulation increases the PPP flux¹⁰⁵. This reasoning suggests that the PPP pathway will be upregulated in L-asparaginase treated cells.

Furthermore, pyrimidine and/or purine metabolism differed between control and L-asparaginase treated samples of all cell lines, which may point towards L-asparaginase induced changes in cellular proliferation and growth¹¹⁰. Lastly, we also found that the sialic acid as well as the glycine, alanine and threonine metabolisms were changed in all cell lines, indicating that L-asparaginase also influences cellular pathways linked to other amino acids apart from asparagine, glutamine and cysteine. Together with the observed cell line dependent heterogeneity in targeted analysis and the double peak pattern in both cystine and GSH stains, this suggests that the observed reduction in oxidative stress after L-asparaginase treatment is presumably not solely due to upregulation of SLC7A11.

Recently, a study on AML has shown that inhibiting SLC7A11 potentiates the anti-leukemic effect of standard-of-care therapies¹⁰⁰. Because we found that L-asparaginase induced *SLC7A11* upregulation was associated with lower intracellular oxidative stress levels, we speculated that inhibiting this antiporter in T-ALL cells would similarly increase the efficiency of L-asparaginase treatment. Surprisingly, addition of erastin to L-asparaginase did not affect cell viability in most T-ALL cell lines. RT-qPCR analysis revealed that this was most likely due to erastin induced *SLC7A11* upregulation. The fact that a similar upregulation has been reported by other publications in which, despite this upregulation, erastin treatment still led to increased cell death^{43,111}, made us wonder in which regard the response in T-ALL cells differed from those studies.

Combination treatment of L-asparaginase and erastin in T-ALL cells did not alter cystine levels in the majority of cell lines and induced similarly as with L-asparaginase single treatment an extra minor peak of increased cystine expression, the latter raising similar reasonings as described for L-asparaginase single treatment. Even though GSH levels were more variably expressed, the majority of cell lines showed increased levels after combination therapy. Both observations of cystine and GSH are in large contrast with studies showing an effect on cell viability^{112,113}, indicating that this difference could be the origin of the lack of effect on cell viability. Furthermore, we observed that, similarly as in experiments in which an effect on cell viability was reported^{113,114}, cellular oxidative stress levels were upregulated after combination treatment. This was highly remarkable, since erastin is known to exert its function by inducing ferroptosis via the accumulation of oxidative stress^{114,115}, questioning why we did not observe a decrease in cell viability.

Given the fact that both cystine and GSH levels did not match with what we would expect based on the observed erastin induced *SLC7A11* upregulation, and given these levels also did not match cellular oxidative stress, we suggest that the absence of an effect on cell viability will be not only due to the SLC7A11-GSH axis. Indeed, based on the above described observation that L-asparaginase single treatment induces a plethora of cellular responses next to the SLC7A11-GSH axis, we presume a similar complexity to occur after combination treatment, suggesting that other, non-explored effects probably rescue T-ALL cells from oxidative stress induced cell death. Consequently, future experiments should exploit a knock-out of *SLC7A11* to explore in a reliable manner to which extent SLC7A11 could function as a chemotherapy-induced therapeutic target. With a view to the clinic, it might also be interesting to explore whether the FDA-approved SLC7A11 inhibitor sulfasalazine is capable of potentiating L-asparaginase function, since this inhibitor has already proven to be advantageous in anti-leukemia therapy^{100,116}.

In conclusion, our results demonstrated that baseline *SLC7A11* expression is highly variable between cell lines of different T-ALL subtypes, encouraging further research to explore its predictiveness for R/R T-ALL. In addition, we validated that L-asparaginase treatment of T-ALL cells upregulates *SLC7A11* expression and associated this with a decrease in cellular oxidative stress, suggesting that *SLC7A11* upregulation indeed plays a role in the chemotherapy response of T-ALL. However, because metabolomic analysis revealed a plethora of cellular responses to L-asparaginase treatment next to the SLC7A11-GSH axis, further experiments will be needed to determine the extent to which SLC7A11 is involved in reducing oxidative stress in response to L-asparaginase treatment. Lastly, we showed that combining L-asparaginase treatment with the SLC7A11 inhibitor erastin does not decrease cell viability although it increases cellular oxidative stress. Because SLC7A11 inhibition has been shown to be advantageous in anti-leukemia therapy^{100,116}, additional studies should be performed to both elucidate the mechanisms rescuing T-ALL cells from erastin induced cell death and further explore the potential of SLC7A11 as a chemotherapy-induced therapeutic target.

8. References

- 1 Rieger, M. A. & Schroeder, T. Hematopoiesis. *Cold Spring Harb Perspect Biol* **4**, doi:10.1101/cshperspect.a008250 (2012).
- 2 Cheng, H., Zheng, Z. & Cheng, T. New paradigms on hematopoietic stem cell differentiation. *Protein Cell* **11**, 34-44, doi:10.1007/s13238-019-0633-0 (2020).
- 3 Olson, O. C., Kang, Y. A. & Passegué, E. Normal Hematopoiesis Is a Balancing Act of Self-Renewal and Regeneration. *Cold Spring Harb Perspect Med* **10**, doi:10.1101/cshperspect.a035519 (2020).
- 4 Laurenti, E. & Göttgens, B. From haematopoietic stem cells to complex differentiation landscapes. *Nature* **553**, 418-426, doi:10.1038/nature25022 (2018).
- 5 Swerdlow, S. H. *et al.* *WHO classification of tumours of haematopoietic and lymphoid tissues*. Vol. 2 (International agency for research on cancer Lyon, 2008).
- 6 Swerdlow, S. H. *et al.* The 2016 revision of the World Health Organization classification of lymphoid neoplasms. *Blood, The Journal of the American Society of Hematology* **127**, 2375-2390 (2016).
- 7 Arber, D. A. *et al.* The 2016 revision to the World Health Organization classification of myeloid neoplasms and acute leukemia. *Blood, The Journal of the American Society of Hematology* **127**, 2391-2405 (2016).
- 8 Terwilliger, T. & Abdul-Hay, M. Acute lymphoblastic leukemia: a comprehensive review and 2017 update. *Blood Cancer J* **7**, e577-e577, doi:10.1038/bcj.2017.53 (2017).
- 9 Paul, S., Kantarjian, H. & Jabbour, E. J. Adult Acute Lymphoblastic Leukemia. *Mayo Clin Proc* **91**, 1645-1666, doi:<https://doi.org/10.1016/j.mayocp.2016.09.010> (2016).
- 10 Richard-Carpentier, G., Kantarjian, H. & Jabbour, E. Recent Advances in Adult Acute Lymphoblastic Leukemia. *Curr Hematol Malig Rep* **14**, 106-118, doi:10.1007/s11899-019-00503-1 (2019).
- 11 Hefazi, M. & Litzow, M. R. Recent Advances in the Biology and Treatment of T Cell Acute Lymphoblastic Leukemia. *Curr Hematol Malig Rep* **13**, 265-274, doi:10.1007/s11899-018-0455-9 (2018).
- 12 Karrman, K. & Johansson, B. Pediatric T-cell acute lymphoblastic leukemia. *Genes Chromosomes Cancer* **56**, 89-116, doi:10.1002/gcc.22416 (2017).
- 13 Szymańska, K. & Park, S. in *Encyclopedia of Cancer (Third Edition)* (eds Paolo Boffetta & Pierre Hainaut) 1-8 (Academic Press, 2019).
- 14 Zhao, Y., Wang, Y. & Ma, S. Racial Differences in Four Leukemia Subtypes: Comprehensive Descriptive Epidemiology. *Sci Rep* **8**, 548-548, doi:10.1038/s41598-017-19081-4 (2018).
- 15 Belver, L. & Ferrando, A. The genetics and mechanisms of T cell acute lymphoblastic leukaemia. *Nat Rev Cancer* **16**, 494-507, doi:10.1038/nrc.2016.63 (2016).
- 16 Krueger, A., Ziętara, N. & Łyszkiwicz, M. T Cell Development by the Numbers. *Trends Immunol* **38**, 128-139, doi:10.1016/j.it.2016.10.007 (2017).
- 17 Halkias, J., Melichar, H. J., Taylor, K. T. & Robey, E. A. Tracking migration during human T cell development. *Cell Mol Life Sci* **71**, 3101-3117, doi:10.1007/s00018-014-1607-2 (2014).
- 18 Seo, W. & Taniuchi, I. Transcriptional regulation of early T-cell development in the thymus. *Eur J Immunol* **46**, 531-538, doi:10.1002/eji.201545821 (2016).
- 19 James, K. D., Jenkinson, W. E. & Anderson, G. T-cell egress from the thymus: Should I stay or should I go? *J Leukoc Biol* **104**, 275-284, doi:10.1002/jlb.1mr1217-496r (2018).
- 20 Passaro, D., Quang, C. T. & Ghysdael, J. Microenvironmental cues for T-cell acute lymphoblastic leukemia development. *Immunological Reviews* **271**, 156-172, doi:<https://doi.org/10.1111/imr.12402> (2016).
- 21 Koch, U. & Radtke, F. Mechanisms of T cell development and transformation. *Annu Rev Cell Dev Biol* **27**, 539-562, doi:10.1146/annurev-cellbio-092910-154008 (2011).
- 22 De Smedt, R., Morscio, J., Goossens, S. & Van Vlierberghe, P. Targeting steroid resistance in T-cell acute lymphoblastic leukemia. *Blood reviews* **38**, 100591, doi:10.1016/j.blre.2019.100591 (2019).
- 23 Bene, M. C. *et al.* Proposals for the immunological classification of acute leukemias. European Group for the Immunological Characterization of Leukemias (EGIL). *Leukemia* **9**, 1783-1786 (1995).
- 24 Bongiovanni, D., Saccomani, V. & Piovani, E. Aberrant Signaling Pathways in T-Cell Acute Lymphoblastic Leukemia. *Int J Mol Sci* **18**, 1904, doi:10.3390/ijms18091904 (2017).
- 25 Girardi, T., Vicente, C., Cools, J. & De Keersmaecker, K. The genetics and molecular biology of T-ALL. *Blood* **129**, 1113-1123, doi:<https://doi.org/10.1182/blood-2016-10-706465> (2017).

- 26 Mroczek, A., Zawitkowska, J., Kowalczyk, J. & Lejman, M. Comprehensive Overview of Gene Rearrangements in Childhood T-Cell Acute Lymphoblastic Leukaemia. *Int J Mol Sci* **22**, 808, doi:10.3390/ijms22020808 (2021).
- 27 Raetz, E. A. & Teachey, D. T. T-cell acute lymphoblastic leukemia. *Hematology Am Soc Hematol Educ Program* **2016**, 580-588, doi:10.1182/asheducation-2016.1.580 (2016).
- 28 Luskin, M. R. & DeAngelo, D. J. T-cell acute lymphoblastic leukemia: Current approach and future directions. *Advances in Cell and Gene Therapy* **2**, e70 (2019).
- 29 Follini, E., Marchesini, M. & Roti, G. Strategies to Overcome Resistance Mechanisms in T-Cell Acute Lymphoblastic Leukemia. *Int J Mol Sci* **20**, 3021, doi:10.3390/ijms20123021 (2019).
- 30 Ferrando, A. Can one target T-cell ALL? *Best Pract Res Clin Haematol* **31**, 361-366, doi:10.1016/j.beha.2018.10.001 (2018).
- 31 McMahon, C. M. & Luger, S. M. Relapsed T Cell ALL: Current Approaches and New Directions. *Curr Hematol Malig Rep* **14**, 83-93, doi:10.1007/s11899-019-00501-3 (2019).
- 32 Li, B. *et al.* Therapy-induced mutations drive the genomic landscape of relapsed acute lymphoblastic leukemia. *Blood* **135**, 41-55, doi:10.1182/blood.2019002220 (2020).
- 33 Kunz, J. B. *et al.* Pediatric T-cell lymphoblastic leukemia evolves into relapse by clonal selection, acquisition of mutations and promoter hypomethylation. *Haematologica* **100**, 1442-1450, doi:10.3324/haematol.2015.129692 (2015).
- 34 Bardelli, V. *et al.* T-Cell Acute Lymphoblastic Leukemia: Biomarkers and Their Clinical Usefulness. *Genes (Basel)* **12**, doi:10.3390/genes12081118 (2021).
- 35 De Smedt, R. *et al.* Targeting cytokine- and therapy-induced PIM1 activation in preclinical models of T-cell acute lymphoblastic leukemia and lymphoma. *Blood* **135**, 1685-1695, doi:10.1182/blood.2019003880 (2020).
- 36 Lewerenz, J. *et al.* The cystine/glutamate antiporter system xc⁻ in health and disease: from molecular mechanisms to novel therapeutic opportunities. *Antioxidants & redox signaling* **18**, 522-555 (2013).
- 37 Lin, W. *et al.* SLC7A11/xCT in cancer: biological functions and therapeutic implications. *Am J Cancer Res* **10**, 3106 (2020).
- 38 Tang, X. *et al.* Research progress on SLC7A11 in the regulation of cystine/cysteine metabolism in tumors. *Oncology Letters* **23**, 1-9 (2022).
- 39 Koppula, P., Zhang, Y., Zhuang, L. & Gan, B. Amino acid transporter SLC7A11/xCT at the crossroads of regulating redox homeostasis and nutrient dependency of cancer. *Cancer Commun (Lond)* **38**, 12, doi:10.1186/s40880-018-0288-x (2018).
- 40 Koppula, P., Zhuang, L. & Gan, B. Cystine transporter SLC7A11/xCT in cancer: ferroptosis, nutrient dependency, and cancer therapy. *Protein Cell*, doi:10.1007/s13238-020-00789-5 (2020).
- 41 Liu, L. *et al.* Cystine-glutamate antiporter xCT as a therapeutic target for cancer. *Cell Biochem Funct*, doi:10.1002/cbf.3581 (2020).
- 42 Jyotsana, N., Ta, K. T. & DelGiorno, K. E. The Role of Cystine/Glutamate Antiporter SLC7A11/xCT in the Pathophysiology of Cancer. *Front Oncol* **12**, doi:10.3389/fonc.2022.858462 (2022).
- 43 Dixon, S. J. *et al.* Ferroptosis: an iron-dependent form of nonapoptotic cell death. *Cell* **149**, 1060-1072, doi:10.1016/j.cell.2012.03.042 (2012).
- 44 Jiang, X., Stockwell, B. R. & Conrad, M. Ferroptosis: mechanisms, biology and role in disease. *Nature Reviews Molecular Cell Biology* **22**, 266-282, doi:10.1038/s41580-020-00324-8 (2021).
- 45 Cao, J. Y. & Dixon, S. J. Mechanisms of ferroptosis. *Cell Mol Life Sci* **73**, 2195-2209, doi:10.1007/s00018-016-2194-1 (2016).
- 46 Shi, Z. Z., Tao, H., Fan, Z. W., Song, S. J. & Bai, J. Prognostic and Immunological Role of Key Genes of Ferroptosis in Pan-Cancer. *Front Cell Dev Biol* **9**, 748925, doi:10.3389/fcell.2021.748925 (2021).
- 47 Ji, X. *et al.* xCT (SLC7A11)-mediated metabolic reprogramming promotes non-small cell lung cancer progression. *Oncogene* **37**, 5007-5019, doi:10.1038/s41388-018-0307-z (2018).
- 48 Shin, S.-S. *et al.* Participation of xCT in melanoma cell proliferation in vitro and tumorigenesis in vivo. *Oncogenesis* **7**, 86, doi:10.1038/s41389-018-0098-7 (2018).
- 49 Sugano, K. *et al.* Expression of xCT as a predictor of disease recurrence in patients with colorectal cancer. *Anticancer research* **35**, 677-682 (2015).
- 50 Takeuchi, S. *et al.* Increased xCT expression correlates with tumor invasion and outcome in patients with glioblastomas. *Neurosurgery* **72**, 33-41; discussion 41, doi:10.1227/NEU.0b013e318276b2de (2013).

- 51 Lee, J. R. *et al.* Overexpression of cysteine-glutamate transporter and CD44 for prediction of recurrence and survival in patients with oral cavity squamous cell carcinoma. *Head Neck* **40**, 2340-2346, doi:10.1002/hed.25331 (2018).
- 52 Zhao, X., Li, Y. & Wu, H. A novel scoring system for acute myeloid leukemia risk assessment based on the expression levels of six genes. *Int J Mol Med* **42**, 1495-1507, doi:10.3892/ijmm.2018.3739 (2018).
- 53 Wang, S. F. *et al.* Activated Integrated Stress Response Induced by Salubrinal Promotes Cisplatin Resistance in Human Gastric Cancer Cells via Enhanced xCT Expression and Glutathione Biosynthesis. *Int J Mol Sci* **19**, doi:10.3390/ijms19113389 (2018).
- 54 Polewski, M. D. *et al.* Increased Expression of System xc- in Glioblastoma Confers an Altered Metabolic State and Temozolomide Resistance. *Mol Cancer Res* **14**, 1229-1242, doi:10.1158/1541-7786.Mcr-16-0028 (2016).
- 55 Lo, M., Ling, V., Wang, Y. Z. & Gout, P. W. The xc- cystine/glutamate antiporter: a mediator of pancreatic cancer growth with a role in drug resistance. *Br J Cancer* **99**, 464-472, doi:10.1038/sj.bjc.6604485 (2008).
- 56 Lei, G. *et al.* The role of ferroptosis in ionizing radiation-induced cell death and tumor suppression. *Cell Research* **30**, 146-162, doi:10.1038/s41422-019-0263-3 (2020).
- 57 Cobler, L., Zhang, H., Suri, P., Park, C. & Timmerman, L. A. xCT inhibition sensitizes tumors to γ -radiation via glutathione reduction. *Oncotarget* **9**, 32280-32297, doi:10.18632/oncotarget.25794 (2018).
- 58 Lanzardo, S. *et al.* Immunotargeting of Antigen xCT Attenuates Stem-like Cell Behavior and Metastatic Progression in Breast Cancer. *Cancer Res* **76**, 62-72, doi:10.1158/0008-5472.Can-15-1208 (2016).
- 59 Polewski, M. D., Reveron-Thornton, R. F., Cherryholmes, G. A., Marinov, G. K. & Aboody, K. S. SLC7A11 overexpression in glioblastoma is associated with increased cancer stem cell-like properties. *Stem Cells and Development* **26**, 1236-1246 (2017).
- 60 Xu, X. *et al.* Targeting SLC7A11 specifically suppresses the progression of colorectal cancer stem cells via inducing ferroptosis. *Eur J Pharm Sci* **152**, 105450, doi:10.1016/j.ejps.2020.105450 (2020).
- 61 Wada, F. *et al.* High expression of CD44v9 and xCT in chemoresistant hepatocellular carcinoma: Potential targets by sulfasalazine. *Cancer Sci* **109**, 2801-2810, doi:10.1111/cas.13728 (2018).
- 62 Yoshikawa, M. *et al.* xCT inhibition depletes CD44v-expressing tumor cells that are resistant to EGFR-targeted therapy in head and neck squamous cell carcinoma. *Cancer Res* **73**, 1855-1866, doi:10.1158/0008-5472.Can-12-3609-t (2013).
- 63 Sato, H. *et al.* Redox Imbalance in Cystine/Glutamate Transporter-deficient Mice*. *Journal of Biological Chemistry* **280**, 37423-37429, doi:<https://doi.org/10.1074/jbc.M506439200> (2005).
- 64 Gout, P. W., Buckley, A. R., Simms, C. R. & Bruchovsky, N. Sulfasalazine, a potent suppressor of lymphoma growth by inhibition of the x(c)- cystine transporter: a new action for an old drug. *Leukemia* **15**, 1633-1640, doi:10.1038/sj.leu.2402238 (2001).
- 65 Dolma, S., Lessnick, S. L., Hahn, W. C. & Stockwell, B. R. Identification of genotype-selective antitumor agents using synthetic lethal chemical screening in engineered human tumor cells. *Cancer Cell* **3**, 285-296, doi:[https://doi.org/10.1016/S1535-6108\(03\)00050-3](https://doi.org/10.1016/S1535-6108(03)00050-3) (2003).
- 66 Robe, P. A. *et al.* Early termination of ISRCTN45828668, a phase 1/2 prospective, randomized study of sulfasalazine for the treatment of progressing malignant gliomas in adults. *BMC Cancer* **9**, 372, doi:10.1186/1471-2407-9-372 (2009).
- 67 Azadkhan, A. K., Truelove, S. C. & Aronson, J. K. The disposition and metabolism of sulphasalazine (salicylazosulphapyridine) in man. *Br J Clin Pharmacol* **13**, 523-528, doi:10.1111/j.1365-2125.1982.tb01415.x (1982).
- 68 Stockwell, B. R. & Jiang, X. The Chemistry and Biology of Ferroptosis. *Cell Chem Biol* **27**, 365-375, doi:10.1016/j.chembiol.2020.03.013 (2020).
- 69 Bolli, E. *et al.* A Virus-Like-Particle immunotherapy targeting Epitope-Specific anti-xCT expressed on cancer stem cell inhibits the progression of metastatic cancer in vivo. *Oncoimmunology* **7**, e1408746, doi:10.1080/2162402x.2017.1408746 (2018).
- 70 Donofrio, G. *et al.* Bovine herpesvirus 4-based vector delivering the full length xCT DNA efficiently protects mice from mammary cancer metastases by targeting cancer stem cells. *Oncoimmunology* **7**, e1494108, doi:10.1080/2162402x.2018.1494108 (2018).
- 71 Zhou, B., Xiao, J. F., Tuli, L. & Ressom, H. W. LC-MS-based metabolomics. *Mol Biosyst* **8**, 470-481, doi:10.1039/c1mb05350g (2012).

- 72 Dettmer, K., Aronov, P. A. & Hammock, B. D. Mass spectrometry-based metabolomics. *Mass Spectrom Rev* **26**, 51-78, doi:10.1002/mas.20108 (2007).
- 73 Issaq, H. J., Van, Q. N., Waybright, T. J., Muschik, G. M. & Veenstra, T. D. Analytical and statistical approaches to metabolomics research. *J Sep Sci* **32**, 2183-2199, doi:10.1002/jssc.200900152 (2009).
- 74 Fiehn, O. Metabolomics – the link between genotypes and phenotypes. *Plant Molecular Biology* **48**, 155-171, doi:10.1023/A:1013713905833 (2002).
- 75 Lopes, A. S., Cruz, E. C., Sussulini, A. & Klassen, A. Metabolomic Strategies Involving Mass Spectrometry Combined with Liquid and Gas Chromatography. *Adv Exp Med Biol* **965**, 77-98, doi:10.1007/978-3-319-47656-8_4 (2017).
- 76 Villas-Bôas, S. G., Mas, S., Akesson, M., Smedsgaard, J. & Nielsen, J. Mass spectrometry in metabolome analysis. *Mass Spectrom Rev* **24**, 613-646, doi:10.1002/mas.20032 (2005).
- 77 Jacob, M., Lopata, A. L., Dasouki, M. & Abdel Rahman, A. M. Metabolomics toward personalized medicine. *Mass Spectrom Rev* **38**, 221-238, doi:10.1002/mas.21548 (2019).
- 78 Schmidt, D. R. *et al.* Metabolomics in cancer research and emerging applications in clinical oncology. *CA Cancer J Clin* **71**, 333-358, doi:<https://doi.org/10.3322/caac.21670> (2021).
- 79 Schraw, J. M. *et al.* Metabolomic profiling identifies pathways associated with minimal residual disease in childhood acute lymphoblastic leukaemia. *EBioMedicine* **48**, 49-57, doi:10.1016/j.ebiom.2019.09.033 (2019).
- 80 Virgiliou, C., Gika, H. G. & Theodoridis, G. A. in *Metabolic Profiling: Methods and Protocols* (eds Georgios A. Theodoridis, Helen G. Gika, & Ian D. Wilson) 65-81 (Springer New York, 2018).
- 81 Alseekh, S. *et al.* Mass spectrometry-based metabolomics: a guide for annotation, quantification and best reporting practices. *Nature Methods* **18**, 747-756, doi:10.1038/s41592-021-01197-1 (2021).
- 82 Jang, C., Chen, L. & Rabinowitz, J. D. Metabolomics and Isotope Tracing. *Cell* **173**, 822-837, doi:<https://doi.org/10.1016/j.cell.2018.03.055> (2018).
- 83 Pitt, J. J. Principles and applications of liquid chromatography-mass spectrometry in clinical biochemistry. *Clin Biochem Rev* **30**, 19-34 (2009).
- 84 Liu, Y. *et al.* The genomic landscape of pediatric and young adult T-lineage acute lymphoblastic leukemia. *Nat Genet* **49**, 1211-1218, doi:10.1038/ng.3909 (2017).
- 85 Verboom, K. *et al.* A comprehensive inventory of TLX1 controlled long non-coding RNAs in T-cell acute lymphoblastic leukemia through polyA+ and total RNA sequencing. *Haematologica* **103**, e585-e589, doi:10.3324/haematol.2018.190587 (2018).
- 86 Kemp, K. & Poe, C. Stressed: The Unfolded Protein Response in T Cell Development, Activation, and Function. *Int J Mol Sci* **20**, 1792, doi:10.3390/ijms20071792 (2019).
- 87 Meyers, R. M. *et al.* Computational correction of copy number effect improves specificity of CRISPR–Cas9 essentiality screens in cancer cells. *Nat Genet* **49**, 1779-1784, doi:10.1038/ng.3984 (2017).
- 88 Van Trimont, M. *et al.* Novel Insights on the Use of L-Asparaginase as an Efficient and Safe Anti-Cancer Therapy. *Cancers (Basel)* **14**, 902, doi:10.3390/cancers14040902 (2022).
- 89 Jiang, G. *et al.* Comprehensive comparison of molecular portraits between cell lines and tumors in breast cancer. *BMC Genomics* **17 Suppl 7**, 525-525, doi:10.1186/s12864-016-2911-z (2016).
- 90 Vincent, K. M., Findlay, S. D. & Postovit, L. M. Assessing breast cancer cell lines as tumour models by comparison of mRNA expression profiles. *Breast Cancer Research* **17**, 114, doi:10.1186/s13058-015-0613-0 (2015).
- 91 Domcke, S., Sinha, R., Levine, D. A., Sander, C. & Schultz, N. Evaluating cell lines as tumour models by comparison of genomic profiles. *Nat Commun* **4**, 2126, doi:10.1038/ncomms3126 (2013).
- 92 Chen, B., Sirota, M., Fan-Minogue, H., Hadley, D. & Butte, A. J. Relating hepatocellular carcinoma tumor samples and cell lines using gene expression data in translational research. *BMC Medical Genomics* **8**, S5, doi:10.1186/1755-8794-8-S2-S5 (2015).
- 93 Peng, H.-Y. *et al.* Metabolic Reprogramming and Reactive Oxygen Species in T Cell Immunity. *Frontiers in Immunology* **12**, doi:10.3389/fimmu.2021.652687 (2021).
- 94 Zhao, R. Z., Jiang, S., Zhang, L. & Yu, Z. B. Mitochondrial electron transport chain, ROS generation and uncoupling (Review). *Int J Mol Med* **44**, 3-15, doi:10.3892/ijmm.2019.4188 (2019).
- 95 Yarosz, E. L. & Chang, C.-H. The Role of Reactive Oxygen Species in Regulating T Cell-mediated Immunity and Disease. *Immune Netw* **18**, e14-e14, doi:10.4110/in.2018.18.e14 (2018).

- 96 Fine, B. M., Kaspers, G. J., Ho, M., Loonen, A. H. & Boxer, L. M. A genome-wide view of the in vitro response to L-asparaginase in acute lymphoblastic leukemia. *Cancer Res* **65**, 291-299 (2005).
- 97 Yin, F. *et al.* Microarray-based identification of genes associated with prognosis and drug resistance in ovarian cancer. *Journal of Cellular Biochemistry* **120**, 6057-6070, doi:<https://doi.org/10.1002/jcb.27892> (2019).
- 98 Robert, S. M. *et al.* SLC7A11 expression is associated with seizures and predicts poor survival in patients with malignant glioma. *Sci Transl Med* **7**, 289ra286-289ra286, doi:10.1126/scitranslmed.aaa8103 (2015).
- 99 Zhang, L. *et al.* Overexpression of SLC7A11: a novel oncogene and an indicator of unfavorable prognosis for liver carcinoma. *Future Oncol* **14**, 927-936, doi:10.2217/fon-2017-0540 (2018).
- 100 Pardieu, B. *et al.* Cystine uptake inhibition potentiates front-line therapies in acute myeloid leukemia. *Leukemia*, doi:10.1038/s41375-022-01573-6 (2022).
- 101 Chiu, M., Taurino, G., Bianchi, M. G., Kilberg, M. S. & Bussolati, O. Asparagine Synthetase in Cancer: Beyond Acute Lymphoblastic Leukemia. *Front Oncol* **9**, doi:10.3389/fonc.2019.01480 (2020).
- 102 Lin, C.-Y. *et al.* Deficiency in asparagine synthetase expression in rectal cancers receiving concurrent chemoradiotherapy: negative prognostic impact and therapeutic relevance. *Tumor Biology* **35**, 6823-6830, doi:10.1007/s13277-014-1895-z (2014).
- 103 Su, N. *et al.* Correlation between asparaginase sensitivity and asparagine synthetase protein content, but not mRNA, in acute lymphoblastic leukemia cell lines. *Pediatr Blood Cancer* **50**, 274-279, doi:10.1002/pbc.21213 (2008).
- 104 Shah, B. D. *et al.* Multi-Institution Review of Adult Early T-Cell Precursor Acute Lymphoblastic Leukemia/Lymphoma (ETP-ALL). *Blood* **126**, 3715, doi:<https://doi.org/10.1182/blood.V126.23.3715.3715> (2015).
- 105 Liu, X. *et al.* Cystine transporter regulation of pentose phosphate pathway dependency and disulfide stress exposes a targetable metabolic vulnerability in cancer. *Nat Cell Biol* **22**, 476-486, doi:10.1038/s41556-020-0496-x (2020).
- 106 Hermanova, I. *et al.* Pharmacological inhibition of fatty-acid oxidation synergistically enhances the effect of L-asparaginase in childhood ALL cells. *Leukemia* **30**, 209-218, doi:10.1038/leu.2015.213 (2016).
- 107 Purwaha, P., Lorenzi, P. L., Silva, L. P., Hawke, D. H. & Weinstein, J. N. Targeted metabolomic analysis of amino acid response to L-asparaginase in adherent cells. *Metabolomics* **10**, 909-919, doi:10.1007/s11306-014-0634-1 (2014).
- 108 Wishart, D. S. *et al.* HMDB 5.0: the Human Metabolome Database for 2022. *Nucleic Acids Res* **50**, D622-D631, doi:10.1093/nar/gkab1062 (2021).
- 109 Goji, T., Takahara, K., Negishi, M. & Katoh, H. Cystine uptake through the cystine/glutamate antiporter xCT triggers glioblastoma cell death under glucose deprivation. *Journal of Biological Chemistry* **292**, 19721-19732, doi:<https://doi.org/10.1074/jbc.M117.814392> (2017).
- 110 Rashkovan, M. & Ferrando, A. Metabolic dependencies and vulnerabilities in leukemia. *Genes Dev* **33**, 1460-1474, doi:10.1101/gad.326470.119 (2019).
- 111 Wang, L. *et al.* ATF3 promotes erastin-induced ferroptosis by suppressing system Xc⁻. *Cell Death & Differentiation* **27**, 662-675, doi:10.1038/s41418-019-0380-z (2020).
- 112 Sato, M. *et al.* The ferroptosis inducer erastin irreversibly inhibits system xc⁻ and synergizes with cisplatin to increase cisplatin's cytotoxicity in cancer cells. *Sci Rep* **8**, 968, doi:10.1038/s41598-018-19213-4 (2018).
- 113 Dixon, S. J. *et al.* Pharmacological inhibition of cystine-glutamate exchange induces endoplasmic reticulum stress and ferroptosis. *Elife* **3**, e02523, doi:10.7554/eLife.02523 (2014).
- 114 Haß, C., Belz, K., Schoeneberger, H. & Fulda, S. Sensitization of acute lymphoblastic leukemia cells for LCL161-induced cell death by targeting redox homeostasis. *Biochemical Pharmacology* **105**, 14-22, doi:<https://doi.org/10.1016/j.bcp.2016.01.004> (2016).
- 115 Sun, Y., Deng, R. & Zhang, C. Erastin induces apoptotic and ferroptotic cell death by inducing ROS accumulation by causing mitochondrial dysfunction in gastric cancer cell HGC-27. *Mol Med Rep* **22**, 2826-2832, doi:10.3892/mmr.2020.11376 (2020).
- 116 Boutter, J. *et al.* Image-based RNA interference screening reveals an individual dependence of acute lymphoblastic leukemia on stromal cysteine support. *Oncotarget* **5**, 11501-11512, doi:10.18632/oncotarget.2572 (2014).

9. Poster

L-asparaginase treatment modulates SLC7A11 expression in T-cell acute lymphoblastic leukemia

Amber Boutens, Julie Morscio, Pieter van Vlierberghe

Department of Biomolecular Medicine, Ghent University, Ghent, Belgium

Introduction and objectives

T-cell acute lymphoblastic leukemia (T-ALL) is an aggressive hematological malignancy that arises from T-cell progenitors. Despite high dose multiagent chemotherapy regimens, still a significant number of patients experience therapy failure. Unfortunately, the underlying mechanisms for this therapy resistance are mostly unknown. Preliminary experiments showed that solute carrier family 7 member 11 (SLC7A11), the light chain functional subunit of the cystine/glutamate antiporter system x_c^- , is transiently upregulated after L-asparaginase treatment. This suggests that this antiporter could be involved in therapy resistance.

The aim of this study is to further explore the effect of L-asparaginase treatment on the SLC7A11 antiporter.

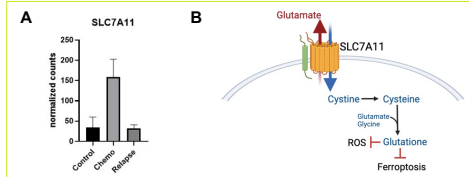


Figure 1. (A) RNA-Seq data of SLC7A11 expression in hCD45⁺ T-cells of chemotherapy-treated versus control T-ALL PDX models. SLC7A11 gene expression is transiently upregulated after chemotherapy treatment. (B) SLC7A11 imports cystine in exchange for glutamate (1:1). Once imported, cystine is converted into cysteine, the rate-limiting precursor for glutathione synthesis. Glutathione can protect cells both from oxidative stress caused by reactive oxygen species (ROS) and ferroptosis caused by lipid hydroperoxides.

Methods

Two T-ALL cell lines, KOPT-K1 and Loucy, were treated for 48 hours with either L-asparaginase (IC₅₀) or vehicle. Subsequently, 2 million cells were pelleted, further processed and analyzed for metabolites as described in figure 2. On the remainder of the cells, RNA was extracted for a SLC7A11 qPCR analysis.

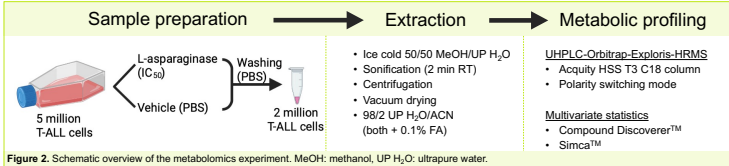


Figure 2. Schematic overview of the metabolomics experiment. MeOH: methanol, UP H₂O: ultrapure water.

Results

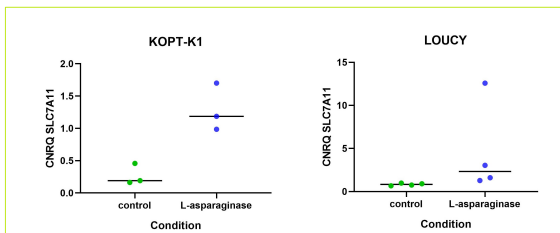


Figure 3. RT-qPCR results showing that L-asparaginase, a compound incorporated in standard T-ALL treatment regimens, upregulates SLC7A11 expression in KOPT-K1 and Loucy T-ALL cell lines (One tailed two sample t-test, $p = .01$).

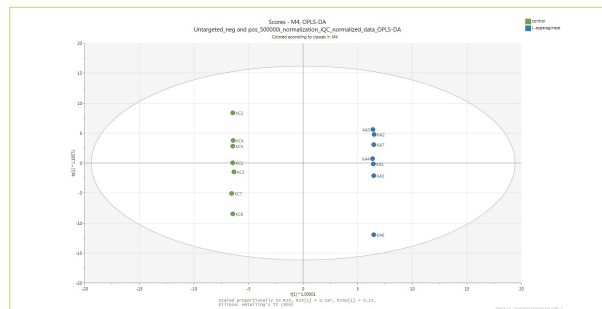


Figure 5. OPLS-DA score plot of L-asparaginase treated versus control KOPT-K1 T-ALL cells allowing to predict group membership based on differences in the metabolome. The plot shows a separation by phenotype between the L-asparaginase-treated and the control group, indicating a change in the metabolomic profile of KOPT-K1 T-ALL cells after treatment.

Conclusion

SLC7A11 is upregulated in various T-ALL cells after L-asparaginase treatment. L-asparaginase treatment changes the intracellular amino acid content in line with its mechanism of action. The metabolic profile can distinguish treated from untreated KOPT-K1 cells, suggesting that SLC7A11 upregulation induces metabolic changes in T-ALL cells which might be involved in therapy resistance. **SLC7A11 represents a potential chemotherapy-induced therapeutic target in T-ALL.**

Contact: Amber.Boutens@ugent.be

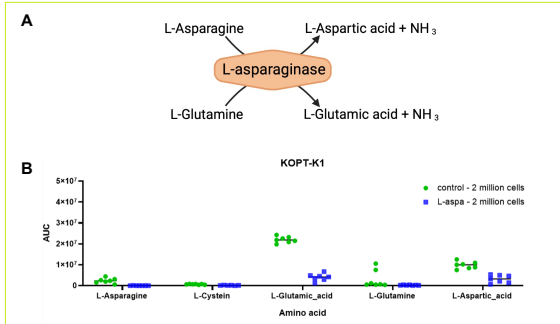


Figure 4. (A) L-asparaginase exerts its anti-leukemic effect not only by catalyzing the extracellular degradation of L-asparaginase into L-aspartic acid and ammonia (NH₃), but also by converting L-glutamine into L-glutamic acid and NH₃ via its glutaminase activity. (B) Metabolic profiling of the intracellular amino acid content of L-asparaginase-treated versus control T-ALL cell lines. L-asparagine, L-glutamic acid and L-aspartic acid levels are decreased after L-asparaginase treatment.

10. Addendum

Gene of interest (5 μ M)	
SLC7A11	Fw - TCCTGCTTTGGCTCCATGAACG
	Rv - AGAGGAGTGTGCTTGCGGACAT
Reference genes (5 μ M)	
TBP	Fw - CACGAACCACGGCACTGATT
	Rv - TTTTCTTGCTGCCAGTCTGGAC
UBC	Fw - ATTTGGTGCGCGTTCTTG
	Rv - TGCCTTGACATTCTCGATGGT
YWHAZ	Fw - ACTTTTGGTACATTGTGGCTTCAA
	Rv - CCGCCAGGACAAACCAGTAT
HMBS	Fw - GGCAATGCGGCTGCAA
	Rv - GGGTACCCACGCGAATCAC
SDHA	Fw - TGGGAACAAGAGGGCATCTG
	Rv - CCACCACTGCATCAAATTCATG

Supplementary Table 1 – Forward and reverse primer sequences of genes used in the qRT-PCR experiments. All primers were purchased at Integrated DNA Technologies and diluted to a concentration of 5 μ M.

A

ID194_D-Aspartic_acid
ID200_D-alanine
 ID193_D-alfa-aminobutyric_acid
 ID007_Glycerol
 ID020_D-Glucuronic_acid
 ID071_Glucaric_acid
 ID134_D-Gluconic_acid_solution
 ID244_Allantoin
 ISTD
 ID222_2-(Dimethylamino)acetonitrile
 ID009_1,3-Propanediol
 ID045_Mesalazine
 ID084_DL-Maleic_acid
 ID057_Acetic_acid_optima
 ID072_3-Hydroxybutyric_acid
 ID105_gamma-Butyrolactone
 ID010_Pyrogallol
 ID580_DL-Phenylalanine
 ID026_3,4-Dihydroxybenzoic_acid
 ID023_3,4-Dihydroxyphenylacetic_acid_n
 D206_N-Acetyl-L-methionine
 ID232_2,6-Dimethylpyrazine
 ID003_3-(Methylthio)-1-propanol
 ID059_Butyric_acid
 ID024_3,4-Dihydroxyhydrocinnamic_acid
 ID030_4-Hydroxyphenylacetic_acid
 ID047_Phenylacetic_acid
 ID021_Caffeic_acid
 ID032_3-Hydroxybenzoic_acid
 ID074_2-Hydroxyhexanoic_acid
 ID031_3-(4-Hydroxyphenyl)propionic_acid
 ID022_Suberic_acid
 ID002_2-Butoxyethanol
 ID066_(S)-(+)-2-Methylbutyric_acid
 ID042_Sinapic_acid
 ID040_trans-3-Hydroxycinnamic_acid
 ID046_Benzoic_acid
 ID161_4-Methyl-3-penten-2-one
 ID050_4-Methylvaleric_acid
 ID017_Hesperetin
 ID018_Naringenin
 ID048_3-Phenylpropionic_acid=ID1509
 ID151_2-Methyl-3-pentanone
 ID288_Glycoursodeoxycholic_acid_(GUC)
 ID061-Octanoic_acid
 ID156_3-Heptanone
 ID167_trans_3-Octen-2-one
 ID113_Hexyl_propionate
 ID063_Dodecanoic_acid_(Lauric_acid)
 ID149_2-Dodecanone
 ID067_Eicosapentaenoic_acid

B

ID189_L-Lysine
 ID195_D-Glutamic_acid
 ID127_D(-)-Ribose
 ID130_Maltose
 ID173_L-Proline
 ID192_2-Aminoisobutyric_acid
 ID015_D-Pinitol
 ID107_L-Gulonic_gamma-lactonew
 ID184_5-aminovaleric_acid
 ID186_beta-Alanine
 ID187_Thiazolidine-4-carboxylic_acid
 ID190_L-Cysteine_hydrochloride
 ISTD
 ID182_D-Valine-d8
 ID095_Malonic_acid
 ID120_L-ascorbic_acid
 ID087_Fumaric_acid
 ID162_Acetoin
 ID090_Glutaric_acid
 ID029_Gentisic_acid
 ID1542_N-acetylvaline
 ID037_4-Hydroxybenzoic_acid
 ID231_2,5-Dimethylpyrazine
 ID027_3,4-Dihydroxyhydrocinnamic_acid
 ID159_3-Penten-2-one
 ID044_Vanillic_acid
 ID324_4-Methyl-2-oxovaleric_acid
 ID144_2,3-Heptanedione_NOK
 ID106_gamma-Caprolactone
 ID033_2-Hydroxyphenylacetic_acid
 ID157_3-Methyl-2-cyclohexen-1-one
 ID154_2-Pentanone
 ID123_1,3-Dimethoxybenzene-NOK
 ID147_2-Acetyl-5-methylfuran
 ID034_3-(2-Hydroxyphenyl)propionic_acid
 ID160_4-Hexen-3-one
 ID118_Methyl_isobutyrate
 ID051_Hexanoic_acid
 ID150_2-Hexanone
 ID163_Acetophenone
 ID004_3-Phenyl-1-propanol
 ID103_S-Methyl_butaneithioate
 ID112_Ethyl_heptanoate
 ID283_Sodium_taurodeoxycholate_hydrate_(T)
 ID284_Sodium_glycodeoxycholate_(GDCA)
 ID735_Skatole_(3-Methylindole)
 ID143_1-Octen-3-one
 ID117_Methyl_cyclohexanecarboxylate
 ID148_2-Decanone
 ID111_Ethyl_decanoate
 ID155_2-Tridecanone

C

ID216_Spermine
 ID211_Sarcosine
 ID012_Mannitol
 ID292_Metformin_(1,1-Dimethylbiguanide_hydr)
 ID239_Pyridine
 ID273_rac-Glycerol_1-phosphate
 ID309_D-Erythronic_acid
 ID311_L-Dihydroorotic_acid
 ID318_D(+)-Xylose
 ISTD
 ID274_Phospho(enol)pyruvic_acid
 ID272_Adenosine_5'-diphosphate
 ID238_Pyrimidine
 ID005_alfa-Tocopherol_NOK
 ID221_Cyclohexylamine
 ID234_2-Methylpyrazine
 ID235_4-Methylthiazole
 ID303_beta-Phenylethylamine
 ID472_trans-Zeatin
 ID060_Isobutyric_acid
 ID567_Pantolactone
 ID952_Butyrlcarnitine
 ID246_Crotonaldehyde
 ID256_Furfural
 ID204_Pyrrole-2-carboxylic_acid
 ID255_Phenylacetaldehyde-NOK
 ID1529_Methyl_nicotinate
 ID241_Thiabendazole
 ID229_N-Nitrosodiethylamine
 ID036_3-Hydroxyphenylacetic_acid
 ID252_3-Methyl-2-butenal
 ID1707_D-biotin
 ID233_2-Acetyl-2-thiazoline
 ID038_Desaminotyrosine
 ID165_Cyclohexanone
 ID299_DL-Hexanoylcarnitine_chloride
 ID041_Salicylic_acid
 ID321_L-Thyroxine_(T4)
 ID879_Glycitein
 ID280_Taurocholic_acid_sodium
 ID278_Tauroursodeoxycholic_acid
 ID258_Cinnamaldehyde
 ID323_Corticosterone
 ID214_Tolbutamide
 ID146_2,4-Dimethyl-3-pentanone
 ID282_Sodium_glycochenodeoxycholate_(GC)
 ID302_Lyso-phosphatidylcholine_C14:0_(14:0)
 ID213_Glyburide_(Glibenclamide)
 ID209_Palmitoyl-L-carnitine
 ID208_Oleoyl-L-carnitine
 ID287_Glycolithocholic_acid_(GLCA)

D

ID1410_1-methylhistamine
 ID328_S-(5I-Adenosyl)-L-methionine
 ID176_L-Aspartic_acid
 ID197_L-Asparagine
 ID460_Triethanolamine_hydrochloride
 ID509_L-2-Aminobutyric_acid
 ID852_Pyridin
 ID304_6-Phosphogluconic_acid
 ID507_D(-)Quinic_acid
 ISTD
 ID1067__L(+)-L-Ascorbic_Acid
 ID297_Adenosine_5-monophosphate
 ID540_Nicotinamide
 ID515_4-Vinylpyridine
 ID538_Adenosine_(Adenosyl)
 ID454_6-O-Methylguanine
 ID326_3-Methoxytyramine
 ID1501_3-Methyl-2-oxobutyric_acid
 ID487_Pantothenic_acid
 ID560_(+/-)Pantothenol
 ID577_2-Acetylthiazole
 ID062_L-3-Phenyllactic_acid
 ID471_Gibberellic_acid_(GA3)
 ID1477_N-acetyl-DL-tryptophan
 ID1408_Indole-3-carboxaldehyde_(I3A)
 ID1405_trans-3-Indoleacrylic_acid
 ID1407_3-(2-Hydroxyethyl)indole_(Tryptophol)
 ID330_3,3',5-Triiodo-L-tyrosine_(T3)
 ID470_Abscisic_acid
 ID290_Cortisol
 ID953_Decanoylcarnitine
 ID873_Genistein
 ID877_Coumestrol
 ID878_Equol
 ID286_Taurochenodeoxycholic_acid_sodium_s
 ID869_Chrysin
 ID1409_D-erythro-dihydrosphingosine
 ID279_Ursodeoxycholic_acid_(UDCA)
 ID329_Testosterone
 ID876_Biochanin_A
 ID322_Deoxycorticosterone
 ID559_Allylanthranilate
 ID508_Carvacrol
 ID501_trans,trans-2,4-Decadienal
 ID1469_Linoleamide

E

ID1479_N6,N6-dimethyllysine
 ID1431_Phosphocholine
 ID1414_L(-)-Aralitol
 ID1465_N1-methylnicotinamide
 ID1478_L-Methionine_sulfone
 ID1419_D-(+)-Fucose
 ID1492_Orotic_acid
 ID1493_Methylguanidine
 ISTD
 ID1462_Homocysteine
 ID1467_N6-acetyl-L-lysine
 ID1415_3,4-Dihydroxyphenylalanine_(L-DOP)
 ID1488_N-Acetylglycine
 ID1430_7-Methylguanosine
 ID1424_2,4,6-Trimethyl-pyridine
 ID1432_Isobutyrylglycine
 ID1502_2-Oxoisopentanoate
 ID1428_Adipoylcarnitine_(C16)
 ID1506_3,5-Dihydroxybenzoic_acid
 ID1425_Alpha-hydroxyisovalerate
 ID1494_Ethylmalonate
 ID1483_N-Tigloylglycine
 ID1495_N-Isovalerylglycine
 ID575_5-Hydroxytryptophol
 ID1496_2-Methylbutyryl-L-carnitine
 ID1500_Homovanillic_acid
 ID1486_Bradykinin_acetate_salt
 ID1505_4-Hydroxybenzaldehyde
 ID1548_DL-leucyl-dl-phenylalanine
 ID1438_trans-2-Octenoyl-L-carnitine
 ID1481_Octanoyl-L-carnitine_C8:0
 ID1468_Aldosterone
 ID1499_3,4,5-Trimethoxycinnamic_acid
 ID871_Daidzein
 ID1480_Decanoyl-L-carnitine_(C10:0)
 ID1509_3-Phenylpropionate
 ID1435_Dodecanoylcarnitine_(12:1)
 ID1426_Dodecanoylcarnitine_C12:0
 ID1474_Dehydroisoandrosterone_sulfate_(DH)
 ID872_Formononetin
 ID1461_Hydroxyhexadecanoylcarnitine_(C16)
 ID1427_Tetradecanoylcarnitine_C14:0
 ID1437_Glycolithocholate_sulfate
 ID1491_2-Methoxyestradiol
 ID1441_trans-2-Hexadecanoyl-L-carnitine
 ID1412_Myristoleic_acid_(14:1_n5)
 ID1436_N-arachidonoylethanolamide
 ID1459_Anandamide_C17:1
 ID1440_N-palmitoylglycine
 ID1498_Stearamide_(Octadecanamide)

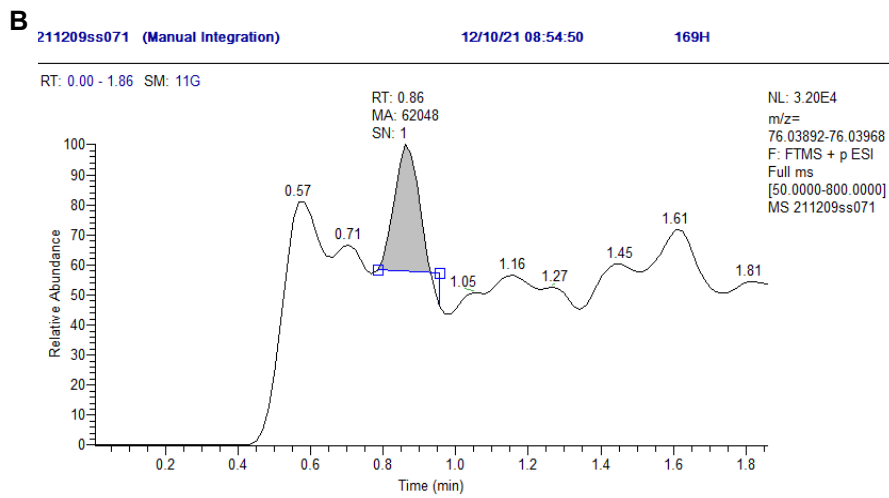
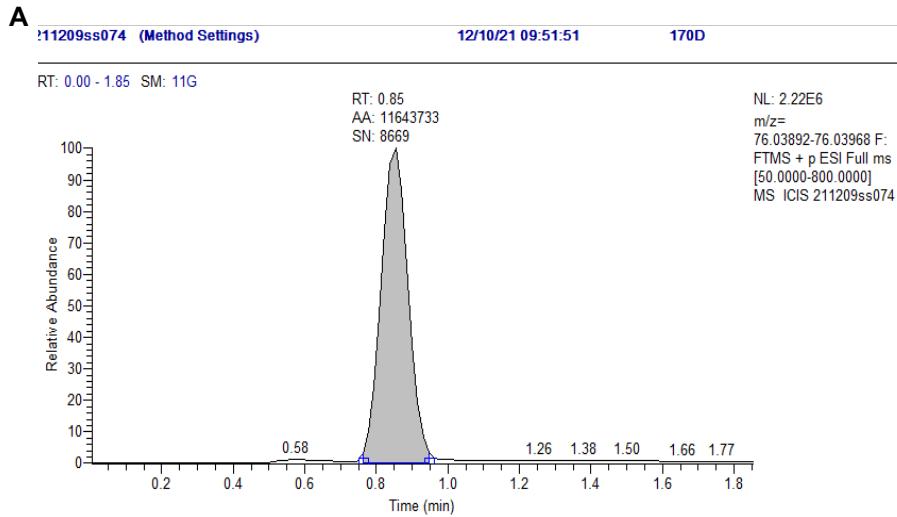
F

ID1580_Agmatine_sulfate
 ID1603_Glucosamine
 ID1608_L-cysteine
 ID1567_N-acetylglucosamine_1-phosphate
 ID1541_D(-)-3-Phosphoglyceric_acid
 ID1512_2-Hydroxyethanesulfonate
 ID1538_Hypotaurine
 ID1544_Xylitol(=ribitol)
 ID1545_L-threonic_acid
 ID1703_Thiamine
 ISTD
 ID1533_N-acetyl-arginine
 ID1581_4-guanidinobutyric_acid
 ID1704_Pyridoxine
 ID1543_2-picolinic_acid
 ID1565_Pseudouridine
 ID1582_N-Acetylglutamine_(acetate_salt)
 ID1534_S-adenosylhomocysteine_(SAH)
 ID1525_(-)Cotinine
 ID1522_3-Hydroxy-3-methylglutarate
 ID1519_2'-Deoxyuridine
 ID1600_N-Acetyl-L-cysteine
 ID1524_Leucylglycine
 ID1429_8-Hydroxy-2I-deoxyguanosine
 ID1571_N6-methyladenosine
 ID1517_4-Hydroxyphenylpyruvic_acid
 ID1532_(R)-Pantetheine
 ID1550_3-Methyl-2-oxopentanoic_acid
 ID1569_Gamma-glutamylphenylalanine
 ID1514_5-Methoxytryptamine
 ID1706_Cyanocobalamin
 ID1705_Pteroylmonoglutamic_acid
 ID1708_Riboflavin
 ID1528_2,6-Dihydroxybenzoic_acid
 ID1573_2-Hydroxy-3-methylvalerate
 ID125_Dipropyl_disulfide_RTNOK
 ID310_(+/-)-2-Hydroxyisocaproic_acid
 ID1701_Retinyl_palmitate_NOK
 ID1575_3-Pentanone-2,2,4,4-d4
 ID1584_Melatonin
 ID1511_3-Hexanone_10ng_μL
 ID1690_Sulfinpyrazone
 ID1518_3-Phenylbutyric_acid
 ID510_1-Acetyl-3-indolecarboxaldehyde
 ID1689_Fenbufen
 ID1691_Sulindac
 ID1520_Piperine
 ID1570_Hexadecanamide_(Palmitamide)
 ID1530_Oleamide
 ID1523_Adrenic_acid_22:4
 ID1521_3-Ethylphenol_NOK
 ID1702_Cholecalciferol_NOK

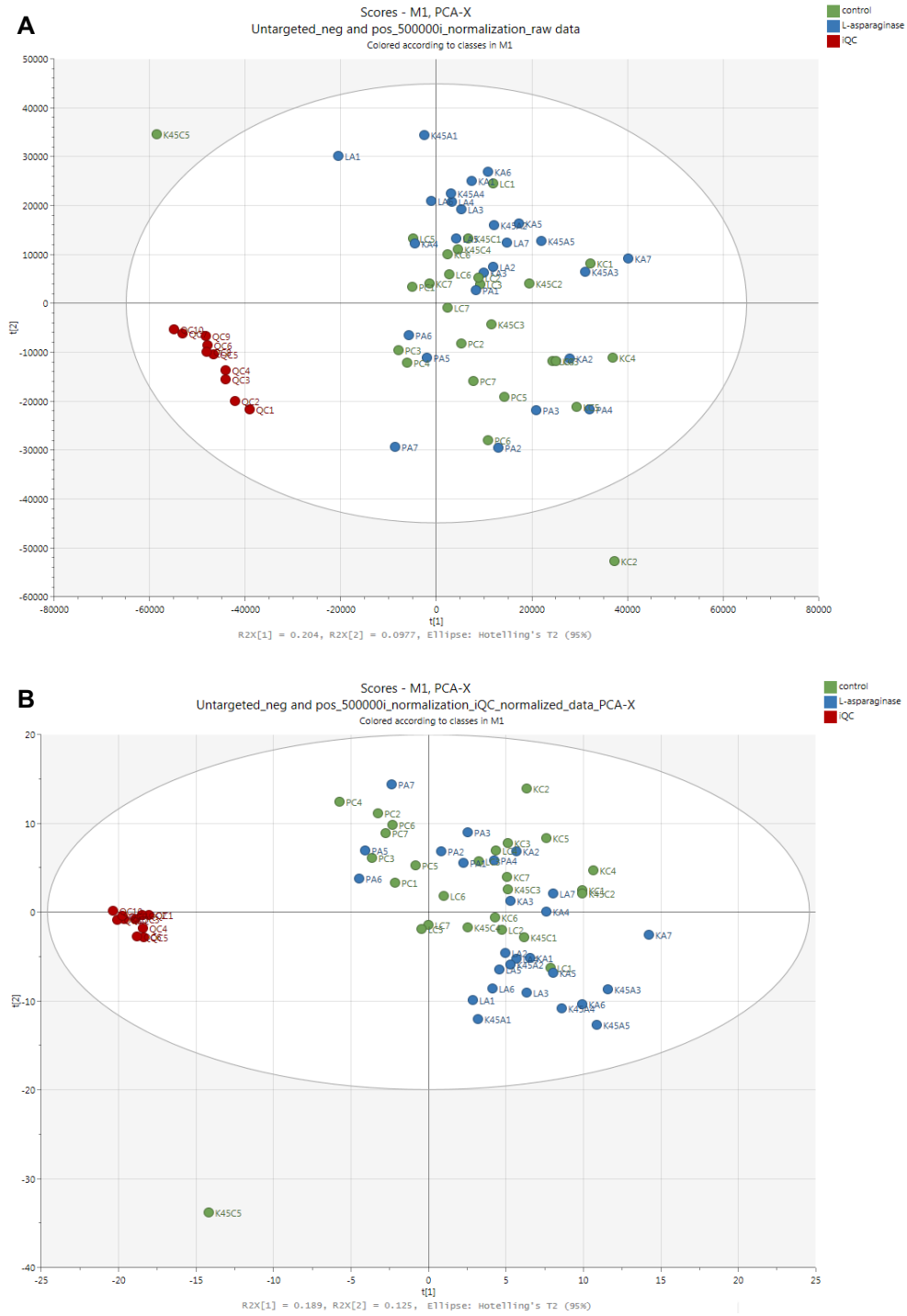
G

196_L-arginine
332_choline_chloride
562_Trimethylamine_solution
169_21_L-alanine
331_Alanine-d3
1345_Trimethylamine-N-oxide
294_L-carnitine
316_creatinine
131_glucose
315_creatine
ISTD
76_Malic_acid
558_cytidine
576_Adenine
170_21_L-valine
523_Guanine
1551_Uric_acid
207_Acetylcarnitine
81_21_Oxoglutaric_acid
98_21_uroncanic_acid
1578_Dopamine-d4
218_Dopamine
96_21_Citric_acid
178_21_L-pyroglutamic_acid
1576_Tyrosine-d2
181_Tyrosine
172_21_L-isoleucine
224_Tyramine
171_21_L-leucine
1393_5-Hydroxytryptophan
82_Pyruvic_acid
320_Kynurenine
1583_Phenylalanine-d2
180_L-phenylalanine
212_21_2-piperidinone
86_21_Methylsuccinic_acid
185_D-pantothenic_acid_hemicalcium_salt
1585_Xanthurenic_acid
1564_N-Acetyltyrosine
223_Tryptamine
569_Kynurenic_acid
1516_Hippuric_acid
1401_Anthranilic_acid
1485_N-acetyl-L-phenylalanine
1397_indole-3-lactic_acid
49_Valeric_acid
89_Azeleic_acid
1577_Indole-3-acetic_acid-d5
201_3-indole-acetic_acid
91_Sebacic_acid
1391_Indole-3-propionic_acid
1563_7-Ketodeoxycholate
1579_Deoxycholic_acid-d4
289_DCA
277_LCA
68_21_alfa-linolenic_acid

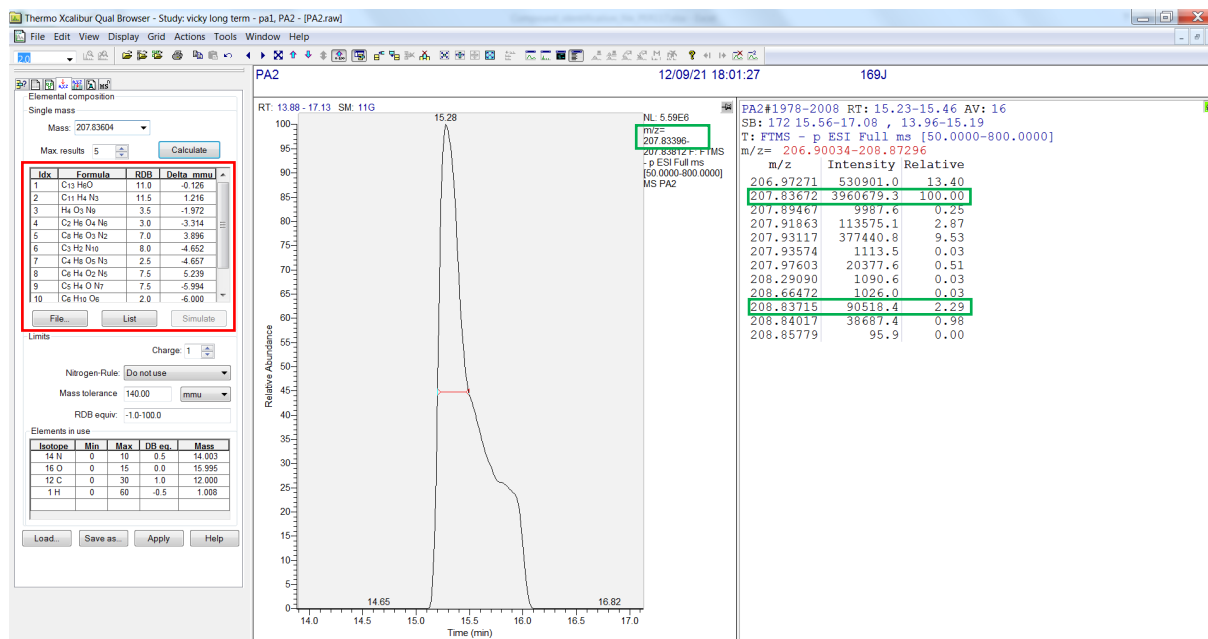
Supplementary Figure 1 – Standard mixtures of 349 target analytes, including all amino acids.
These mixtures were injected before and after the sample analyses to check the operational conditions of the device as well as to allow targeted metabolomics data analysis.



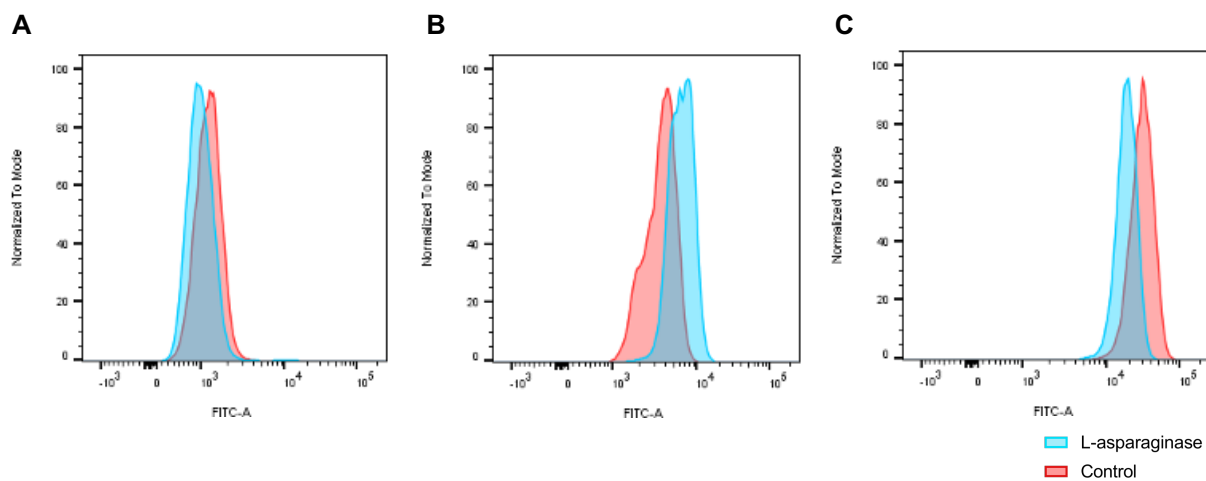
Supplementary Figure 2 – Areas under the curve (AUCs) were manually adjusted in case a peak at an amino specific retention time (RT) was not included correctly. Glycine chromatograms of two different samples showing (A) a clean peak in which no intervention was needed and (B) a peak that had to be manually selected due to high background signal.



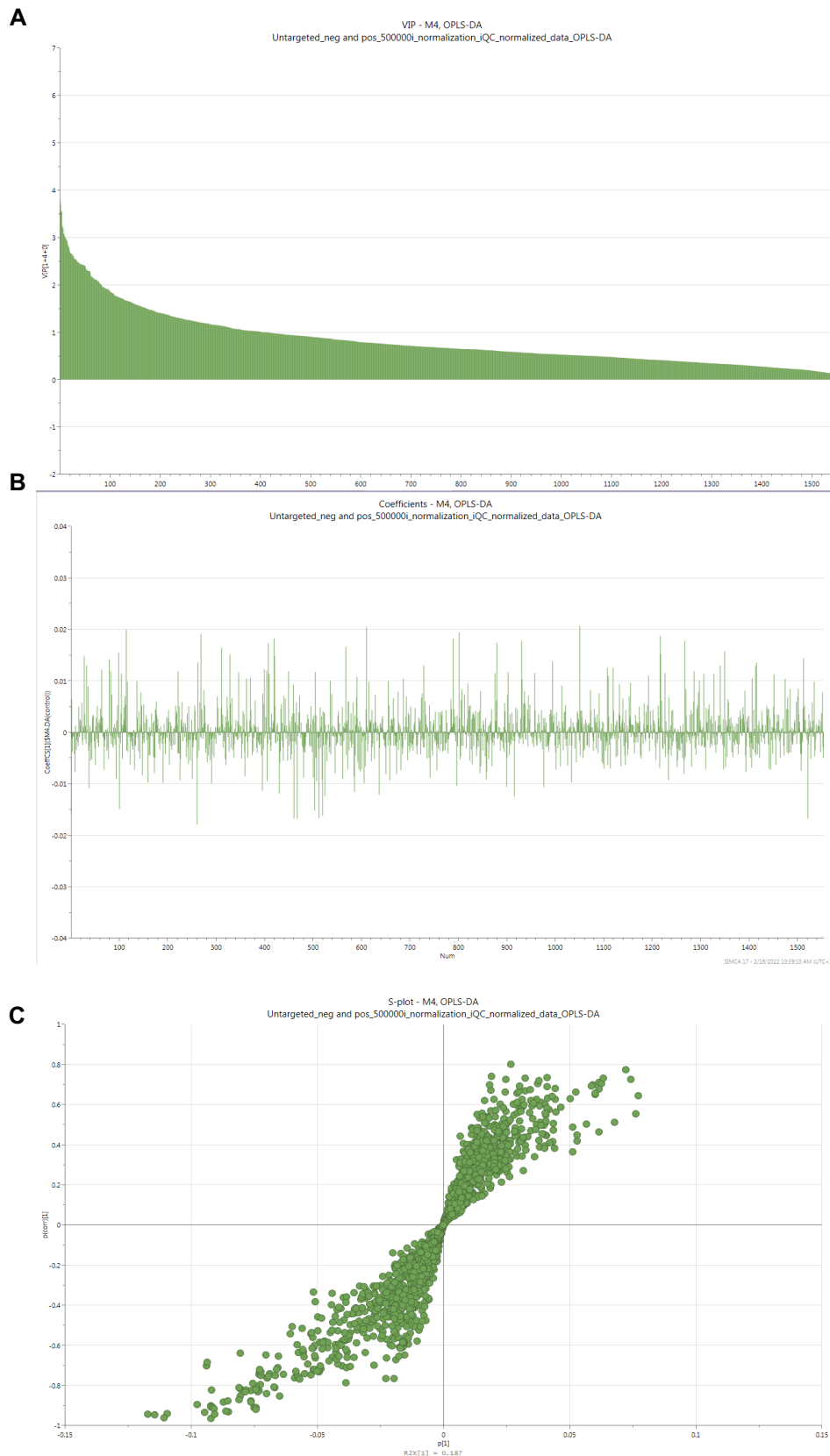
Supplementary Figure 3 – Comparison of unnormalized and normalized data. PCA-X models based on (A) unnormalized and (B) normalized AUC data. Strong clustering of internal QC (iQC) samples indicates that normalization is beneficial.



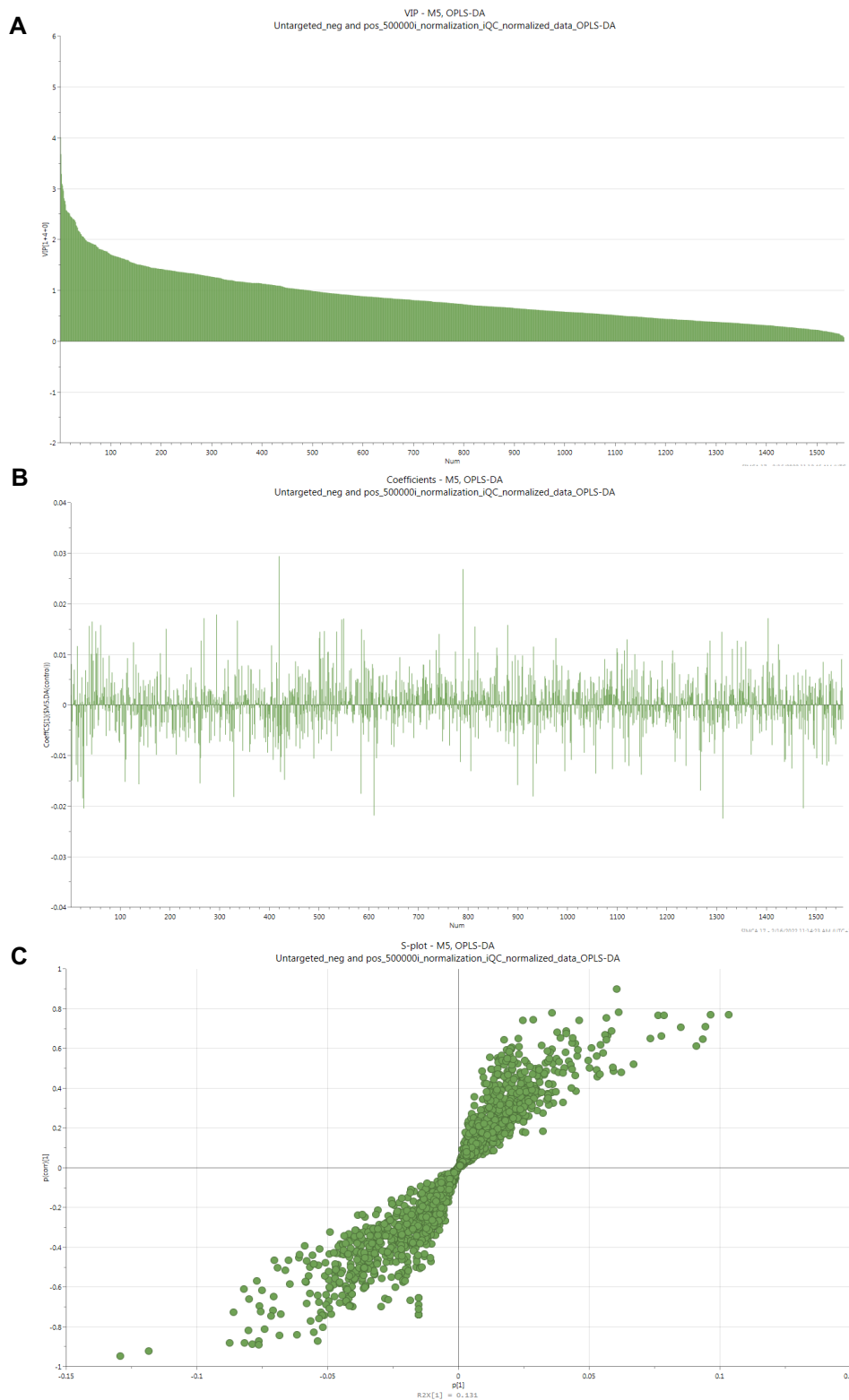
Supplementary Figure 4 – Example indicating the method used to predict the number of carbon atoms in the metabolite based on the relative abundances of ^{12}C and ^{13}C atoms. The relative abundance of ^{12}C was determined by searching the m/z value generated by Xcalibur 3.0 software (green box in the middle) in a generated list of m/z values with corresponding relative abundance values (top green box on the right). ^{13}C relative abundance were subsequently found in that same list by adding 1.008 to the m/z value of ^{12}C (bottom green box on the right). The number of carbon atoms could then be calculated as follows: $2.29/100 * 100/1.1 = 2$. Based on this number of C-atoms, a corresponding putative chemical formula was identified from a list containing suggested possible chemical formulas (red box), which was in this example $\text{C}_2\text{H}_6\text{O}_4\text{N}_6$.




Supplementary Figure 5 – L-asparaginase induced SLC7A11 upregulation modulates downstream cystine, GSH and general oxidative stress levels. Flow cytometric analysis of (A) intracellular cystine (B) cellular GSH and (C) general oxidative stress after L-asparaginase treatment of HPB-ALL cell lines.




Supplementary Figure 6 – Identification of metabolites discriminating control and L-asparaginase treated samples in the validated OPLS-DA KOPT-K1 model. Metabolites were selected based on three parameters: VIP-score > 1 (1), Jack-knifed confidence interval > 0 (2), and S-plot score $0.5 < y < -0.5$ (3). (A) VIP-score plot, (B) Jack-knifed confidence interval plot, (C) S-plot score plot of the validated OPLS-DA KOPT-K1 model.



Supplementary Figure 7 – Identification of metabolites discriminating control and L-asparaginase treated samples in the validated OPLS-DA PER-117 model. Metabolites were selected based on three parameters: VIP-score > 1 (1), Jack-knifed confidence interval > 0 (2), and S-plot score $0.5 < y < -0.5$ (3). (A) VIP-score plot, (B) Jack-knifed confidence interval plot, (C) S-plot score plot of the validated OPLS-DA PER-117 model.

A**Detailed result table**Mouse over the **Help** icon to find more information on each columns 

Pathway Name	Total ↑↓	Hits (all) ↑↓	Hits (sig.) ↑↓	Expected ↑↓	P-value ↑↓	Gamma P ↑↓	Details
Vitamin B9 (folate) metabolism	2	2	2	0.22857	0.010955	0.017691	View
Glycerophospholipid metabolism	6	6	3	0.68571	0.01586	0.017807	View
Alanine and Aspartate Metabolism	4	4	2	0.45714	0.05842	0.018851	View
Pyrimidine metabolism	5	5	2	0.57143	0.091771	0.019724	View
Lysine metabolism	5	5	2	0.57143	0.091771	0.019724	View
Chondroitin sulfate degradation	1	1	1	0.11429	0.11111	0.020255	View
Galactose metabolism	1	1	1	0.11429	0.11111	0.020255	View
Keratan sulfate degradation	1	1	1	0.11429	0.11111	0.020255	View
Caffeine metabolism	1	1	1	0.11429	0.11111	0.020255	View
Fructose and mannose metabolism	1	1	1	0.11429	0.11111	0.020255	View
Heparan sulfate degradation	1	1	1	0.11429	0.11111	0.020255	View
Porphyrin metabolism	1	1	1	0.11429	0.11111	0.020255	View
N-Glycan Degradation	1	1	1	0.11429	0.11111	0.020255	View
Nitrogen metabolism	1	1	1	0.11429	0.11111	0.020255	View
Glycine, serine, alanine and threonine metabolism	6	6	2	0.68571	0.12973	0.020783	View
Tryptophan metabolism	6	6	2	0.68571	0.12973	0.020783	View
Glycolysis and Gluconeogenesis	2	2	1	0.22857	0.21127	0.023324	View
Glycosphingolipid biosynthesis - ganglioseries	2	2	1	0.22857	0.21127	0.023324	View
Sialic acid metabolism	2	2	1	0.22857	0.21127	0.023324	View


B**Detailed result table**Mouse over the **Help** icon to find more information on each columns 

Pathway Name	Total ↑↓	Hits (all) ↑↓	Hits (sig.) ↑↓	Expected ↑↓	P-value ↑↓	Gamma P ↑↓	Details
Pyrimidine metabolism	6	6	4	1.6	0.022834	NaN	View
N-Glycan biosynthesis	4	4	3	1.0667	0.039321	NaN	View
Glycosphingolipid biosynthesis - ganglioseries	2	2	2	0.53333	0.056452	NaN	View
Glycosphingolipid biosynthesis - globoseries	2	2	2	0.53333	0.056452	NaN	View
Glycosphingolipid metabolism	2	2	2	0.53333	0.056452	NaN	View
Glycerophospholipid metabolism	5	5	3	1.3333	0.085373	NaN	View
Glycolysis and Gluconeogenesis	3	3	2	0.8	0.14677	NaN	View
Sialic acid metabolism	3	3	2	0.8	0.14677	NaN	View
Tryptophan metabolism	3	3	2	0.8	0.14677	NaN	View
Alanine and Aspartate Metabolism	3	3	2	0.8	0.14677	NaN	View
Phosphatidylinositol phosphate metabolism	3	3	2	0.8	0.14677	NaN	View
Starch and Sucrose Metabolism	3	3	2	0.8	0.14677	NaN	View
Chondroitin sulfate degradation	1	1	1	0.26667	0.25	NaN	View
Di-unsaturated fatty acid beta-oxidation	1	1	1	0.26667	0.25	NaN	View
Vitamin B2 (riboflavin) metabolism	1	1	1	0.26667	0.25	NaN	View
Keratan sulfate degradation	1	1	1	0.26667	0.25	NaN	View
Alkaloid biosynthesis II	1	1	1	0.26667	0.25	NaN	View
Vitamin B1 (thiamin) metabolism	1	1	1	0.26667	0.25	NaN	View

Supplementary Figure 8 – Differentially expressed pathways between control and L-asparaginase treated Loucy cells. Pathway analysis was performed using all identified (A) positively and (B) negatively ionized metabolites.

A

Pathway Name	Total ↑↓	Hits (all) ↑↓	Hits (sig.) ↑↓	Expected ↑↓	P-value ↑↓	Gamma P ↑↓	Details
Aminosugars metabolism	3	3	2	0.38571	0.039437	0.0027663	View
Glycosphingolipid biosynthesis - lactoseries	1	1	1	0.12857	0.125	0.0035204	View
Blood Group Biosynthesis	1	1	1	0.12857	0.125	0.0035204	View
Glycosphingolipid biosynthesis - neolactoseries	1	1	1	0.12857	0.125	0.0035204	View
Keratan sulfate biosynthesis	1	1	1	0.12857	0.125	0.0035204	View
O-Glycan biosynthesis	1	1	1	0.12857	0.125	0.0035204	View
Glycerophospholipid metabolism	6	6	2	0.77143	0.16023	0.003894	View
Glycosphingolipid biosynthesis - ganglioseries	2	2	1	0.25714	0.23592	0.0048534	View
Sialic acid metabolism	2	2	1	0.25714	0.23592	0.0048534	View
Hexose phosphorylation	2	2	1	0.25714	0.23592	0.0048534	View
Glycosphingolipid biosynthesis - globoseries	2	2	1	0.25714	0.23592	0.0048534	View
Phosphatidylinositol phosphate metabolism	2	2	1	0.25714	0.23592	0.0048534	View
N-Glycan biosynthesis	3	3	1	0.38571	0.33415	0.0065151	View
Glutathione Metabolism	3	3	1	0.38571	0.33415	0.0065151	View
Glycosphingolipid metabolism	5	5	1	0.64286	0.49764	0.010944	View
Pyrimidine metabolism	5	5	1	0.64286	0.49764	0.010944	View
Lysine metabolism	5	5	1	0.64286	0.49764	0.010944	View
Glycine, serine, alanine and threonine metabolism	6	6	1	0.77143	0.56512	0.013755	View
Aspartate and asparagine metabolism	7	7	1	0.9	0.62442	0.01698	View
Carnitine shuttle	8	8	1	1.0286	0.67642	0.020624	View

B**Detailed result table**Mouse over the **Help** icon to find more information on each columns 

Pathway Name	Total ↑↓	Hits (all) ↑↓	Hits (sig.) ↑↓	Expected ↑↓	P-value ↑↓	Gamma P ↑↓	Details
Purine metabolism	8	8	5	1.8567	0.004794	NaN	View
Pyrimidine metabolism	6	6	3	1.4	0.10101	NaN	View
Vitamin B3 (nicotinate and nicotinamide) metabolism	3	3	2	0.7	0.1129	NaN	View
Alanine and Aspartate Metabolism	3	3	2	0.7	0.1129	NaN	View
Aspartate and asparagine metabolism	4	4	2	0.93333	0.2005	NaN	View
Aminosugars metabolism	4	4	2	0.93333	0.2005	NaN	View
Di-unsaturated fatty acid beta-oxidation	1	1	1	0.23333	0.21875	NaN	View
Vitamin B2 (riboflavin) metabolism	1	1	1	0.23333	0.21875	NaN	View
Alkaloid biosynthesis II	1	1	1	0.23333	0.21875	NaN	View
Vitamin B1 (thiamin) metabolism	1	1	1	0.23333	0.21875	NaN	View
Vitamin B5 - CoA biosynthesis from pantothenate	1	1	1	0.23333	0.21875	NaN	View
Glycosphingolipid biosynthesis - lactoseries	1	1	1	0.23333	0.21875	NaN	View
Bile acid biosynthesis	1	1	1	0.23333	0.21875	NaN	View
Propanoate metabolism	1	1	1	0.23333	0.21875	NaN	View
Blood Group Biosynthesis	1	1	1	0.23333	0.21875	NaN	View
Vitamin H (biotin) metabolism	1	1	1	0.23333	0.21875	NaN	View
Vitamin E metabolism	1	1	1	0.23333	0.21875	NaN	View
De novo fatty acid biosynthesis	1	1	1	0.23333	0.21875	NaN	View
Vitamin A (retinol) metabolism	1	1	1	0.23333	0.21875	NaN	View


Supplementary Figure 9 – Differentially expressed pathways between control and L-asparaginase treated PER-117 cells. Pathway analysis was performed using all identified (A) positively and (B) negatively ionized metabolites.

A

Pathway Name	Total ↑↓	Hits (all) ↑↓	Hits (sig.) ↑↓	Expected ↑↓	P-value ↑↓	Gamma P ↑↓	Details
Pyrimidine metabolism	5	5	5	1.5	0.0014544	0.0033905	View
Aspartate and asparagine metabolism	7	7	6	2.1	0.0019576	0.0033948	View
Purine metabolism	8	8	6	2.4	0.0062929	0.003432	View
Glycine, serine, alanine and threonine metabolism	6	6	5	1.8	0.0069897	0.0034381	View
Urea cycle/amino group metabolism	7	7	5	2.1	0.01957	0.003549	View
N-Glycan biosynthesis	3	3	3	0.9	0.0223	0.0035736	View
Histidine metabolism	3	3	3	0.9	0.0223	0.0035736	View
Glutathione Metabolism	3	3	3	0.9	0.0223	0.0035736	View
Beta-Alanine metabolism	3	3	3	0.9	0.0223	0.0035736	View
Tryptophan metabolism	6	6	4	1.8	0.055831	0.0038914	View
Alanine and Aspartate Metabolism	4	4	3	1.2	0.071749	0.004053	View
Methionine and cysteine metabolism	9	9	5	2.7	0.074891	0.0040858	View
Glycolysis and Gluconeogenesis	2	2	2	0.6	0.08216	0.0041627	View
Glycosphingolipid biosynthesis - ganglioseries	2	2	2	0.6	0.08216	0.0041627	View
Sialic acid metabolism	2	2	2	0.6	0.08216	0.0041627	View
Glycosphingolipid biosynthesis - globoseries	2	2	2	0.6	0.08216	0.0041627	View
Vitamin B5 - CoA biosynthesis from pantothenate	2	2	2	0.6	0.08216	0.0041627	View
Vitamin B9 (folate) metabolism	2	2	2	0.6	0.08216	0.0041627	View
Valine, leucine and isoleucine degradation	2	2	2	0.6	0.08216	0.0041627	View
CoA Catabolism	2	2	2	0.6	0.08216	0.0041627	View

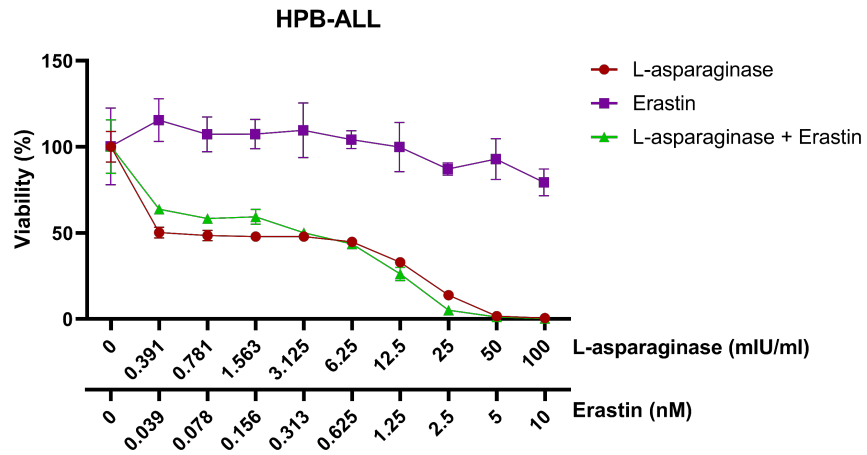
B

Detailed result table

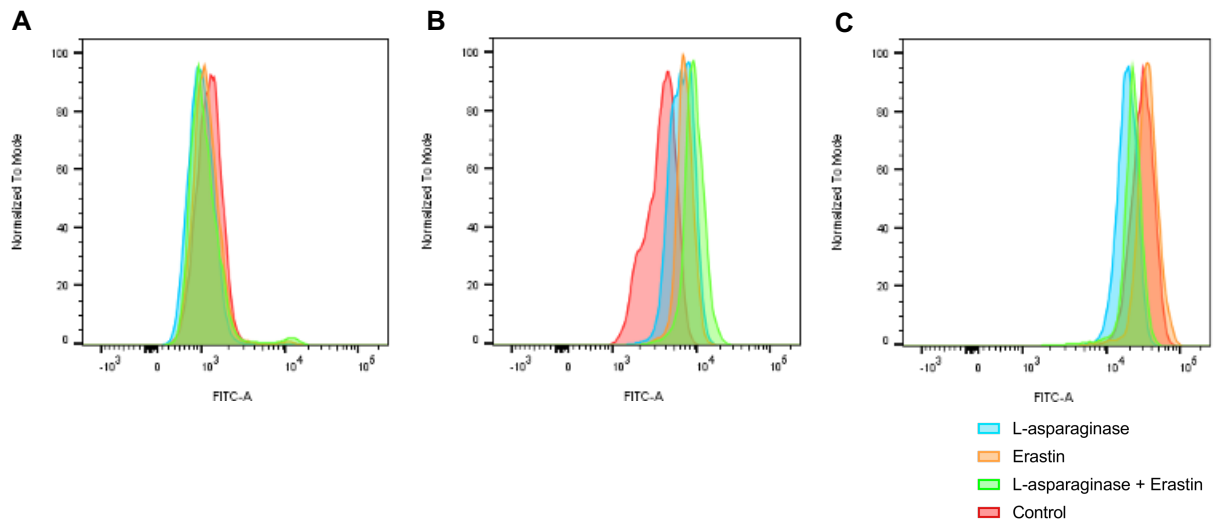
Mouse over the **Help** icon to find more information on each columns 

Pathway Name	Total ↑↓	Hits (all) ↑↓	Hits (sig.) ↑↓	Expected ↑↓	P-value ↑↓	Gamma P ↑↓	Details
Histidine metabolism	3	3	3	1.0	0.024194	NaN	View
Tryptophan metabolism	3	3	3	1.0	0.024194	NaN	View
Pyrimidine metabolism	6	6	4	2.0	0.059881	NaN	View
N-Glycan biosynthesis	4	4	3	1.3333	0.079255	NaN	View
Glycosphingolipid biosynthesis - ganglioseries	2	2	2	0.66667	0.090726	NaN	View
Glycosphingolipid biosynthesis - globoseries	2	2	2	0.66667	0.090726	NaN	View
Glycine, serine, alanine and threonine metabolism	2	2	2	0.66667	0.090726	NaN	View
Arachidonic acid metabolism	2	2	2	0.66667	0.090726	NaN	View
Glycosphingolipid metabolism	2	2	2	0.66667	0.090726	NaN	View
Prostaglandin formation from arachidonate	2	2	2	0.66667	0.090726	NaN	View
Leukotriene metabolism	2	2	2	0.66667	0.090726	NaN	View
Purine metabolism	8	8	4	2.6667	0.18781	NaN	View
Glycolysis and Gluconeogenesis	3	3	2	1.0	0.22379	NaN	View
Sialic acid metabolism	3	3	2	1.0	0.22379	NaN	View
Phosphatidylinositol phosphate metabolism	3	3	2	1.0	0.22379	NaN	View
Starch and Sucrose Metabolism	3	3	2	1.0	0.22379	NaN	View
Methionine and cysteine metabolism	3	3	2	1.0	0.22379	NaN	View
Pyruvate Metabolism	1	1	1	0.33333	0.3125	NaN	View

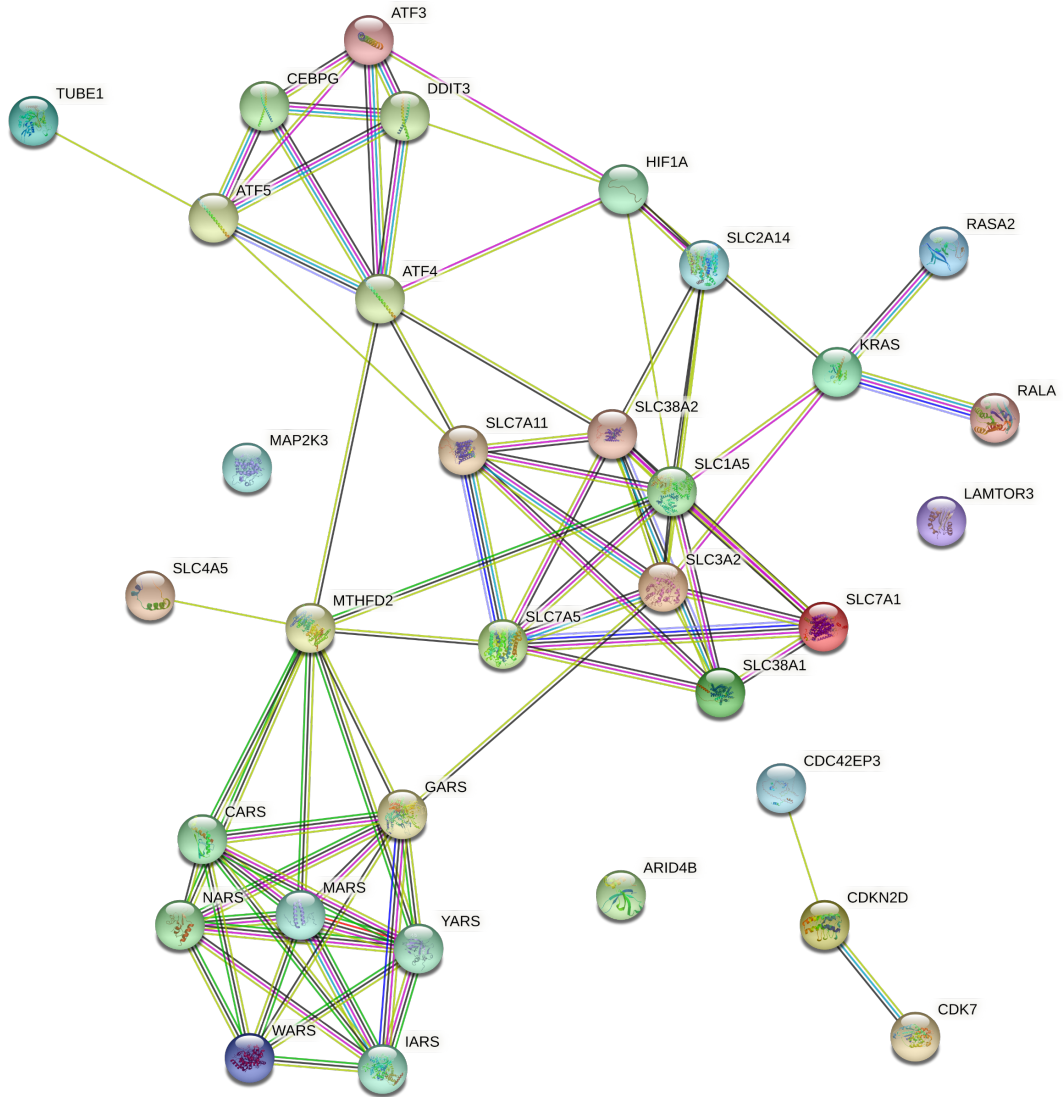
Supplementary Figure 10 – Differentially expressed pathways between control and L-asparaginase treated KOPT-K1 cells. Pathway analysis was performed using all identified (A) positively and (B) negatively ionized metabolites.



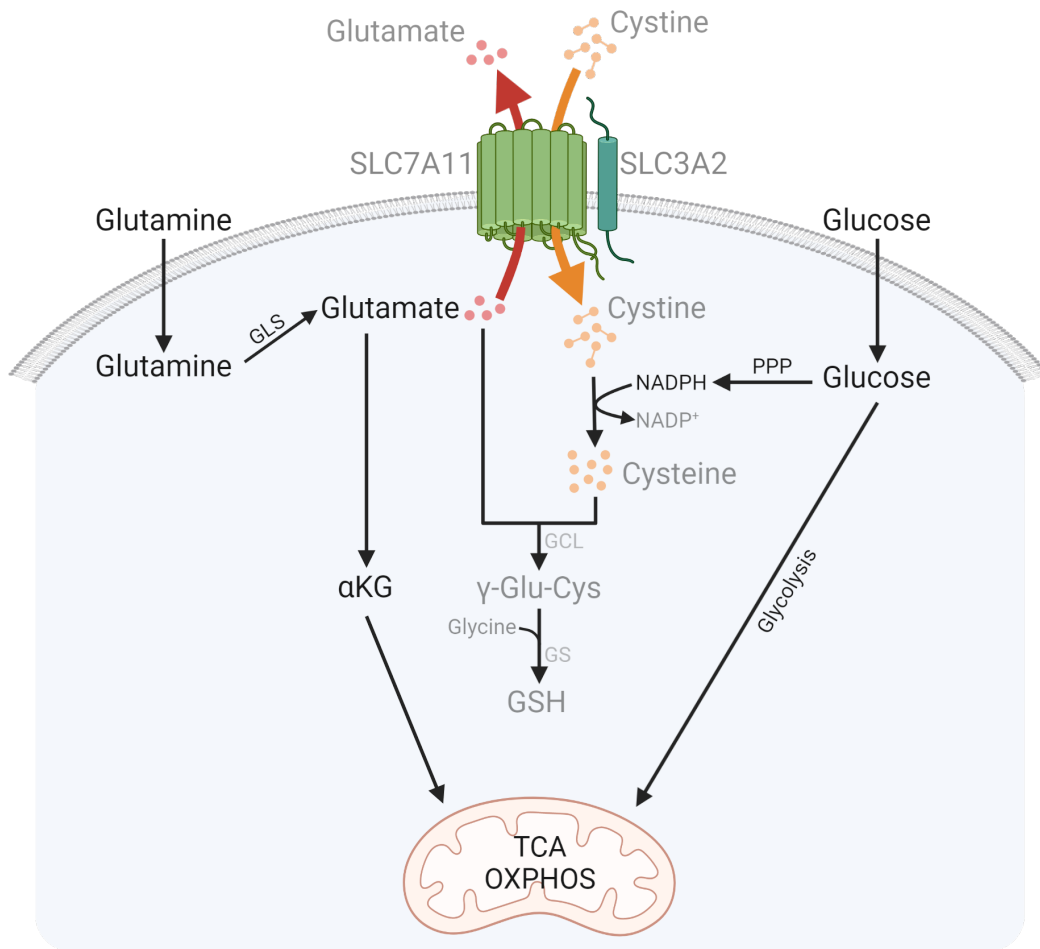
Supplementary Figure 11 – Inhibiting L-asparaginase upregulated SLC7A11 with erastin does not decrease cell viability. Viability of HPB-ALL cells measured by CellTiter Glo viability assay after L-asparaginase/erastin mono-treatment or combination treatment. Error bars represent the SD of two technical replicates.



Supplementary Figure 12 – Inhibiting L-asparaginase induced SLC7A11 with erastin does not modulate downstream cystine, GSH and general oxidative stress levels in accordance with its effect on SLC7A11 expression levels. Flow cytometric analysis of (A) intracellular cystine levels, (B) cellular GSH and (C) general oxidative stress after L-asparaginase, erastin or combination treatment of HPB-ALL cells.



Supplementary Figure 13 – STRING analysis (<https://string-db.org>) on microarray data of L-asparaginase treated T-ALL cells⁹⁶.



Supplementary Figure 14 – Glutamine and glucose dependency of SLC7A11 overexpressing T-ALL cells. TCA, tricarboxylic acid; OXPHOS, oxidative phosphorylation; GLS, glutaminase; αKG, α-ketoglutarate; PPP, pentose phosphate pathway; GCL, glutamate-cysteine ligase; GS, glutathione synthetase. Created with BioRender.com.